April 2003

Advanced Fuel Cycle Initiative

October – December 2002

Quarterly Report – Volume I

SAND2003-1179P

Idaho Accelerator Center

Argonne National Laboratory, Brookhaven National Laboratory, Burns & Roe, Enterprises, Inc.
General Atomics, Idaho National Engineering & Environmental Laboratory
Idaho Accelerator Center, Lawrence Livermore National Laboratory
Los Alamos National Laboratory, Oak Ridge National Laboratory
Sandia National Laboratories, University of Nevada, University of Michigan
University of California, University of Texas
University Research Alliance, Westinghouse Savannah River Company

Sandia is a multiprogram laboratory operated by Sandia Corporation, a Lockheed Martin Company, for the United States Department of Energy's National Nuclear Security Administration under contract DE-AC04-94AL85000

Advanced Fuel Cycle Initiative Quarterly Report
October – December 2002

Approval

Signature on File

_____ Date _____

John Kelly
AFCI Program Manager

This page intentionally left blank

Table of Contents

Acronyms and Symbols

AAA	Advanced Accelerator Applications
AC	Accelerating cavities
ACP	Advanced Crystallization Process
ACRR	Annular Core Research Reactor
ADS	Accelerator-Driven System
ADTF	Accelerator-Driven Test Facility
ADMAB	Accelerator-Driven Minor Actinide Burner
AES	Advanced Energy Systems (formerly Northrup-Grumman Corp.)
AET	Ability Engineering Technology
AFCI	Advanced Fuel Cycle Initiative
AFM	Atomic Force Microscopy
A•h	Ampere-Hour
AHA	Acetohydroxamic acid
Am	Americium
AMUSE	Argonne Model for Universal Solvent Extraction, the generic TRUEX model expanded to include UREX and PUREX processing
ANL	Argonne National Laboratory (Chicago)
ANL-W	Argonne National Laboratory-West (Idaho Falls)
ANRC	Amarillo National Research Center
ANS	American Nuclear Society
ANSYS	structural analysis modeling code
ANTT	Advanced Nuclear Transformation Technology
appm	atomic parts per million
APT	Accelerator Production of Tritium
ASME	American Society of Mechanical Engineers
ATR	Advanced Test Reactor (INEEL)
ATW	Accelerator Transmutation of Waste
Ba	Barium
BCM	Beam-Current Monitor
BCP	Baseline Change Proposal
BCP	Buffered Chemical Polishing
Be	Beryllium
Beta (β)	Ratio to the speed of light
Bi	Bismuth
BISTRO	Two-Dimensional Discrete Ordinates Code
BNFL	British Nuclear Fuels, Ltd
BNL	Brookhaven National Laboratory
BOF	Balance of Facility
BOL	Beginning of Life
BOP	Balance of Plant
BOR-60	Sodium-Cooled Fast Reactor (Dmitrovgrad, Russia)
BPM	Beam-Position Monitor
BSE	backscattered electron (images)
CCDTL	Coupled-Cavity Drift-Tube Linac
CCL	Coupled-Cavity Linac
Ce	Cerium
CEA	Commissariat à l'Energie Atomique (France)
CEM	Cascade Exciton Model code (Model-based Monte-Carlo particle transport code)
CERCA	Compagnie Pour L'Etude Et La Realisation De Combustibles Atomiques
cercer	Ceramic-Ceramic
cermet	Ceramic-Metal
CFD	Computational Fluid Dynamics
CINDER90	Computer Code
CLWR	Commercial Light-Water Reactor

Cm	Curium
CMPO	Neutral Extractant
CMR	Chemistry and Metallurgy Research (facility at LANL)
CONCERT	COmbined Neutron Center for European Research and Technology
Cr	Chromium
Cs	Cesium
Cu	Copper
CVD	Chemical Vapor Deposition
cw	Continuous Wave (100% duty factor)
DACS	Data Acquisition and Control System
DAS	Data Acquisition System
DBTT	Ductile-To-Brittle Transition Temperature
DCR	Design Change Request
DDN	Design Data Need
DELTA	Development of Liquid Metal Technologies and Applications
DIAMEX	Aqueous Solvent Extraction Process for TRU Recovery
DOE	Department of Energy
dpa	Displacements per Atom
EBR	Experimental Breeder Reactor
ED&D	Engineering Development and Demonstration
EDS	Energy Dispersive Spectrometry
EFPD	Effective Full-Power Day
EFTTRA-T4	Radiation Test Sponsored by the European Union
EIS	Electrochemical Impedance Spectroscopy
EIS	Environmental Impact Statement
EMT	Electrometallurgical Treatment
ENDF	Evaluated Nuclear Data File – Evaluations that can be used in MCNPX for more accurate predictions of fission, criticality, transport, and radiation damage
EOI	End of Irradiation
EOL	End of Life
EPICS	Experimental Physics and Industrial Control System
ERANOS	Computer modeling code
ERC	External Review Committee
ES&H	Environmental, Safety, and Health
ESS	European Spallation Source
ESSAB	Energy System Acquisition Advisory Board (DOE)
Eu	Europium
FC	Fuel Cycle
FCF	Fuel Conditioning Facility
FCOPT	Fuel Cycle Optimization
FDD	Facility Design Description
F&OR	Functional and Operational Requirement
Fe	Iron
FFTF	Fast Flux Test Facility
FMF	Fuel Manufacturing Facility
FNFB	Fast Neutron Flux Booster
FODO	Focus-Drift-Defocus-Drift
FPY	Full-Power Year
FWHM	Full Width Half Maximum
FZJ	Forschungs Zentrum Jülich (German Laboratory)
FZK	Forschungs Zentrum Karlsruhe (German Laboratory)
GEN IV	Generation IV
g/L	Grams per Liter
GA	General Atomics Inc.
GFR	Gas-cooled Fast Reactor
GIF	Generation IV International Forum

GNASH	Nuclear Reaction Code
gpm	gallons per minute
GSI	Gesellschaft für Schwerionenforschung (Darmstadt, Germany)
GT-MHR	Gas Turbine Modular Helium Reactor
H	Hydrogen
HAN	Hydroxylamine
HCP	Hazard Control Plan
He	Helium
HEBT	High-Energy Beam Transport
HEU	Highly enriched uranium
Hf	Hafnium
HFEF	Hot Fuel Examination Facility
HFIR	High Flux Isotope Reactor (ORNL)
HFR	High Flux Reactor (Petten, Netherlands)
Hg	Mercury
HIP	Hot Isostatic Process (for bonding materials)
HLW	High-Level Waste
HM	Heavy metal
HPRF	High-Power Radio Frequency
HS/WS	Halo-Scraper/Wire-Scanner (diagnostic device)
HX	Heat exchanger
I&C	Instrumentation and Control
IAC	Idaho Accelerator Center
IAEA	International Atomic Energy Association (Vienna, Austria)
ICP-MS	Inductively Coupled Plasma-Mass Spectrometry
ICS	Integrated Control System
IFMIF	International Fusion Materials Irradiation Facility
IFR	Integral Fast Reactor
IHX	Intermediate Heat Exchanger
IMS	Information Management System
INEEL	Idaho National Engineering and Environmental Laboratory
I-NERI	International Nuclear Energy Research Initiative
IPBT	In-Pile Beam Tube
IPPE	Institute of Physics and Power Engineering, Obninsk, Russia.
ISABEL	Physics Modeling Code
ISTC	International Science and Technology Centre (Moscow)
ITER	International Thermonuclear Experimental Reactor
ITU	Institute for Transuranium Elements (Karlsruhe, Germany)
JAERI	Japan Atomic Energy Research Institute
JCNNM	Johnson Controls Northern New Mexico
JLAB	Jefferson Laboratory (VA)
K	Potassium
KAERI	Korean Atomic Energy Research Institute
KEK	National Laboratory for High-Energy Physics (Tsukuba, Japan)
keV	Kiloelectron Volt
kW	kilowatt
LA150n	Los Alamos generated nuclear data library, extending up to 150 MeV
LAHET	Los Alamos High-Energy Transport
LANL	Los Alamos National Laboratory
LANSCE	Los Alamos Neutron Science Center
LBE	Lead-bismuth eutectic
LBHM	Low- Hot Model
L/d	Length-to-diameter ratio
LFR	Lead-Cooled Fast Reactor
L/hr	Liter per hour
LEBT	Low-Energy Beam Transport

LEDA	Low-Energy Demonstration Accelerator
LHGR	linear heat generation rate
LINAC	A computer code based on PARMILA that has been modified to include CCDTL and SCRF elliptical cavities as options
LLFP	Long-lived fission product
LLNL	Lawrence Livermore National Laboratory
LLRF	Low-level radio frequency
LME	Liquid-metal embrittlement
LMR	Liquid-metal reactor
LTA	Lead Test Assembly
LUA	Lead Use Assembly
LWR	Light-water reactor
M	Molar
MA	Minor actinide
mb	Millibarn
MCA	Multi-criteria analysis
mCi	Millicurie
MCNP	Monte Carlo N-Particle Transport Code
MCNPX	Merged code—Los Alamos High-Energy Transport (LAHET) and Monte Carlo N-Particle Codes (MCNP)
MCWO	MCNP Coupling With ORIGEN2 (burnup calculation code)
MDD	Modified Direct Denitration
MEAM	Molecular Embedded Atom Method
MEGAPIE	Megawatt Pilot Experiment
MFM	Magnetic Flow Meter
MIT	Massachusetts Institute of Technology
mL	Milliliter
Mo	Molybdenum
MOX	Mixed oxide fuel
mR	Millirad (a measure of radiation)
MSR	Molten Salt Reactor
MT	Metric Ton
MTL	Materials Test Loop
MUSE	CEA-Cadarache Zero-Power Subcritical Experiments
MW	Megawatt
MWD/T	Megawatt Days per Ton (standard unit for burnup)
MWth	Megawatt thermal
MYRRHA	Multipurpose hYbrid Research Reactor for High-Tech Applications
N	Nickel or nitride
Na	Sodium
Ni	Nickel
Np	Neptunium
n/p	Neutrons per proton
NDA	Nondestructive analyses
NE	DOE Office of Nuclear Energy, Science, and Technology
NEA	Nuclear Energy Agency (Paris)
NEPA	National Environmental Protection Agency
NERAC	Nuclear Energy Research Advisory Committee
NERI	Nuclear Energy Research Initiative
NFC	Nuclear Fuel Cycle
NFF	Nonfertile Fuel
NRC	Nuclear Regulatory Commission
O&M	Operations and Maintenance
OCRWM	Office of Civilian Radioactive Waste Management
OECD-NEA	Organization for Economic Cooperation and Development-Nuclear Energy Agency (Paris)

ORIGEN	A computer code system for calculating the buildup, decay, and processing of radioactive materials
ORNL	Oak Ridge National Laboratory
P&ID	Piping and Instrumentation Diagram
P&T	Partitioning and transmutation
PACS	Personnel Access Control System
PARMTEQM	RFQ simulation code
Pb	Lead
PCM	Pulse Control Modulation
Pd	Paladium
PFD	Process Flow Diagram
PHA	Preliminary Hazards Assessment
PHENIX	Fast Reactor in France
PIE	Post-irradiation examination
PNNL	Pacific Northwest National Laboratory
POP	Proof of Performance, Proof of Principle
PRAD	Proton Radiography
PRISM	Power Reactor Innovative Small Module
PSAR	Preliminary Safety Analysis Report
PSS	Personnel Safety System
PSI	Paul Scherrer Institute (Switzerland)
Pu	Plutonium
PUREX	Plutonium-Uranium Extraction
PWR	Pressurized Water Reactor
PYRO	Pyrochemical process
Q	Quality factor
QA	Quality Assurance
QAC	Quick ATW Costing
QC	Quality Control
R	Rad (a measure of radiation)
R&D	Research and Development
RAMI	Reliability, Availability, Maintainability, and Inspectability
RBS	Rutherford Backscattering Spectrometry
RERTR	Reduced Enrichment for Research and Test Reactors program
RF	Radio Frequency
RFQ	Radio-Frequency Quadrupole
RCCS	Resonance-Control Cooling System
RIA	Rare Isotope Accelerator
RIAR	Russian Institute of Atomic Reactors
rms	root mean square
RRR	Residual Resistance Ratio
RSICC	Radiation Safety Information Computational Center
RTD	Surface Temperature Detector
RTH	Royal Institute of Technology (Stockholm, Sweden)
Ru	Ruthenium
SAA	Systems Approaches Analysis
SANEX	Aqueous Solvent Extraction Process for Am and Cm Recovery
SAR	Safety Analysis Report
SC	Superconducting
SCK CEN	Studiecentrum Voor Kernenergie Centre D'Etude De L'Energie Nucleaire
SCM	Subcritical Multiplier
SCRF	Superconducting RF
SCWR	Supercritical Water-Cooled Reactor
SDD	System Design Description
SEM	Scanning Electron Microscopy
SFR	Sodium-Cooled Fast Reactor

SFT	Stacking-Fault Tetrahedral
SHR	shutdown heat-removal
SINQ	Spallation Neutron Source at Paul Scherrer Institute (Switzerland)
SNF	Spent Nuclear Fuel
SNL	Sandia National Laboratories
SRS	Savannah River Site
SRTC	Savannah River Technology Center
STAYSL	A computer code to analyze results of activation foil measurements
STAYSL2	A computer code to analyze results of activation foil measurements in both a proton and neutron flux
Star-CD	Computational fluid dynamics code
STP	Standard Temperature and Pressure
STIP	Spallation Target Irradiation Program (at PSI)
STIP	Spallation Target Irradiation Program
Ta	Tantalum
T/B	Target / Blanket
TBP	Tri-*n*-butyl Phosphate or Tributylphosphate
Tc	Technitium
TEM	Transmission Electron Microscopy
TESLA	International Collaboration on a TeV Superconducting Linear Accelerator
TGA	Thermal Gravimetric Analysis
Ti	Titanium
TiN	Titanium Nitride
TJNAF	Thomas Jefferson National Accelerator Facility
TMT	Target and Materials Test Station
T/p	Tritons (nucleii of tritium atoms) per Proton
TRAC	Transient Reactor Analysis Code
TRACE 3-D	Interactive computer code that calculates the envelopes of a bunched beam through a user-defined transport system
TREACS	TReat Experiment for ACcelerator-driven Systems
TREAT	Transient Reactor Test Facility
TRISO	Tri-isotropic, referring to a multi-layered fuel-particle coating consisting of pyrolytic carbon and silicon carbide
TRADE	TRIGA Accelerator Driven Experiment
TRIGA	Small Reactor Type
TRISPAL	Refers to the French APT Program
TRL	Technical Readiness Level
TRU	Transuranics (americium, curium, neptunium, and plutonium)
TRUEX	Aqueous solvent extraction process for TRU recovery
U	Uranium
UFP	University Fellowship Program
UNLV	University of Nevada Las Vegas
UPP	University Participation Program
UREX	Uranium Extraction (an aqueous partitioning process)
URA	University Research Alliance
URP	University Research Program
USQD	Unreviewed Safety Question Determination
V	Vanadium
VHTR	Very-High Temperature Reactor
VPS	Vapor Plasma Spray
VARIANT	Three-Dimensional Nodal Transport Code
W	Tungsten
WBS	Work Breakdown Structure
WNR	Weapons Neutron Research (facility at LANL)
WPPT	Working Party on Partitioning and Transmutation
WSRC	Westinghouse Savannah River Company

Xe	Xenon
XRD	X-ray Diffraction
Y	Yttrium
ZPPR	Zero Power Physics Reactor
Zr	Zirconium
ZrC	Zirconium Carbide
ZrN	Zirconium Nitride

1 INTRODUCTION

The mission of the Advanced Fuel Cycle Initiative (AFCI) is to develop and implement spent fuel treatment and transmutation technologies to enhance the performance of the proposed repository and reduce the cost of geologic disposal for the United States. The AFCI is closely coupled with the Generation IV Nuclear Energy Systems Program (Generation IV) that seeks to deploy a new generation of nuclear power plants by 2030 to provide a transmutation capability. Together, these two programs enable an expanded role for nuclear power as a sustainable resource that will address long-term U.S. energy security, environmental, and economic concerns. The AFCI also provides for an effective transition from the current once-through nuclear fuel cycle to the future sustainable cycle. Such a closed nuclear fuel cycle could provide a number of benefits, including:

- Reducing the cost of geologic disposal of commercial spent nuclear fuel,
- Recovering the energy value from commercial spent nuclear fuel,
- Reducing the inventories of civilian plutonium in the U.S.,
- Reducing the toxicity of high-level nuclear waste requiring geologic disposal, and
- Eliminating or significantly delaying the technical need for a second geologic repository in the U.S.

Key to the mission of the AFCI is the development and demonstration of technologies that can be employed in a number of facilities that will need to be constructed. The first of these is a light water reactor (LWR) Spent Fuel Treatment (SFT) facility that would begin operation in FY 2015. This facility will process the spent fuel from both the existing and newly constructed advanced LWR systems. It can be sized to treat fuel at a rate equal to the current spent nuclear fuel discharge rate. In this facility, cesium and strontium will be extracted and managed separately. Minor actinides will be stored for transmutation in future systems. Slightly enriched uranium, plutonium, neptunium, and possibly other minor actinides will be recycled into LWRs through fabrication of a proliferation-resistant fuel in a facility that will begin operation by FY 2018. Most existing and newly constructed LWRs are expected to utilize proliferation-resistant fuel to the maximum degree possible for their operational lifetimes.

Processing of LWR spent nuclear fuel in the U.S. could offer significant advantages over direct disposal. Separation of the uranium, which constitutes more than 95% of spent nuclear fuel, results in a dramatic decrease in the volume of material bound for geologic disposal. Separate management of cesium and strontium significantly decreases the short-term heat load in the repository and removal of the minor actinides decreases the long-term heat load. Together, these effects could result in substantial decreases in the number of waste packages that must be disposed. Recycling of plutonium in the proliferation-resistant fuel would also begin to slow the growth of the U.S. civilian inventories of plutonium.

Fully closing the nuclear fuel cycle requires the introduction of one or more fast-spectrum systems found among the Generation IV systems and possibly an Accelerator-Driven System (ADS) to provide a transmutation capability. A preliminary determination will be made by FY 2007 as to whether an ADS will be required to supplement the transmutation capability provided by Generation IV fast reactors. In a fast reactor system, unburned plutonium and minor actinides from the LWR SFT facility could be consumed, helping to close the nuclear fuel cycle. The

small quantity of waste eventually disposed under this approach would have dramatically reduced toxicity and long-term heat load when compared to the existing inventory of spent nuclear fuel. The AFCI will develop the nuclear fuel for a range of Generation IV fast reactor systems and help guide the selection of the fast reactor to be used for transmutation. In order to support performance testing of these systems and a decision on their deployment by FY 2030, engineering-scale demonstration of prototypic candidate Generation IV fast reactor fuels will be performed by FY 2022.

Implementing a closed nuclear fuel cycle could significantly reduce the cost of geologic disposal of spent nuclear fuel. A preliminary analysis has shown that the implementation of AFCI technologies could reduce the cost of the first geologic repository by approximately $5 billion. These savings result from decreasing the number of waste packages and drip shields, as well as from reduced operational costs. With full implementation of the AFCI, a second repository and its associated $50 billion cost would either not be needed or would be delayed significantly. The AFCI could provide other economic benefits as well. It has been estimated that recycling the LWR fuel into proliferation-resistant fuel could produce a gross revenue of $12 billion between 2018 and 2040. Overall, the AFCI could result in a net savings of between $35 and $50 billion between 2010 and 2040.

The AFCI could provide substantial intangible benefits in addition to these projected cost savings. The closed nuclear fuel cycle is essential to enabling an increased role for nuclear power in the future, enhancing our energy security. Nuclear energy can also address energy security concerns through decreasing oil imports. Nuclear energy can serve a critical role in addressing environmental concerns by providing large-scale power generation without carbon emissions and clean hydrogen for the transportation sector. The energy value contained in the spent nuclear fuel currently stored in this country is equivalent to over 6 billion barrels of oil, or about two full years of U.S. oil imports. The reduction of civilian plutonium inventories in the U.S. would reduce the associated physical protection and material control and accounting requirements, in addition to reducing the proliferation risk from these materials.

This report is Volume I of the October through December FY03 Technical Quarterly Report for the Advanced Fuel Cycle Initiative. Volume I covers research activities for the Technical Integration, Systems Analysis, Fuels Development, Transmutation, and University Programs elements. Volume II will cover the Separations element of the AFCI. For more information on the contents of this report, please contact the following people:

- Technical Integration – John Kelly, SNL, (505) 844-8993, jekelly@sandia.gov
- Systems Analysis – Ralph Bennett, INEEL, (208) 526-7708, rcb@inel.gov
- Fuels Development – Kemal Pasamehmetoglu, LANL, (505) 667-8893, kop@lanl.gov
- Transmutation – Mike Cappiello, LANL, (505) 665-6408, mcappiello@lanl.gov
- Idaho Accelerator Center – Frank Harmon, (208) 282-5875, harmon@physics.isu.edu
- UNLV Programs – Tony Hechanova, UNLV, (702) 895-1457, hechanova@unlv.edu
- Fellowship Program – Cathy Dixon, URA, (806) 376-5533, dixon@uraweb.org

2 TECHNICAL INTEGRATION

2.1.1 Technical Integration Objective and Scope

The Technical Integration program element serves as the mechanism for interpreting the myriad of technical efforts into a single overarching cohesive program focused upon resolving spent nuclear fuel issues. The scope of Technical Integration encompasses all technical program elements including systems analysis, separations, fuels, and transmutation, and abstracts the salient elements of each program element to perform a technical and programmatic synthesis to derive a consolidated overview of the advanced fuel cycle.

2.1.2 Technical Integration Highlights

- Completed a final draft of the Five-Year Program Management Plan
- NERAC/ANTT Presentation
- Began preparations for the Semi-Annual Review Meeting held in Albuquerque in January, 2003
- Coordinated with Burns & Roe and NTDs the draft Work Package submission for FY03 work scope

2.1.3 Technical Integration Summary

The two most significant highlights of the Technical Integration effort for the first quarter of FY 2003 consisted of development and submittal of the overall Program Management Plan, and preparation and presentation of the forthcoming and five-year technical plans to the ANTT and associated NERAC subcommittee. Development of the Program Management Plan was a significant effort entailing analysis and integration of both the coming year outlying five-year technical program and associated resource allocations. Continuous interactions with Headquarters, the National Technical Directors, and Laboratory, Industry and University Principal Investigators were necessary to formulate activities and schedules. Several iterations were required to distill and prioritize work schedules to accommodate anticipated budget scenarios over the 5-year time span, and simultaneously achieve both near and long term programmatic goals.

Additional efforts included initiation of preparations for the Semi-Annual AFCI Review Meeting to be held during January, and coordinating the development of Work Packages with DOE Headquarters and the National Laboratories. Among the tasks initiated in anticipation of the review meeting were development and distribution of the draft agenda, negotiations with the proposed conference center, and the consolidation, editing, and printing of both posters and presentations. Coordination efforts for the technical and management Work Packages required development of an integrated task and associated budget spreadsheet for the entire AFCI Program, from which the individual site-generated forms were developed and managed.

3 SYSTEMS STUDIES AND ANALYSIS

3.1.1 Systems Studies and Analysis Scope and Objectives

Systems Analysis activity crosscuts the AFCI technical areas (Fuels, Separations, and Transmuters) and provides the tools and analyses to inform key decisions in the program. Systems Analysis also includes work related to the transmutation of radionuclides. The Systems Analysis activity is integrated between the Generation IV Program and the AFCI, and coordinated with the Technical Integration function of each program.

3.1.2 Systems Studies and Analysis Highlights

Due to the continuing resolution, the accomplishments summarized in this report reflect those organizations with carryover scope and funding from FY02.

- An extensive update on Systems Analysis and Reactor-Based Transmutation studies was prepared and presented for the NERAC Advanced Nuclear Transformation Technology (ANTT) subcommittee meeting.
- An overview of AAA and CEA LWR Recycle Approaches was prepared and presented to the AFCI Blue Ribbon Panel on Proliferation Resistant Characteristics of Recycle Fuels.
- A summary report on systems studies of multi-tier transmutation strategies was completed.
- An updated report was completed including the pyroprocess facility layout and the process flows was prepared to establish safeguards options.
- An AFCI-oriented Nuclear Fuel Cycle (NFC) model was implemented in a partial-equilibrium energy sector optimization (MARKAL) model.
- Calculations were performed using the Monteburns code to estimate the mass flows of multiple recycling of Pu in light water reactors (LWR).

3.1.3 Systems Studies and Analysis Technical Summary

Systems Studies and Analysis [ANL]

An extensive update on Systems Analysis and Reactor-Based Transmutation studies was prepared and presented for the NERAC Advanced Nuclear Transformation Technology (ANTT) subcommittee meeting. The FY02 progress on deep burnup in Tier 1 PWRs, advanced LWR transmutation of waste, low conversion fast burner reactors, and dynamic fuel cycle studies was presented. The ability to stabilize the plutonium inventory with the CORAIL multi-recycle concept was contrasted to once-through UO_2 and MOX fuel cycles. Elemental management scenarios for LWR recycle, including Pu+Np recycle, were compared; and the practical issues arising from high minor actinide content with TRU recycle were highlighted. The impact of deep burnup in LWRs on Tier 2 performance and capacity requirements was shown; and low conversion ratio fast reactors options were discussed. The LANL studies on equilibrium and dynamic fuel cycle scenarios were also summarized. The importance of continued transmutation studies to compare and refine fuel cycle strategies was recognized.

An overview of AAA and CEA LWR Recycle Approaches was prepared and presented to the AFCI Blue Ribbon Panel on Proliferation Resistant Characteristics of Recycle Fuels. Background studies of LWR recycle, including the French Charpin report, OECD Working Party on Plutonium Recycling, and the FY01 AAA multi-tier study, were summarized. Recent work on deep burnup in Tier 1 PWRs was highlighted including the CORAIL results and CONFU assembly concepts. Particular attention was given to the techniques and impact of multi-recycle strategies. The fuel cycle impact was quantified in detail including evaluations of mass flows, fuel composition, critical mass, radiation properties, heat load, and fresh fuel dose rates.

Three technical papers based on AFCI systems analyses were published and presented at the winter ANS meeting in Washington:

- T. A. Taiwo, T. K. Kim, J. A. Stillman, M. Salvatores, R. N. Hill, and P. J. Finck, "Assessment of Proliferation and Fuel Handling Issues for a Multirecycle PWR Assembly Concept," *Trans. Am. Nucl. Soc.*, 87, 404 (2002).
- J. A. Stillman and R. N. Hill, "Performance of an Accelerator-Driven Transmuter for Minor Actinide Burning," *Trans. Am. Nucl. Soc.*, 87, 523 (2002).
- Y. Kim, W. S. Yang, T. A. Taiwo, R. N. Hill, and H. Khalil, "Evaluation of Tc-99 and I-129 Transmutation Potential of PWRs," *Trans. Am. Nucl. Soc.*, 87, 527 (2002).

In addition, several technical papers based on the AAA systems studies were presented and published at the PHYSOR 2002 ANS International Topical Meeting on the New Frontiers of Nuclear Technology held in Seoul, Korea on October 7-10, 2002, and the 7th Information Exchange Meeting on Actinide and Fission Product Partitioning & Transmutation held in Jeju, Korea on October 14-16, 2002:

- T. K. Kim, J. A. Stillman, T. A. Taiwo, R. N. Hill, P. J. Finck, and M. Salvatores, "Assessment of the Transuranics Stabilization in PWRs," *PHYSOR 2002*
- Y. Kim, W. S. Park, W. S. Yang, T. A. Taiwo, and R. N. Hill, "An Investigation of an Optimal Range of Subcriticality for Accelerator-Driven Systems," *PHYSOR 2002*
- Y. Kim, W. S. Yang, T. A. Taiwo, and R. N. Hill, "Reactivity Estimation for Source-Driven Systems Using First-Order Perturbation Theory," *PHYSOR 2002*
- T. K. Kim, T. A. Taiwo, J. A. Stillman, R. N. Hill, and P. Finck, "Assessment of the Equilibrium State in Reactor-Based Plutonium or Transuranics Multirecycling," *Information Exchange*
- Y. Kim, R. N. Hill, W. S. Yang, and H. Khalil, "Transmutation of Long-Lived Fission Products in the ATW System," *Information Exchange*

A summary report on systems studies of multi-tier transmutation strategies was completed. This report included a synopsis of the major FY02 AAA systems research reports. Proliferation resistant and conventional ALWR fuel cycles were evaluated to clarify and *assess the practical limits for Tier 1 partial destruction* of the transuranics (TRU); four distinct reports from this task were summarized. Partial burning of the TRU in a first tier thermal spectrum system will impact the performance of the second tier transmuter; thus, *the Tier 2 fast system performance impact* was also considered; three additional reports on this topic were described. The reactor-based

transmutation reports on advanced LWR recycle techniques and low conversion fast reactor systems were also considered in this comprehensive summary report.

For the first tier thermal system, FY02 work focused on the application of the heterogeneous assembly CORAIL concept. LWR performance results are quite promising for multi-recycle of plutonium. These deep burnup strategies allow a significant fraction of the TRU (up to 75%) to be consumed in LWRs. However, recycle of plutonium and/or minor actinides in a thermal spectrum system leads to a significant buildup of higher actinides. Thus, the deep burnup fuels are progressively more difficult to handle and will complicate fuel storage, reprocessing, and re-fabrication. Initial studies to define the practical limits for TRU recycle in LWRs were completed. It was concluded that multi-recycle of plutonium can be accommodated with technology similar to standard MOX; however, without plutonium separation, only 2 or 3 recycles can be achieved without more elaborate remote handling.

Deep burnup of TRU in the first tier thermal spectrum system leads to a much lower Tier 2 capacity requirement. The ratio of Tier 2 to commercial power capacity is roughly 25% for a single tier strategy (with nonuranium fuel); this can be reduced to ~15% with limited recycle of all TRU, or as low as ~6% with complete recycle of plutonium in the LWR. Despite the significant reduction in transuranic (TRU) production rates in the Tier 1 deep burnup options, the inventory of the problematic minor actinides continues to increase; this implies that the most limiting repository parameters (e.g., long-term heat load and dose) have not been improved by the Tier 1 campaign. Furthermore, the high concentration of minor actinides leads to several adverse impacts on the Tier 2 fuel cycle. The radiation sources for the second tier are nearly an order of magnitude higher for these minor actinide rich compositions.

An alternative approach to reduce the fast system Tier 2 capacity is to enhance the net TRU consumption by removing fertile material. Fast burner reactor designs were adapted for this purpose to assess the feasibility and performance at very low conversion ratio. For the postulated approach, a fuel enrichment of 50% TRU/HM is required for CR~0.25, and 100% TRU/HM for CR~0. Safety analysis results indicate that the low conversion burner designs exhibit favorable passive transient behavior even for beyond design basis (double fault) accidents. In addition, accelerator-driven fast spectrum systems using nonuranium fuel (CR=0) were evaluated and tailored for the consumption of minor actinides resulting from the deep burnup scenarios.

Based on the totality of the systems studies results and comparison to previous international and domestic transmutation studies, three favorable transmutation strategies were identified:

1. Single tier system with a low conversion ratio fast spectrum transmuter.
2. Double tier system with repeated recycle of plutonium (or Pu+Np) in Tier 1 LWRs with a complementary Tier 2 low conversion ratio minor actinide burner.
3. Double tier system with limited recycle of mixed TRU in Tier 1 LWRs with a complementary Tier 2 low conversion ratio fast spectrum transmuter.

The single tier fast spectrum strategy mitigates the generation of additional higher actinides with their associated fuel handling problems. However, the double tier options are attractive based on economic and timing considerations, with existing LWRs exploited to reduce the Tier 2 infrastructure costs. The choice between the Pu and TRU recycle options hinges on policy decisions regarding reprocessing technology and plutonium separation. Repeated recycle of plutonium (or Pu+Np) is better for LWR performance, but may raise proliferation concerns.

In conclusion, double tier transmutation strategies with limited or full recycle of TRUs in thermal spectrum LWRs offer the promise of rapid deployment and reduced dedicated (fast spectrum system) infrastructure. However, this approach will magnify the generation of higher actinides, which are difficult to handle and complicate repository design. Results are promising for LWR multi-recycle of plutonium; however, full TRU recycle will be limited by practical considerations. To truly eliminate TRU wastes, a complementary second tier fast spectrum transmutation system must also be deployed to consume the remaining minor actinides; and it is suspected that this final step is necessary to achieve the desired repository benefits.

Fuel Cycle Analyses

A spent fuel transmutation campaign based solely on mono-recycling of plutonium separated from spent UO_2 in commercial-sector LWRs partially loaded with MOX assemblies was considered. The evaluation assumed a commercial nuclear sector capacity of 300 GWth, with the first loading of 1/3 MOX-fueled cores in 2015, allowing 12 years for the construction of fuel processing and MOX fabrication plants in the U. S. Predictions of the size of the Pu stockpile over the next 100 years are compared in Figure 3-1 for continuation of the once-through fuel cycle and if MOX fuel is utilized in a variable number of reactor units. Of the 109 currently licensed units in the U. S., 35 are of the type (Westinghouse 17x17 or Combustion Engineering System 80 designs) most likely to receive licensing for MOX irradiation.[1] Assuming the fuel cycle conditions outlined above, the annual rate of Pu discharge from UO_2 assemblies can be balanced with the annual rate of Pu charged to MOX assemblies if 41 units receive licenses for MOX deployment; this is a true mono-recycling scenario. Results are also provided for the optimistic scenario of utilizing all currently licensed units (109) for Pu recycle.

Based on the fuel cycle conditions outlined above, the stockpile grows at the rate of ~20 MT/year without Pu recycling. If 35 or 41 units are licensed for MOX deployment beginning in 2015 (1/3 core loading), the stockpile growth rate slows to 13 or 12 MTPu/year, respectively; the corresponding Pu stockpile reductions in 2100 are 27% and 31%. In the optimistic scenario of all currently licensed units burning MOX, there is a short-term reduction of the Pu stockpile at the rate of ~4 MT/year. However, the Pu discharge rate from UO_2 assemblies burned to 50 GWd/MT is 15.2 MT/year, while 53.8 MT/year must be charged to the MOX assemblies. The imbalance of 38.6 MT/year could be drawn from the existing stockpile, but this requires additional LWR spent fuel processing capacity beyond the 2,000 MT/year rate required to service the current fleet. Furthermore, the supply of un-recycled Pu is exhausted in ~35 years after the recycling campaign begins; thus, the mono-recycling was scaled back to 41 units beginning in 2050. In this case, the Pu stockpile in 2100 is roughly half the inventory if no recycling were practiced. However, the inventory of minor actinides (MA) in 2100, which are important for the intermediate and long-term decay heat and repository dose release, would be nearly 40% *higher* compared with the once-through fuel cycle.

[1] H. R. Trellue and J. W. Davidson, Feasibility of Using Light Water Reactors to Transmute Spent Nuclear Fuel, Los Alamos National Laboratory, LAUR015692.

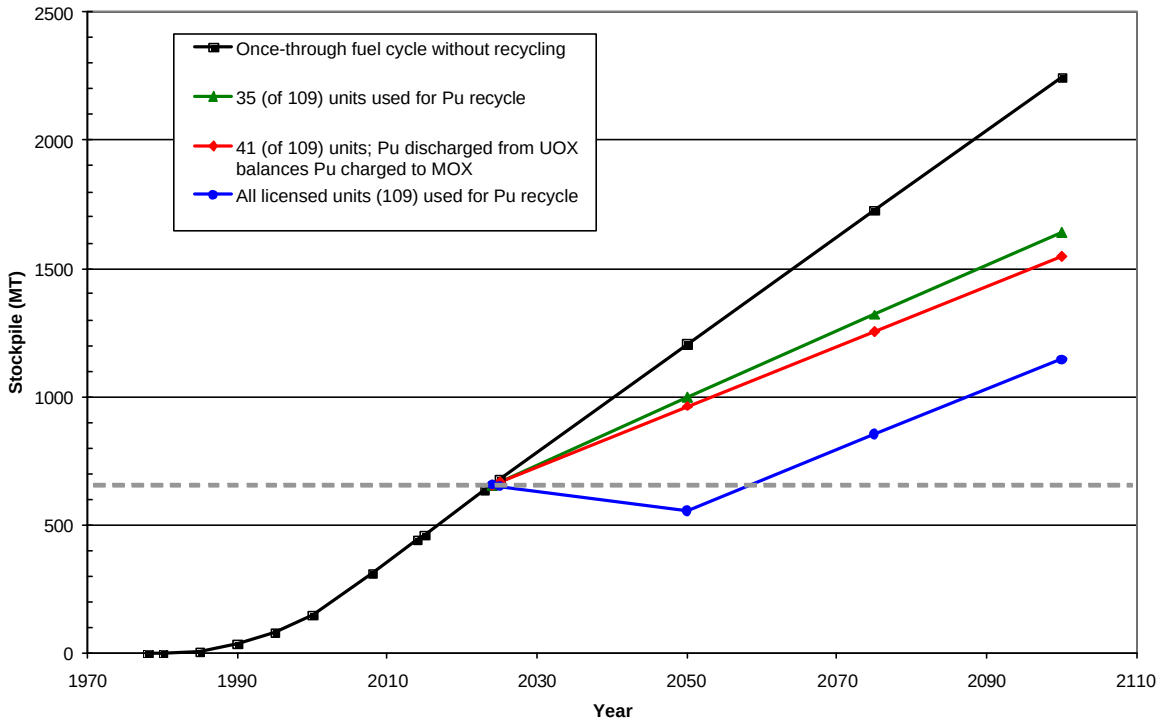

Figure 3-1. Plutonium Stockpile with Pu Recycling in 1/3 MOX Cores.

The impact of longer cooling time before spent fuel disposal and variations in the LWR spent fuel burnup was also evaluated. Due to the rapid cooling of the fission products in spent fuel, delaying placement by 15 years reduces the short-term decay heat in 2100 by ~25%. Delayed placement of the actinides does not reduce the minor actinide (MA) inventory; thus, the long-term heat load is not reduced. However, a modest reduction (roughly 6%) in the intermediate-term actinide heat load is observed.

Figure 3-22 projects the integrated MA stockpile derived from spent UO_2 fuel processing and spent MOX fuel (which is not reprocessed in the mono-recycling campaign) with MOX assemblies in the mono-recycling campaign fabricated from 10- and 25-year cooled Pu. Delaying the processing of the spent UO_2 causes a *25% increase in the amount of MA in the processing waste stream* due to the additional decay of Pu-241 to Am-241 ($t_{1/2}$=14.4 years). Furthermore, the fissile content of the Pu used for MOX fuel is reduced to 63%, requiring a slightly higher assembly average loading (9.6% Pu/HM). Consequently, the discharge rate of MA+Pu-241 (which eventually decays into Am-241) from the MOX assemblies is 3.3% higher when processing is delayed. The net result is a 12.3% increase in the MA stockpile in 2100, which would yield a corresponding increase in their long-term heat load.

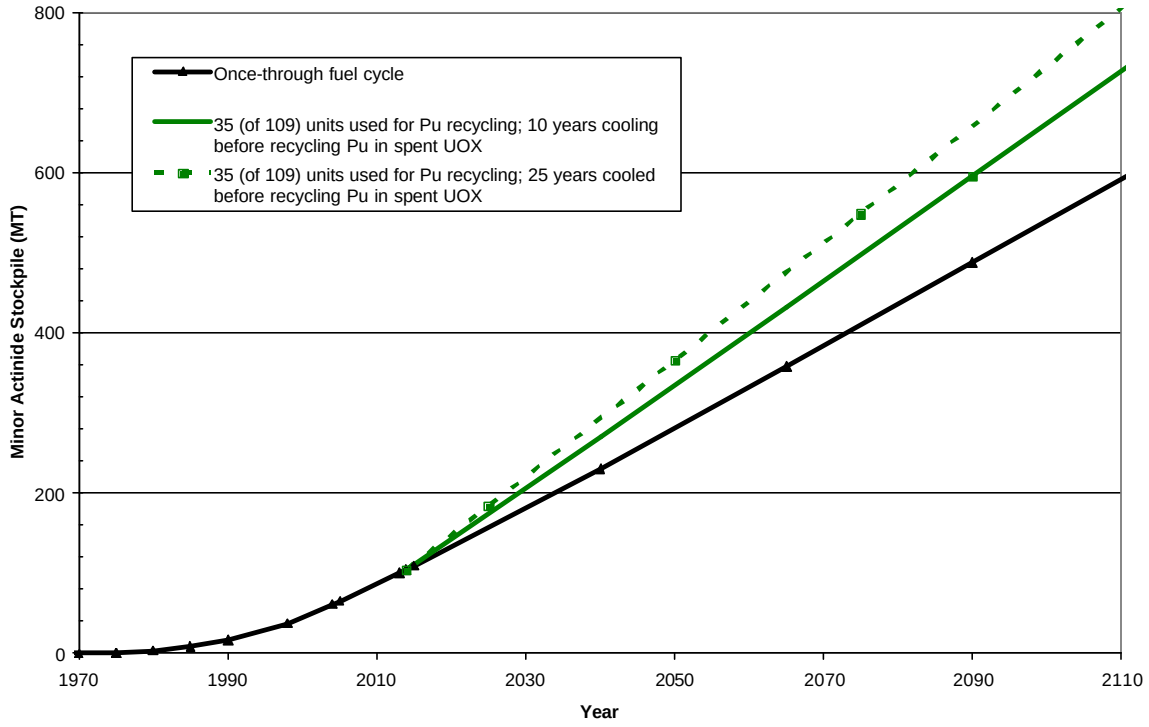

Figure 3-2. Minor Actinide Stockpile with Pu Mono-Recycling in 1/3 MOX Cores.

Repository Benefit Analyses

Work has been initiated to analyze the impact of various fuel cycle options on repository performance. Detailed comparisons were made between the 35-isotope simplified model (SM) obtained from Golder Associates and the total system performance assessment (TSPA) model used for Yucca Mountain site recommendation (SR) analysis. Interest in using the SM for the fuel cycle analysis is driven by the fact that the model is much faster running and less resource intensive than the SR model.

The release rates for Tc-99 and I-129 between the SM and the SR model agree very well. However, Np-237 release rates in the initial results were lower in the SM model by a factor of 3-4. This discrepancy was traced to a lack of modeling the decay of Am-241 to Np-237 in the SM. When this deficiency was corrected, the agreement between the SM and the SR model for the release of Np-237 is nearly as good as in the case of Tc-99 and I-129 results. Plutonium release rates from the EBS agree fairly well between the SM and the SR model, but agreement in the release rates at the unsaturated and saturated zones is not as good; adjusting the partition coefficients for plutonium might fix this problem.

Uranium release rates were also lower in the SM than in the SR model. For the peak release rate, occurring between 100,000 and 300,000 years, the discrepancy was nearly a factor of 3, but was much smaller by 1,000,000 years. Previous work on the SR model indicated a sensitivity to uranium solubility; this discrepancy can probably be eliminated or substantially mitigated by increasing the uranium solubility in the waste packages and in the invert. Since the SM and the SR model use the same correlation for uranium solubility, the real source of the discrepancy is in the pH, temperature, and/or concentrations of carbon dioxide.

The simplified model was used to evaluate the impact of removal of 99% of the actinides and actinide daughters from various waste forms in the Yucca Mountain Repository. In an initial case, actinides and actinide daughters were removed from all waste forms. This resulted in reduction of the peak mean dose rate by a factor of 63, a result consistent with previous estimates based on the site recommendation model. In a second case, actinides and daughters were removed only from commercial spent nuclear fuel. This resulted in a reduction in the mean peak dose rate by a factor of 11. If the actinides and actinide daughters are removed only from defense high-level waste glass or DOE spent nuclear fuel, the reduction in the mean peak dose rate is less than 2.5%.

Work was also initiated to create a representative SINDA thermal model for the repository. A variable mesh-size node structure was created for the repository cross section, so that transient thermal behavior in the repository both near and far from heat-generating waste packages can be analyzed using a single comprehensive thermal model. Smaller nodes in the neighborhood of drifts reflect the need for analyses to capture transient thermal behavior of relatively short duration. Larger nodes are adequate for describing the much more slowly varying temperature fields in regions far away from drifts. Nodalization in the vertical direction also reflects averaged locations of rock strata with different morphologies and thermal properties; this thermal model neglects a slight slope of the rock strata.

Proliferation Resistance Studies

An updated report with the pyroprocess facility layout and the process flows was prepared. The document was provided to LANL to establish safeguards options. Bounding compositions (one with weapons-grade plutonium make up and another with make up actinides coming from a twice-through MOX recycle in LWRs, which in equilibrium results in a high concentration of Cm) were developed and incorporated in the flow sheets. Although several flow sheet options have been studied, the baseline flow sheet includes a two-step electrolysis. The baseline layout of the facility is shown in Figure 3-3.

LANL prepared several safeguards approaches on the baseline facility. The choices were thoroughly described and discussed during a meeting between ANL and LANL, held at LANL in November. Four different safeguards approaches were proposed and discussed. The implications of each option on the process and the operations of the facility were evaluated by ANL.

The preparation of an interim report documenting the safeguards approaches and the implications on the facility was initiated. LANL took the lead with preparing the description of the safeguards options and ANL contributed sections on the description of the material balance areas in the facility, the bounding cases based on make up material assumptions, and the impact of the safeguards option on operations and maintenance.

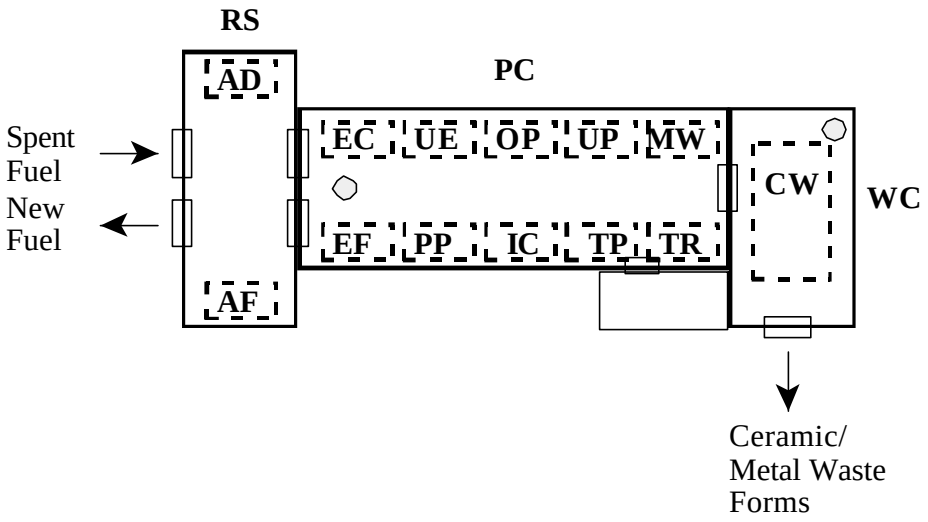

AD:	Assembly Diassembling	**IC:**	Injection Casting
EC:	Element Chopping	**PP:**	Pin Processing
UE:	Uranium Electrorefining	**EF:**	Element Fabrication
OP:	Oxidant Production	**AF:**	Assembly Fabrication
UP:	Uranium Product Processing	**MW:**	Metal Waste Processing
TR:	TRU/U Recovery	**CW:**	Ceramic Waste Processing
TP:	TRU/U Product Processing		

Figure 3-3. Process operations in a baseline advanced Fuel Cycle Facility.

At the request of NNSA (NA-241), the co-sponsor of this task, an abstract summarizing the project was submitted to the IAEA International Conference on Innovative Technologies for Nuclear Fuel Cycles and Nuclear Power, to be held in June 2003:

- J. Roglans, K. Budlong-Sylvester, K. M. Goff, Technology Demonstration of Proliferation Resistance for an Advanced Fuel Cycle Facility.

NFC Modeling in Full-Energy Sector Competition: MARKAL [LANL]

An AFCI-oriented Nuclear Fuel Cycle (NFC) model was implemented in a partial-equilibrium energy sector optimization model, MARKAL (MARKet ALlocation model). MARKAL evaluates options within the context of the entire energy/materials system by: balancing all supply and demand requirements, monitoring capital stock turnover, and adhering to environmental and policy restrictions. MARKAL then selects a time-dependent technology mix based on life-cycle costs of competing alternatives.

Past MARKAL NFC models were found to be outdated and to possess insufficient resolution of technologies. Hence, a present-day LWR fleet along with the possibility of construction of ALWRs capable of MOX multirecycle was implemented. See Fig. 3-1 for a schematic of this model.

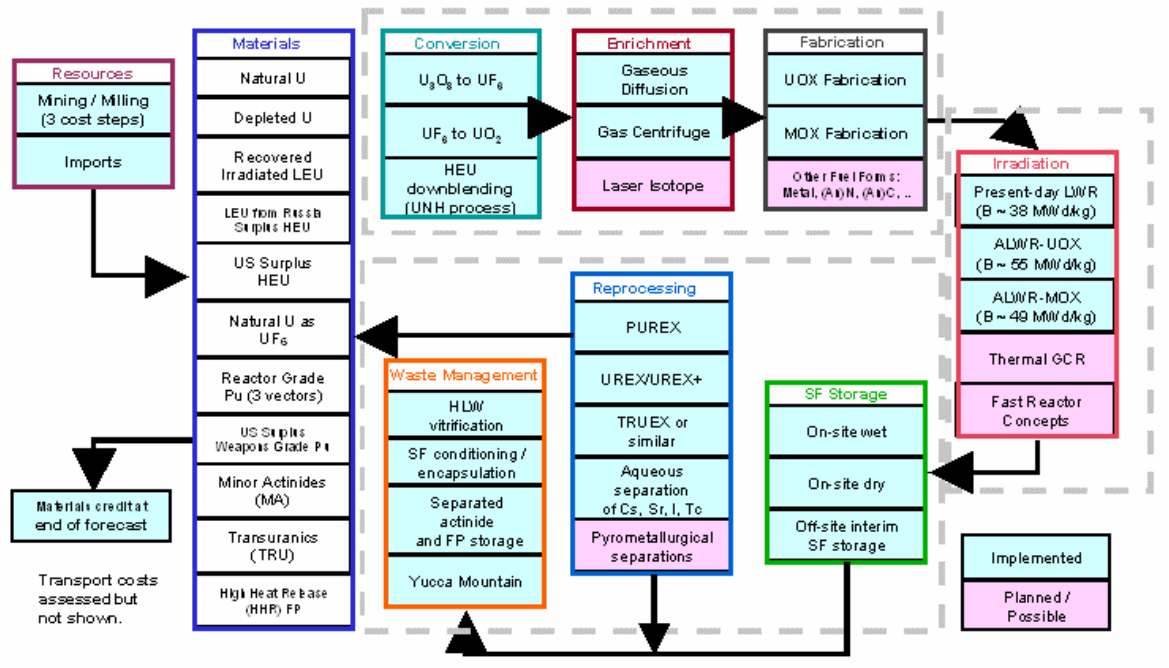

Figure 3-4. Technologies and Materials Implemented in MARKAL Model.

The forecasting period of the database extends to 2035. A reference case was run, with costs and availability dates obtained from US sources where available, and OECD/NEA or IAEA data otherwise. It was found that, under the reference cost database, nuclear would roughly retain its market share through 2035, with moderate ALWR penetration compensating for retirement of the current fleet; see the Fig. 3-5. By 2030, roughly 14% of nuclear generation would be derived from ALWRs, with half of these burning first-pass MOX. It should be noted that in this forecast ALWR penetration is essentially precluded, since certain variables -- perceived-risk barriers to entry, economy-of-scale issues associated with introduction of the new infrastructure – are not captured at this time. Hence, the forecast indicates that market-driven penetration of the ALWR-MOX fuel cycle in the US, highly sensitive to the assumed $1700/kWe capital cost, may be expected to proceed sluggishly at best.

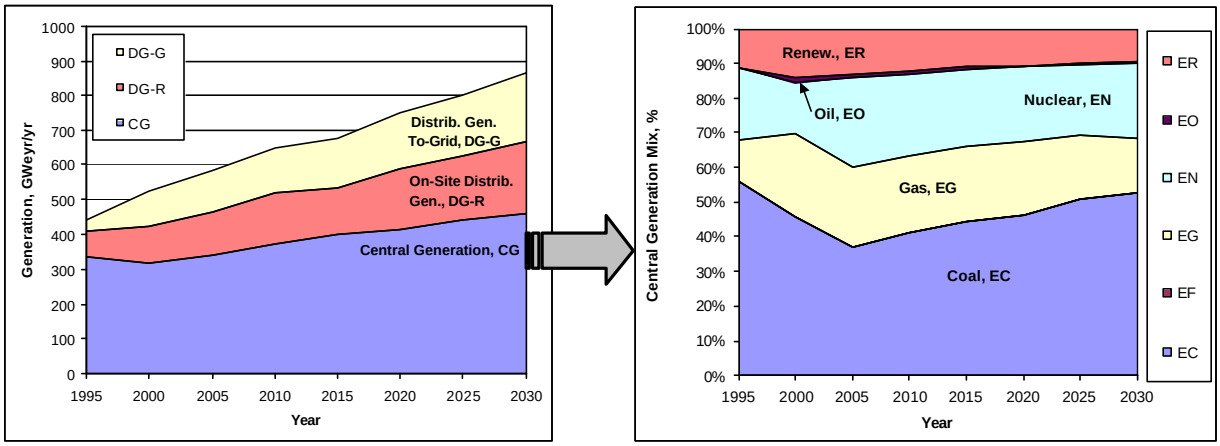

Figure 3-5. The US Generation MOX to 2030, Reference Case.

Financial Impact of Reprocessing Strategies upon the Repository

During FY02, a set of heat release based criteria – focusing upon short- and long-term heat load carried by the repository, as well as heat release and chemical limitations on vitrified glass packing density – was developed at Los Alamos. The relative merit of seven reprocessing scenarios, each leading to unique waste streams, was assessed based upon these criteria. See the Table 1 for a recapitulation of the scenarios.

Table 1. Summary Description of Seven Scenarios Based on Different Degrees of Activation and Fission-Product Removal

	Short Description	**Elaborated Description of Disposed Material Form**	**Presumed Advantage of Scenario**
I	Base Case	Direct disposal of SNF fuel assemblies	Base- or Point-of-Departure (POD) case: direct disposal of SNF fuel assemblies, including VFPs.
II	I – U(ranium)	Vitrified [MA + Pu + NVFP]	Reduce mass but must deal with full short- and long-term heat load, which establishes limits on the degree to which the volume of the waste form can be reduced.
III	II – {Cs,Sr}	Vitrified [MA + Pu + VLHR = LHR]	Reduce mass, as well as short-term heat load associated with HHRs, but with full (TRU = Pu + MA) long-term heat load and proliferation risk.
IV	III - Pu	Vitrified [1 - U - HHR - Pu = MA + VLHR = LHR]	Similar to *nsc = III*, with some reduction in long-term heat load through the removal of Pu (and reduced long-term proliferation risk).
V	II - Pu	Vitrified [1 - U - Pu = MA + NVFP]	Not unlike *nsc = II*, but with some reduction in long-term heat load resulting from Pu removal (and reduced long-term proliferation risk).
VI	V - MA	Vitrified [1 - U - Pu - MA = NVFP]	Reduce mass with full short-term heat load, but with significantly reduced long-term heat load.
VII	IV - MA	Vitrified [1 - U – HHR - Pu – MA = VLHR]	The best it gets; volume and mass reduction along with reductions in both short-term and long-term heat loads

MA = minor actinides Np,Cm, Am
VFP = volatile fission products
LHR = Low heat release radionuclides
TRU = MA + Pu
NVRP = non-volatile fission products
HHR = high heat release radionuclides
VLHR = very low heat release radionuclides

The cost assessment of these scenarios considered only those costs directly connected to the waste streams – namely, vitrification and Yucca Mountain (YM) disposal. Using heat load as the sole YM design criterion, these costs may be formulated based on a High Level Waste (HLW) unit vitrification cost of 300,000 $/m^3 and a Vitrified High Level Waste (VHLW) unit repository disposal cost of 332 $/kgSNF(equivalent) of YM capacity used. This condition

represents the $440/kg Life Cycle Cost (LCC) estimate minus the (avoided) YM cost component relating to spent fuel waste package fabrication. It was found that conditioning and disposal costs alone (reprocessing and storage costs are not included) indicate that a scheme must include removal of high heat-release fission products (Cs, Sr) to be economically worthwhile – scenarios II, V, and VI, for which the vitrification and disposal costs are similar to that of direct disposal -- may be ruled out on this basis. The impact on the NFC as a whole of the scenarios that survive this down select must still be assessed. It must be emphasized that the heat load limits used reflect the current YM design basis. Table 2 summarizes these results.

Table 2. Cost Comparison of Heat-Load Limited Disposal Scenarios

	Waste originating from 1 kgHM [kg waste]	**Unit vitrification cost [$/kg waste]**	**Unit emplacement/ disposal cost [$/kg waste]**	**Total [conditioning + disposal] [$/kgIHM]**	**'Effective' repository capacity [tonneIHM]**
I	1.00	N/A	440	440	83,800[(a)]
II	0.0516	3,231	6,436	498	83,800
III	0.0475	922	4,087	238	143,300
IV	0.0380	757	3,484	161	210,300
V	0.0420	3,686	7,052	451	93,900
VI	0.0407	3,323	6,274	390	108,900
VII	0.0366	480	897	50	846,400

[(a)] The DOE design basis.

Tier-0 Reactor Material Balances For NFCSim: ORIGENInterface

The ORIGENInterface capability is a criticality and burnup engine developed to provide life cycle material balances for a diverse and interacting reactor fleet. It couples with NFCSim; as such, it is designed to address nuclear economies in which a steady state is never obtained, or is a poor approximation. ORIGENInterface operates in transient and equilibrium fuel management regimes at the refueling batch level, derives reactor- and cycle-dependent initial fuel compositions, and invokes ORIGEN2.x to carry out burnup calculations.

ORIGENInterface implements a piecewise linear, reactor-specific reactivity model to perform criticality calculations. The model is piecewise linear since fluence-dependent neutron production and destruction rates are obtained from ORIGEN and tabulated at a resolution of ~ 2 n/kb. The model is reactor-specific because the non-fuel composition and geometry of each reactor may be uniquely specified.

To test the performance of the criticality engine, predicted enrichment and burnup histories for the startup transient of a French N-4 PWR with 1/4 of the core replaced upon refueling and equilibrium burnup 42.5 MWd/kg were compared to those found in the 1994 OECD Economics

of the Nuclear Fuel Cycle study. This acts as a check upon the model's estimate of interassembly power peaking as well, since the enrichment spread for the first core loading is selected based upon the criterion that the average power produced by the hottest or coldest assembly not deviate by greater than 50% from the average. Figure 3-6 illustrates this comparison; it can be seen that the model obtains a realistic initial enrichment spread and burnup history.

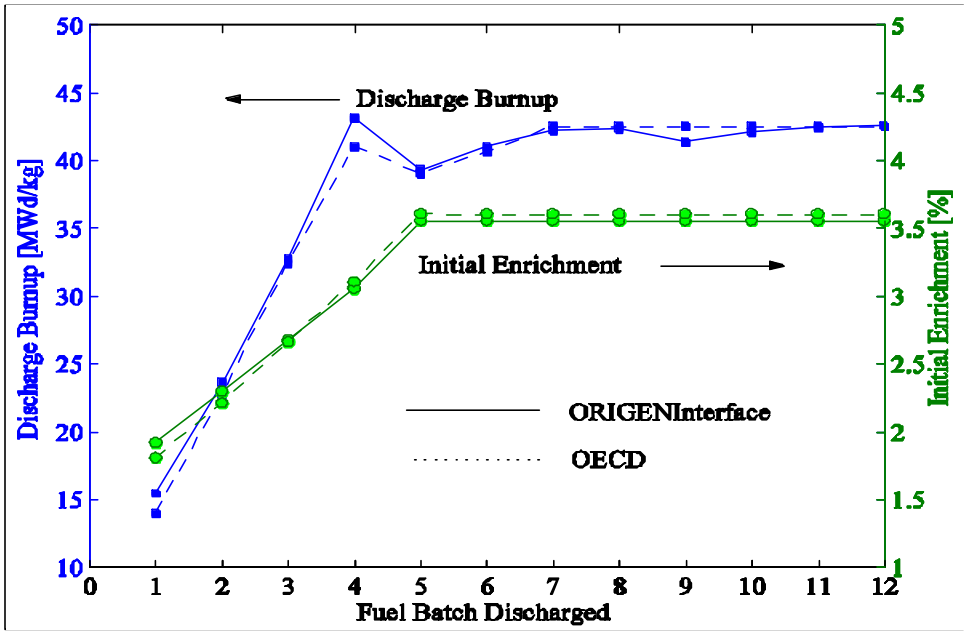

Figure 3-6. Burnup and Enrichment During a Startup Transient.

ORIGENInterface produces life-cycle material balances, providing composition data for each fuel batch at charge and discharge, as well as decay-induced compositional changes. Figure 3-7 shows enrichment-burnup pairs for each batch charged to a LWR with ~40 year lifetime. Burnup is incremented by 5% every 5 years.

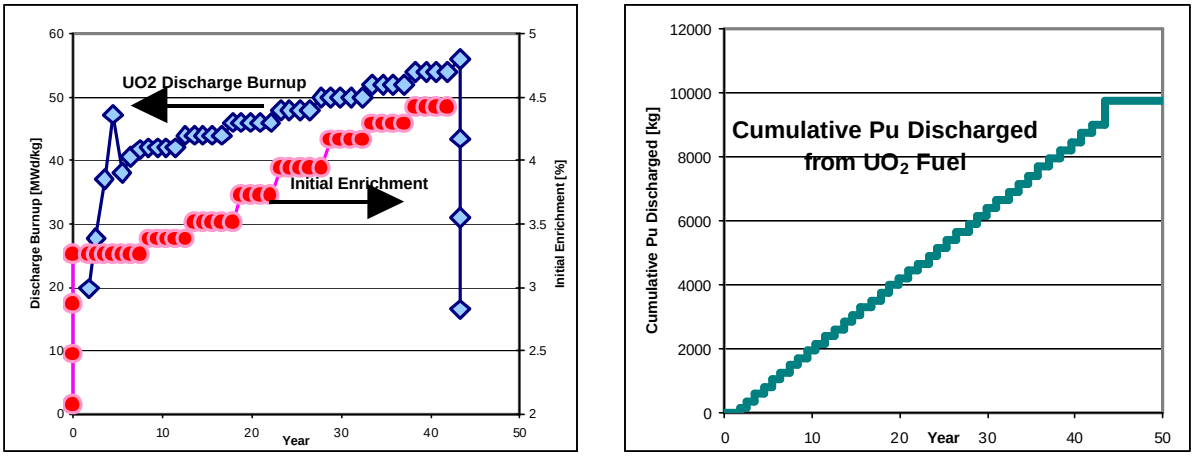

Figure 3-7. Sample Material Balance Data for a Tier-0 PWR.

Sample (Interim) Results from NFCSim Simulation Model

The purpose of this section is to convey the progress that has been made expanding NFCSim capabilities. The primary new capabilities are being able to couple with ORIGEN for fueling details and to model the "back end" of the fuel cycle. Consequently, only the results of a single NFCSim simulation are presented herein to illustrate these capabilities.

Coupling ORIGEN to NFCSim affords increased fidelity in modeling fuel requirements (*e.g.*, enrichment) and discharged fuel impact on separations, recycled fuel fabrication, and storage requirements. This coupling also permits simulation of the start up and shut down transients, which account for nearly 20% of discharged fuel. Figure 3-8 shows ORIGEN results for a representative Pressurized Water Reactor (PWR) and Boiling Water Reactor (BWR) that were used in an NFCSim simulation that starts with the present-day fleet of nuclear reactors.

Figure 3-9 shows results from an NFCSim simulation wherein an exogenous demand for nuclear power is met by installing new ALWRs with an equilibrium burnup of 45 MWt d/kg. The demand at time *t* is assumed to be of the form: $D(t) = P(t_0)[1+ growth]^{Y(t)}$, where $P(t_0)$ is the installed capacity at the time t_0 when the demand is first applied, *growth* is the rate at which demand changes, and $Y(t)= t - t_o$ is the real number of years since time t_0. In Fig. 3-9 the demand increases at 1% per annum beginning September 1, 2012. Small deviations of the installed capacity from the demand curve are observable for short periods of time. The reasons for these deviations are multifold. Inherent to the NFCSim model is the assumption that no response is instantaneous (*i.e.*, new capacity only appears after some delay for installation and/or other reasons). Consequently, NFCSim looks at the demand appropriately shifted into the future. Similarly, NFCSim projects the amount of installed capacity that will still be operating at the appropriate time in the future plus any capacity that has been ordered but not yet installed. The difference between the projected demand and the projected installed capacity yields the capacity deficit that needs to be ordered immediately to meet a future demand. Then NFCSim simulates ordering of the largest integer number of reactors that will not exceed the projected demand. Consequently, NFCSim will always slightly undershoot any demand curve. Nevertheless, these deviations from the demand curve are small compared to the instantaneous-power fluctuations, which can be as large as 30% of the installed capacity. The reactor capital costs dominate the annual charges, as is also shown in Fig. 3-9.

Although the cost of transporting nuclear material throughout the NFC is relatively inexpensive (*i.e.*, 50 $/kg), the transportation costs are nearly 2.3 B$ in 2000. This large transportation cost arises from the large masses that must be transported between the mine and the enrichment plant. The transportation cost starts to rise after 2012 primarily because of the transport of uranium before enrichment occurs that is associated with the fueling requirements of the new ALWRs being brought online [*i.e.*, a new reactor must load an entire core, whereas a running reactor only refuels part (1/3) of a core].

The repository cost ramps up starting in 2010, as expected, but sharply drops in 2042 when repository shipments finally eliminate the backlog of SNF that is older than seven years and sitting in cooling storage. The annual enrichment, mining and milling, fuel fabrication, and conversion costs are small compared to the other costs.

The SNF waste generated by all reactors, also plotted in Fig. 3-9, increases nearly linearly, and reaches a maximum of 146,000 metric tonnes in 2050. The mass in cooling storage appears to bottom out in 2042, because the backlog of SNF in cooling storage that is seven years old or older has been eliminated and the demand growth is small.

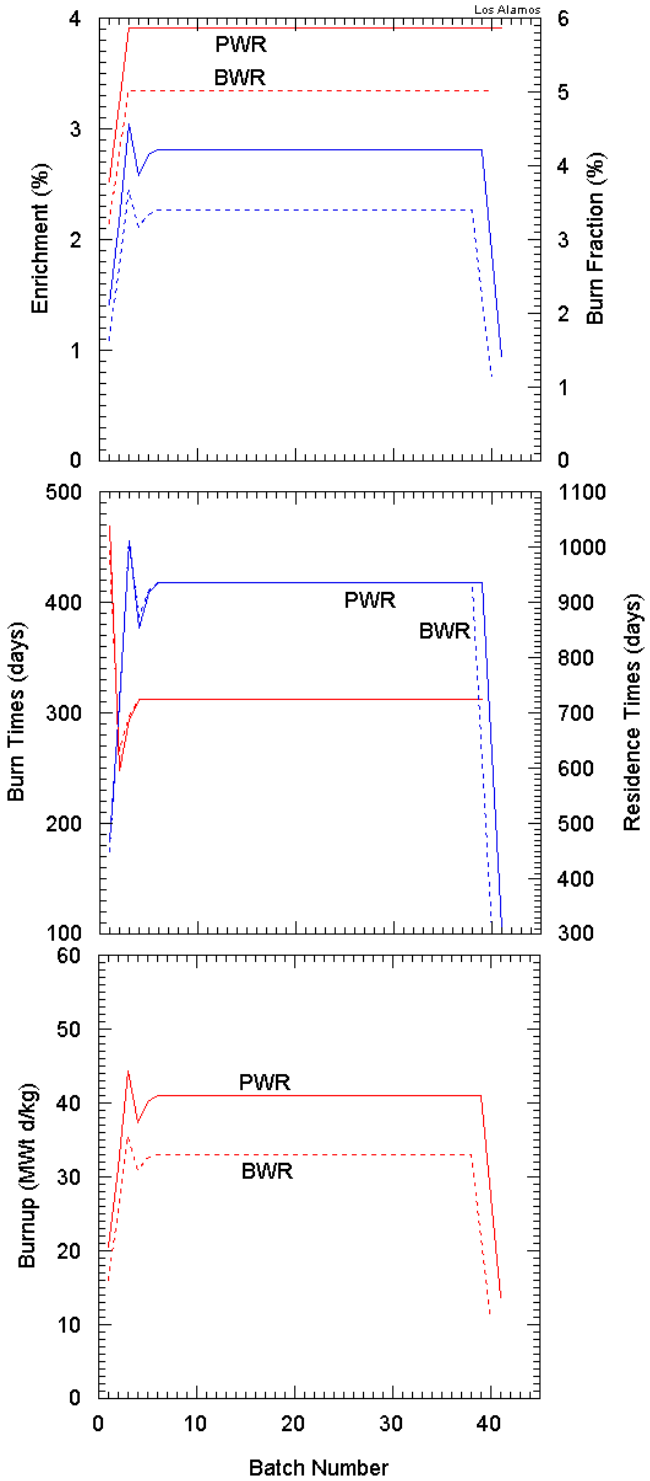

Figure 3-8. The enrichment, burn fraction, (power) burn times, (fuel) residence times, and burnup are shown for a BWR (dashed line) and PWR (solid line) as a function of the reactor fuel charge.

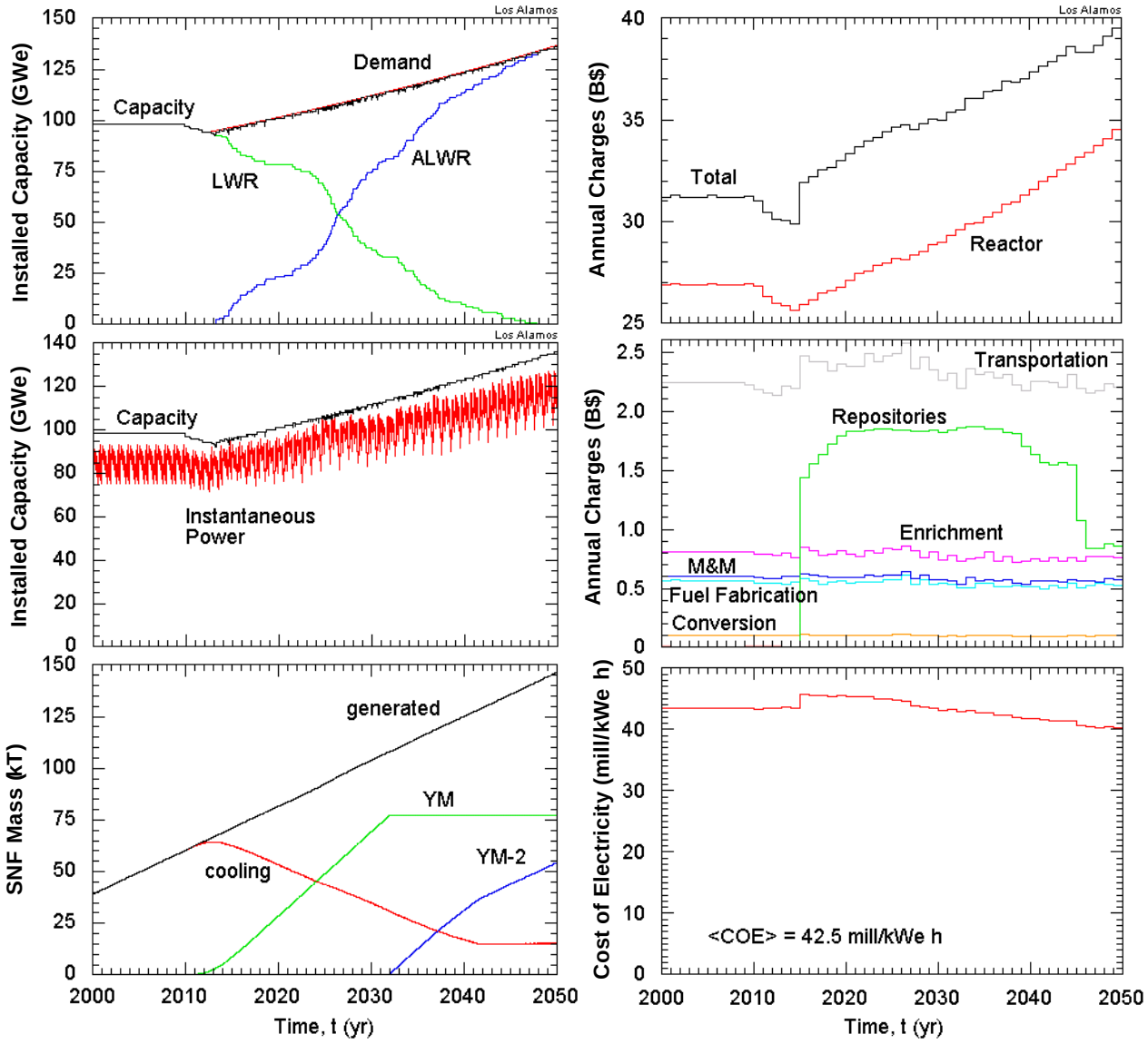

Figure 3-9. The installed capacity, exogenous demand, and reactor mix are plotted as a function of time in the lower right. The mass of SNF generated, stored in cooling ponds, and interred in Yucca Mountain and a second repository are shown in the lower right. The annual charges and cost of electricity are shown on the right.

The instantaneous, undiscounted *COE* is approximately constant over the 50-yr simulation period. The constancy of the *COE* is the result of the annual charges being dominated by the reactor cost, which also track the energy production (*COE* is the ratio of cost to energy production). A discounted *COE* for the 50-yr simulation period is 42.5 mill/kWeh, in agreement with other Los Alamos' models for the same period.

Neutronics Supporting Calculations

Calculations were performed using the Monteburns code to estimate the mass flows of multiple recycling of Pu in light water reactors (LWR). The calculations assumed full MOX core configuration with conventional fuel assemblies (as opposed to CORAIL or APA fuel assemblies). To maintain the safety margins, up to 12 water rods were substituted for fuel rods in each assembly. A fixed number of reactors were specified to be MOX burners and was balanced

such that these reactors would consume 'legacy' spent fuel until that was used up and then they would accept the Pu from a fleet of UO_2 fueled LWRs.

It was necessary to blend "fresh" Pu from spent nuclear fuel with each batch of recycled fuel to keep the in order to maintain a fixed number of MOX-fueled LWR's. Otherwise, the decreasing fissile content of the fuel would necessitate reducing the number of reactors as the number of recycling passes increased.

To estimate the impact of higher residual heat and radioactivity from spent MOX, the cooling time was increased to 7 years, at which point the MOX has about the same activity as extended burnup UO_2 fuel.

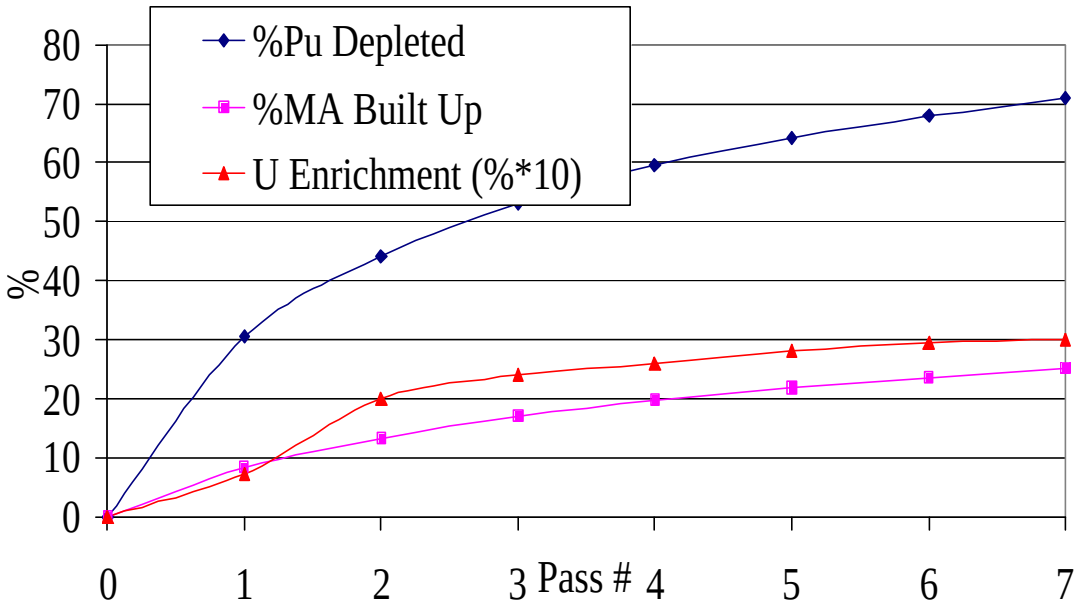

Figure 3-10. The total Pu depleted, the MA buildup, and enrichment required for the uranium diluent in the MOX as a function of the number of recycles.

The Figure 3-10 shows the impact that multiple recycles have on a) total Pu depleted, b) minor actinide (MA) buildup and c) the uranium enrichment required to blend with the MOX for a proper fuel loading. It can be seen that >50% of the Pu can be consumer within three passes with about 1/3 of the Pu converted to MA. The uranium enrichment remains below 5 w% even up to 7 recycles. After three recycles of the Pu, there are diminishing returns on the amount of Pu that is consumed.

4 FUELS DEVELOPMENT

The AFCI fuels development effort will provide proliferation-resistant fuels for use in advanced fuel cycles for both our current light water reactors (LWRs) or advanced light-water reactors (ALWR) (Series One) and for the next generation of nuclear power and transmutation systems (Series Two).

Series One focuses on developing LWR recycle fuels. The objective is to develop proliferation-resistant Plutonium and Uranium Oxide fuels with additional contaminants for use in LWRs. This fuel is referred to as the proliferation-resistant LWR fuel. The Series One fuels and separations technology will provide the means to significantly reduce the quantity of high-level waste materials that must be stored in the repository. Additional irradiation in the LWRs will reduce the plutonium inventory in the spent fuel.

Series Two will develop advanced fuels for use in both Generation IV power systems and in transmutation systems that can be deployed by 2030. Series Two fuels and separations will be designed to maximize transmutation performance and significantly reduce the toxicity, long term-decay heat in the repository and longevity of materials stored in the repository. Depending upon the fuel cycle deployment scenarios, Series Two fuel development addresses fertile-free fuels (accelerator driven systems and fast reactors with inhomogeneous core), low-fertile fuels (fast-reactors with low conversion ratio), fertile-rich fuels with high-burnup (for Generation IV reactors after achieving an equilibrium fuel-cycle including thermal and high-conversion ratio fast reactors).

Detailed descriptions of the scope, short and long-term objectives, goals and schedules for the AFCI fuel development program are provided in the AFCI Program Plan and the reader is referred to this document for additional background information. General questions regarding the fuel development program should be addressed to the National Technical Director (NTD) Kemal Pasamehmetoglu at kop@lanl.gov .

The FY03 quarterly progress for the fuels development activities during the first quarter (October 1st through December 31st 2002) is presented in this section for the following technical categories of activities:

- Integration of Fuel Development Activities
- Series One Fuels Design, Specifications and Analyses
- Series One Fuel Fabrication
- Series One ATR Irradiation Experiments
- Series Two Fuel Design Specification and Analyses
- Series Two Nitride Fuel Development
- Series Two Metallic Fuel Development
- Series Two TRISO Fuel Development
- Series Two Advanced Fuel Forms
- Series Two ATR Irradiation

- Series Two FUTURIX Irradiation
- ATR Fast Flux Booster Design

4.1 Integration of the Fuel Development Activities

The AFCI fuel development is a National effort with participation by multiple institutions and it is lead by a National Technical Director (NTD). The NTDs responsibility is to implement the five-year program plan which includes integrating the efforts over the various institutions, interfacing with the DOE fuels manager and the AFCI Technical Integrator and interfacing with the other elements of the AFCI (Systems, Separations, and Transmutation).

4.1.1 Integration Objectives

The FY03 objectives for the integration activities performed by the NTD are as follows:

- Coordinate and provide technical leadership to all the fuel development activities within the AFCI program, including the International collaboration activities;
- Provide fuels input to the 5-year program plan prepared and maintained by the Technical integrator and update as requested;
- Coordinate and compile the fuels section of the monthly and quarterly reports;
- Coordinate the planning and work-package development for the fuels activities for FY03 and FY04;
- Participate in International Collaboration development activities in support of the DOE staff (specifically, establish an international agreement with Switzerland on advanced dispersion fuels)
- Participate in program-wide meetings and, as necessary, working group meetings of other program elements (Systems, Separations, Transmutation, Generation IV) to assure timely flow of technical information within the program:
- Provide technical and programmatic presentations on behalf of the AFCI program in internal and external review meetings;
- Form a fuel development working group (FDWG), chair the working group meetings and publish the meeting minutes within a month following the meetings;
- Provide assistance to DOE-NE AFCI and fuel managers in resolving technical issues as they emerge within the program.

4.1.2 Integration Highlights

The following are the major highlights of the Integration activities:

- Fuels input for the final DRAFT of the five-year program plan was completed and submitted to AFCI Technical Integrator.
- Fuel development working group was formed after DOE approval of the charter.

4.1.3 Integration Activities Summary

In the area of Integration, the following are the major first quarter activities:

- AFCI Five-Year Program Plan Development;
- Formation of the FDWG;
- NERAC Transmutation sub-committee review of the AFCI program; and
- OECD/NEA Meeting on Future Needs for Nuclear Energy Research.

For additional information on these activities, contact Kemal Pasamehmetoglu at kop@lanl.gov

AFCI Five-Year Program Plan Development. For the AFCI, the five-year development plan for the Series One and Series Two transmutation fuels was drafted and submitted to the Technical Integrator (TI). The plan includes the high-level program objectives, FY03 and five-year milestones, five-year budget estimates and FY03 funding distribution among various tasks and institutions.

Formation of the FDWG. The charter for the FDWG was drafted by the Fuel Development NTD and approved by DOE. The FDWG is currently comprised of technical representatives from ANL, BNL, GA, INEEL, LANL, ORNL, WSRC. It is chaired by the Fuel Development NTD. Other AFCI NTDs, the TI and the DOE program managers and technical leads also are included in the working group meetings as observers. The FDWG is responsible for specific milestones that require inter-institutional integration. The first FDWG meeting is scheduled in January 2003 coincident with the AFCI semi-annual review meeting.

NERAC Transmutation sub-committee review of the AFCI program. The transmutation subcommittee ("Richter committee") of the Nuclear Energy Research Advisory Committee (NERAC) met in Washington, D.C. on December 20-21, 2002 to review the AFCI program plan. The Fuel development NTD presented the Five-Year Program Plan for the Fuel Development and the Recent Accomplishments in the area of transmutation fuel research. The presentations were well received and the questions centered primarily on programmatic issues.

OECD/NEA Meeting on Future Needs for Nuclear Energy Research. The Fuel Development NTD attended the OECD/NEA meeting on the R&D Needs for the Current and Future Nuclear Systems, held in Paris, France on November 6-8, 2003. The NTD presented the AFCI program plan. Noteworthy were the national program presentations made by the French representative (with emphasis on gas-cooled reactors) and by the Japanese representative (with emphasis on accelerator driven systems and the proposed test facility). The NTD also attended the group meeting on the needs of fuels and materials research. Because of the very general nature of the discussions, it was very difficult to identify any specific research needs that are of interest to AFCI program, outside those that are already included in various roadmaps and program plans.

4.2 Series One Fuels Design, Specifications and Analyses

The fuel requirements are developed in close coordination with the National Technical Director for System Analysis on implementation scenarios, system point designs for LWRs/ALWRs, and licensability studies. Industry and NRC interactions, which are essential in developing the requirements, will be conducted under this activity. A NERAC ANTT Blue Ribbon Panel will make recommendations on the fuel proliferation resistance requirements, which will also be incorporated into the fuel design and specifications.

In addition, analyses of LWR/ALWR cores establish required operating conditions for the proliferation-resistant fuel. Fuel pellet specifications and requirements flow down from these analyses. Parametric analyses of irradiated fuel performance guides the development of irradiation test matrices. The results of all fuel tests are used to validate phenomenology in the fuel model. This activity will provide the final fuel pellet design specifications, a data package that documents fuel performance, and an experimentally validated fuel performance model. In the long term, the validated models developed by this activity will become the tools for performing fuel safety analyses required by the licensing process.

The major milestone for this activity is the completion of the fuel specifications and final performance data package by the end of FY 2007. Interim milestones include:

Develop initial set of fuel specifications.	FY 2003
Develop testing requirements and specifications.	FY 2004
Prepare initial LWR licensing and operational requirements.	FY 2004
Initiate fuel performance modeling and validation.	FY 2004
Develop interim set of fuel specifications to be used for loop tests in ATR (LWR-2).	FY 2005
Complete fuel safety modeling.	FY 2006

4.2.1 Series One Fuels Design, Specifications and Analyses Objective and Scope

This activity consists of defining the fuel specifications, which include performance modeling and data validation. This activity leads to final fuel design specifications by FY 2007 to support fuel technology selection. Derivation of the licensability requirements based on the associated systems studies and interactions with private industry and NRC are also performed for this activity.

In FY 2003, the LWR Fuel Design and Specifications Activity will emphasize the preparation of the detailed fuel development plan, initiation of the modeling and analyses activities, and establishing the proper internal and external interfaces required for future fuel licensing and use.

The major FY 2003 milestones include:

- Develop initial set of fuel specifications.
- Complete initial revision of five-year Series One fuel development plan.

- Procure TRANSURANUS code (a Belgian U/Pu MOX fuel performance model) and make the necessary modifications
- Perform initial analysis of fuel irradiation performance.
- Parametric studies that assist with the identification of objectives for the irradiation test program

4.2.2 Series One Fuels Design, Specifications and Analyses Highlights

During the continuing resolution, the first quarter progress in this activity was slow and the following is the major highlight:

- A presentation was made to the Blue Ribbon Panel for the definition of the proliferation resistant mixed oxide fuel for Series One.

4.2.3 Series One Fuels Design, Specifications and Analyses Technical Summary

As part of the fuel design and specifications activities, Ken Chidester (kchidester@lanl.gov) made a briefing to the Blue Ribbon Panel on Proliferation Resistant Characteristics of Recycle Fuels on the subject of "Fabrication and Anticipated In-Reactor Performance of LWR (Series One) recycle Fuel". A summary of this briefing is provided below. Because of the funding rates during the continuing resolution, the activities in other sites (ORNL, INEEL and WSRC) did not start in the first quarter and are expected that the efforts will pick up in the second quarter.

Studying the safeguards and dose issues related to the use of plutonium and uranium oxide fuel for LWRs is a good way to understand the potential effects of any actinide or other material additive might have on oxide fuel manufacturing, transportation, handling at the reactor site, storage, and recycling. The process steps for a proliferation resistant fuel will be very similar to the current MOX manufacturing now practiced in Europe with changes due increased dose and minor changes in process parameters (see Fig. 5-1 for typical MOX process flow diagram). Development and testing of recycle fuel using plutonium recovered from spent nuclear fuel began in the 1950s and continued in the US until the late 1970s. In Europe the development of plutonium and uranium oxide (MOX) fuel continued and today is used in commercial LWRs along with the standard uranium oxide fuel. Typically, commercial MOX fuel contains up to 7% plutonium and 97% depleted uranium oxide. The plutonium isotopic content will vary depending on the burnup and time since separation but it can contain up to 1.5 % ^{238}Pu and up to 1.5 % ^{241}Am.

The designs of MOX plants are usually based on ^{241} Am under 3% and ^{238} Pu values under 2 %. At these levels all the operational steps are designed to be done in shielded gloveboxes and run remotely through automation and centralized control. Typically, each process step is unique to one or a group of gloveboxes. Seldom does one glovebox contain more than one process step. This means that the fuel material is transferred and accounted for between each process step, (see Fig. 5-2). Process losses have to be accounted for immediately and loose powder and dust must be constantly cleaned up for both accountability and worker dose control. The glove ports are set up on each glovebox to enable maintenance of the operating equipment and replacement of wore parts as needed. The dose to workers is minimized for operations personnel but increased for maintenance personnel. The air supply and ventilation systems are designed to keep the risk to the workers and public well below the permit limits. The addition of any new material which

potentially increases the worker dose will have to be thoroughly analyzed for impacts on dose to workers in the fuel processing plant, potential impacts on licensing of the manufacturing plant, shipping, handling at the reactor site, spent fuel storage, shipping, and finally impacts on recycling.

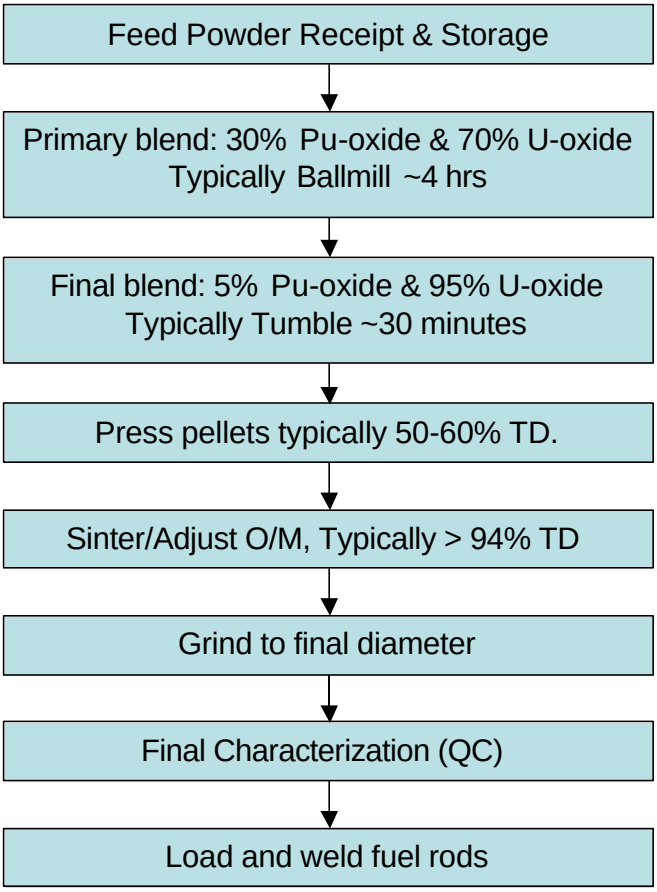

Figure 4-1. MOX Preparation Flow Diagram for LWRs

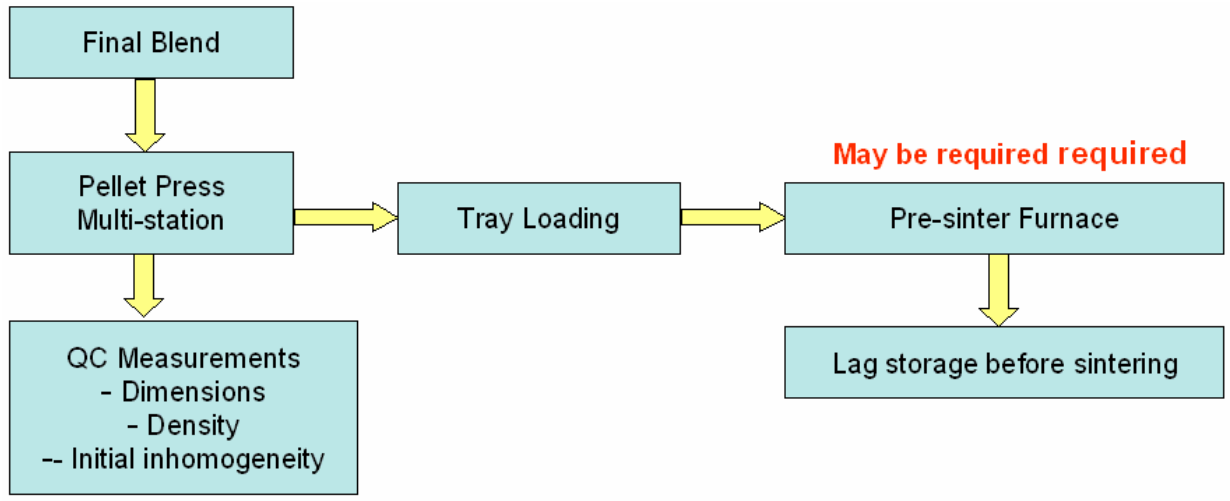

Figure 4-2. Example of some MOX process steps and transfers required.

The potential impact on worker dose can be seen from some anecdotal information gathered during the processing of fuel with americium added, see Table 1. Table 1 shows three area classifications and the relative dose levels defined for each. A glovebox was able to have ~2 kgs of plutonium (^{239} Pu) as oxide and nitride processed/or stored in it and still be considered a buffer area. However when 25 grams of americium as oxide was brought into the glovebox the dose level greatly increased during processing and the box temporarily became a high RAD area.

1. Table – Americium effect on RAD control (anecdotal)

Buffer Area	RAD Area	High RAD Area
Dose < 5 mrem ~ 2 kgs Pu-239	5 < Dose < 100 mrem	100 < Dose < 500 mrem w 25g Am in box ~ 2.5g dispersed (~5g/ batch)

Actinide additives will also impact in-reactor performance. The addition of americium will likely increase helium production under irradiation and therefore potentially impact swelling and fission gas release. Adding actinides like neptunium will likely increase ^{238}Pu production and other higher actinides. There are many options for potentially increasing proliferation resistance but impacts on manufacturing, shipping, handling, and performance have to be heavily considered in the final analysis.

4.3 Series One Fuel Fabrication

Using small-scale fabrication equipment in the LANL TA-55 facility, the test fuels will be characterized, fabricated, and supplied to ATR for irradiation testing. The first two years focus on developing and confirming modifications to commercial fabrication processes to enable the fuel to meet the fuel design specifications. From 2005 to 2007, the activity focuses on optimization of the fabrication process to define process specifications by 2007, supply of fuel from irradiation testing and supporting design requirements for the LTA, and fuel fabrication plant preconceptual design activities.

The major milestone for this activity is the completion of the final fuel fabrication process definition by the end of FY 2007. The interim milestones include:

- Supply fuel pellets, characterization data and test capsules for the initial irradiation tests in ATR (initial part of LWR-1).
- Supply fuel pellets, characterization data, and test capsules for the remaining LWR-1 tests in ATR.
- Supply fuel pellets, characterization data and test capsules for LWR-2 loop tests to be performed in an ATR pressurized loop.
- Supply fuel pellets, characterization data and test capsules for transient tests (safety tests).

4.3.1 Series One Fuel Fabrication Objectives and Scope

In FY 2003, the Fuel Fabrication activities focus on process development and fabrication of (U, Pu, Np) oxide fuel pellets for irradiation testing in the ATR (LWR-1). The fuel composition will vary but will be focused on a nominal 5% Pu with very small amounts of Np and potentially some amount of a depletable neutron absorber. Oxide feed powders will be acquired and the process testing will include varying the blending, milling, pressing, and sintering (temperature, time, and atmospheric) parameters. The development will include key property measurements and initial modeling of material behavior.

Samples of the fabricated pellets will be measured for U, Pu, and Np assay, impurities and all other pertinent parameters. The pellets will be prepared for shipment from LANL to INEEL, where they will be loaded into fuel pins and assembled into capsules for irradiation in the ATR. After all samples are measured, a data package will be assembled to document the condition of the fuel batches. Pellet samples will also be prepared for other potential irradiation tests.

The major FY 2003 milestones for the Fuel Fabrication activity include:

- Acquisition of the oxide feed powders for process development.
- Acquisition of the metal powder for test fuel in the ATR experiments.
- Demonstration of (U, Pu, Np,) oxide fuel.
- Completion of the ATR fuel pellet fabrication.
- Completion of the oxygen diffusion model.

4.3.2 Series One Fuel Fabrication Highlights

The following are the major first quarter highlights for Series One fuel fabrication:

- Modifications and fixes to fuel production facilities are being made to start the pellet fabrication in March.
- A computer program that gives an accurate description of the density of lattice defects in nonstoichiometric cerium oxide (CeO_{2-x}) was developed. Partial free energy of formation (per mol O_2) of nonstoichiometric ceria was calculated as a function of composition with applications in phase stability calculations. After validation, the model will be further extended to include diffusion of oxygen in PuO_{2-x} and $UO_{2-x.}$

4.3.3 Series One Fuel Fabrication Technical Summary

The technical summaries for the following two activities are provided below:

- Fabrication line preparation; and
- Modeling of defect thermo-chemistry in non-stoichiometric ceria.

Fabrication Line Preparation. Figure 5-3a. shows the part of oxygen-to-metal-ratio analyzer that has been updated. This equipment is important for determining the exact stoichiometry of the actinide oxides, which is important when sintering uranium dioxide. The other part of the equipment, the furnace, has been tested out, and a few more modifications that are needed will be done in the next few weeks. The documentation is being written and reviewed for safety. Figure 5-3b. shows a gas bubbler attached to an inert furnace. This bubbler is required to sinter oxides contained uranium dioxide to maintain stoichiometry. Two other small modifications, the replacement of a HEPA filter and the installation of a pressure regulator, will be completed within a couple of weeks. The first mixed oxide sintering is scheduled for mid-March.

Also, six U_3O_8 samples have been run although none have been completely reduced UO_2. We suspect what is observed is a mix of U_3O_8 and UO2 - a yellow brown powder with black (unoxidized?) crumbs in it. It is believed the reason for these results is a leak on the gas inlet side meaning not enough hydrogen is reachingU_3O_8.

Several steps have been made to locate this potential leak. A couple such areas are the rotary flowmeter, and the bubbler system. As we locate the leak and replace components, we are taking the time to do some minor upgrades to the plumbing to make it easier to use the equipment. The bubbler system is very inaccessible and during this time we are taking steps to make it easier to use the bubbler system.

(a) (b)

Figure 4-3. (a) Oxygen to metal ratio analyzer, (b) Gas bubler attached to an inert furnace

Modeling of defect thermo-chemistry in non-stoichiometric ceria (CeO_{2-x}). A computer program was developed to allow for an accurate description of the density of lattice defects in nonstoichiometric cerium oxide (CeO_{2-x}). The simulation tool incorporates statistical – thermodynamic methods and is flexible enough to include the spin of the defect building units and the degeneracy of the electronic state. The code is based on a theoretical model devised by S. Ling[2], and accounts for the coulombian interaction between different defect species, and for exclusion effects. The simulated region spans temperatures in the range 700 - 1500 ^{o}C, and partial oxygen pressures in the range 10^{-30} - 1 atm. A comparison with available experimental data[3],[4] [9,10] is presented in Fig.5-4. Figure 5-5 shows a typical dependence on log(P_{O2}) of the normalized concentration of species containing oxygen vacancies.

[2] S. Ling, Phys. Rev. B, 49, 864, (1994).

[3] R. J. Panlener, R. N. Blumenthal and J. E. Garnier, J. Phys. Chem. Solids, 36, 1213 (1975).

[4] H. L. Tuller and A. S. Nowick, J. Electrochem. Soc. 126, 209 (1979).

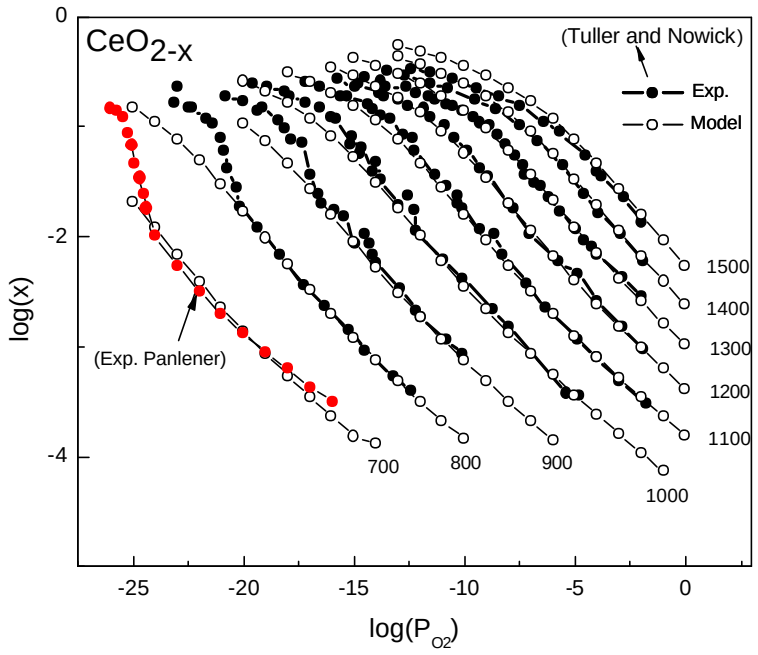

Figure 4-4. Comparison of $\log_{10}(x)$ vs $\log_{10}(P_{O2})$ at different temperatures iwht expweimwntal data from Panlener *et al* [9], Tuller and Nowick [10]. The temperature is measured in Celsius degrees, P_{O2} is measured in atm, and x is the oxygen deficiency in CeO_{2-x}.

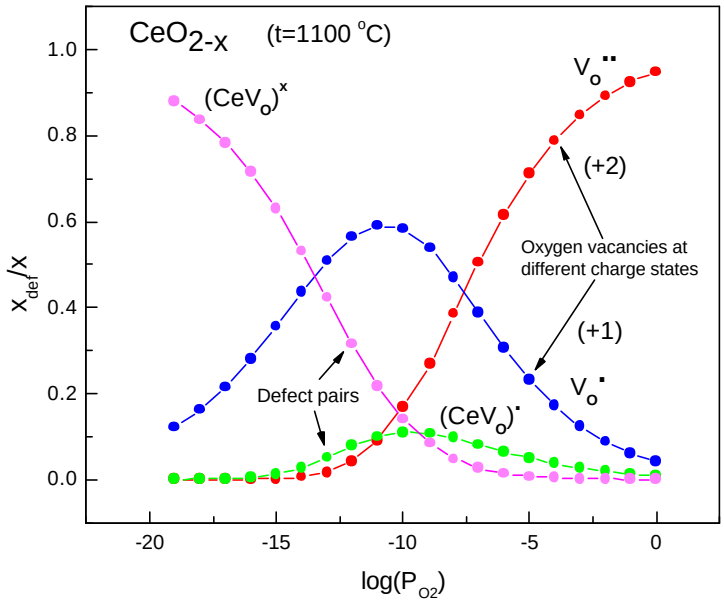

Figure 4-5. Normalized concentration of defect species containing oxygen, at 1100º C, as a function of $\log_{10}(P_{O2})$.

Partial free energy of formation (per mol O_2) of a given nonstoichiometric ceria was calculated as a function of oxygen deficiency (x in CeO_{2-x}). The results are presented in Fig. 5-6. It was noticed that the traditional mass action equations breakdown in the high nonstoichiometric region (log(x)>-2.5), due to a significant contribution from coulombian interaction between

defect species. For the entire region were no phase transitions occur, the numerical results compares well with the available experimental data.

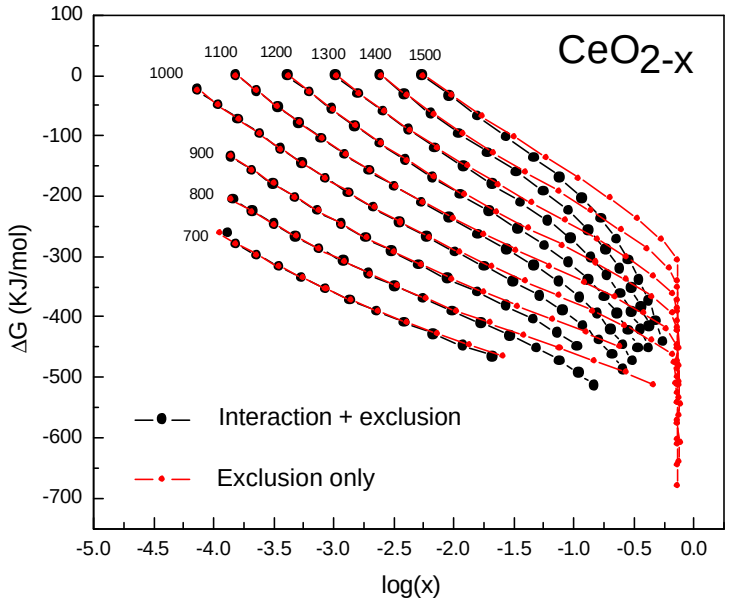

Figure 4-6. Relative partial free energies as a function of nonstoichiometry at different temperatures (ºC).

The intrinsic electronic conductivity (Fig. 5-7) and the electron diffusivity (Fig. 5-8) in CeO_{2-x} were calculated as functions of temperature. From the comparison with experimental data[5],[6], the activation energy for the small-polaron hopping was derived. These results are particularly important in modeling the total electrical conductivity and the oxygen diffusivity for the intrinsic region.

For additional information on this topic, please contact Marius Stan at mastan@lanl.gov.

[5] R. N. Blumenthal, P. W. Lee, R. J. Panlener, J. Electrochem. Soc. 118, 123 (1971).
[6] H. L. Tuller, A. S. Nowick, J. Phys. Chem. Solids, 38, 859 (1977).

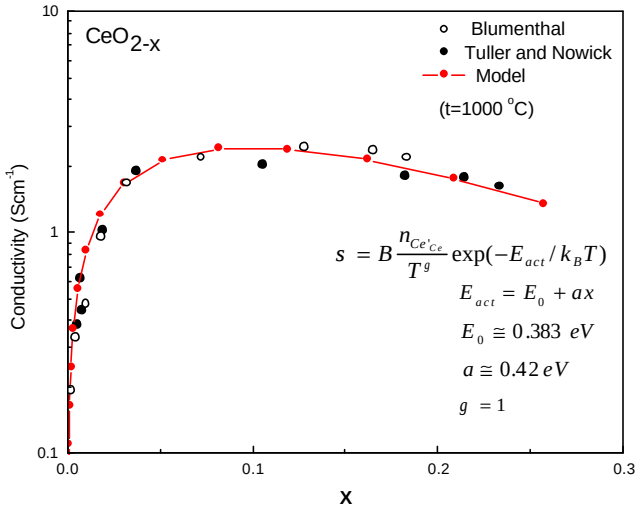

Figure 4-7. Comparison of calculated intrinsic electronic conductivity with experimental data take from Blumenthal *et al*,[7] Tuller and Nowick[8].

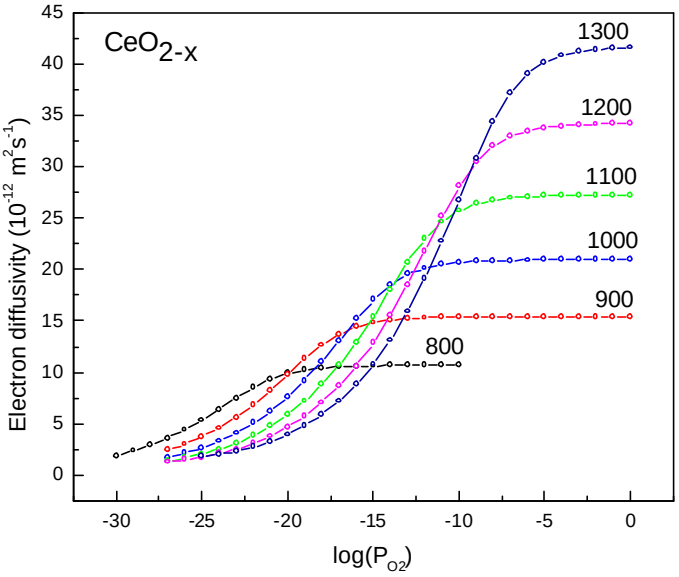

Figure 4-8. Calculated intrinsic electron diffusivity as a function of $\log_{10}(P_{02})$ at different temperatures (ºC).

[7] R. N. Blumenthal, P. W. Lee, R. J. Panlener, J. Electrochem. Soc. 118, 123 (1971).
[8] H. L. Tuller, A. S. Nowick, J. Phys. Chem. Solids, 38, 859 (1977).

4.4 Series One ATR Irradiation Experiments

The first test for Series One fuel is an accelerated burnup irradiation of clad and unclad (U, Pu, Np) oxide fuel pellets and wafers. The primary motivation of these tests is to determine the degree to which the existing MOX fuel performance database is applicable to (U, Pu, Np) oxide fuels. Tests of fuel prototype samples, termed "rodlets," will be irradiated in the LWR-1 test to assess fuel behavior and fuel/cladding interactions, including formation of a rim effect. Tests of wafer-sized samples in easily accessible irradiation positions as part of a series of materials characterization tests will allow more detailed assessment of densification, recrystallization, and modification of the fuel ceramic. Test irradiations will be simulated on the proliferation-resistant fuel performance code, and model-data comparisons will be used to modify and validate the performance codes. These tests are planned to be performed in ATR (and High Flux Isotope Reactor (HFIR) if needed) from the third quarter in FY 2004 through the end of FY 2007.

The performance of prototypic fuel rods in prototypical neutron flux and coolant conditions will be assessed in the LWR-2 irradiation test series. The irradiation tests will focus on confirming behavior of the reference fuel and will be designed to fine tune fuel parameters such as stoichiometry, density, etc. The testing will include tests to demonstrate full lifetime performance and provide supporting licensing and performance data for LTA testing. This test series will be performed in the ATR using a pressurized water test loop. The LWR-2 and ATR test loop design, fabrication, insertion, and irradiation activities will take place between FY 2006 and FY 2013.

Additional tests may be planned as the results of the initial irradiations (LWR-1) are reviewed and the licensing requirements are developed. In addition, the international database on MOX and similar fuels will be reviewed to determine additional testing requirements. Currently, the primary test vehicle is envisioned to be the ATR. Additional tests may be performed in test stations of HFIR, as necessary.

An additional key fuel performance and safety test will be transient testing of an irradiated fuel rodlet from the LWR-1 test in the Annular Core Research Reactor (ACRR) or in the Transient Reactor Test Facility (TREAT). The purpose of this scoping test will be to supplement information on ramp testing in (U, Pu) oxide fuel that will allow the NRC to determine whether more expensive, more rigorous transient testing of proliferation-resistant fuel will be necessary for licensing. The restart of the TREAT or the use of ACRR for transient testing will need to be assessed as licensing requirements are developed. Funding requirements for this activity will be established in FY 2004. If required, these tests will need to be initiated in FY 2006.

The Post-Irradiation Examination (PIE) tasks for examining the samples from the initial first LWR-1 irradiation tests will begin late in FY 2004. More detailed PIE will be performed on fuel retrieved from the LWR-1, LWR-2; transient tests and will continue until the end of FY 2007. However, large scale PIE work will not begin until the fuel in LWR-1 is irradiated at least for a year and thus is not expected to begin until FY 2006. The hot-cells at INEEL and LANL will be the primary PIE locations, but other hot-cells (e.g. ANL-W) may be used if necessary.

4.4.1 Objective and Scope for Series One ATR Irradiation Experiments

In FY 2003, the main task for Fuel Irradiation is LWR-1 testing in ATR. The design test plan and safety analyses for LWR-1 tests will be completed in FY 2003 to prepare for irradiation

testing in ATR in the beginning of FY 2004. In addition, the fuel pellets fabricated at LANL will be used in the fabrication of the fuel pins and irradiation capsule. The FY03 scope also includes the pre-conceptual design for the loop test (LWR-2).

4.4.2 Highlights for Series One ATR Irradiation Experiments

There are no highlights for the first quarter because the activities did not start.

4.4.3 Technical Summary for Series One ATR Irradiation Experiments

The activities are expected to begin in the second quarter of FY03.

4.5 Series Two Fuel Design Specification and Analyses

The Series Two fuels development effort will provide advanced transmutation fuels for Generation IV fast reactor systems that will be deployed by 2030. During the first five years, the Series Two effort is structured to provide fabrication and irradiation test information for a range of promising advanced fuels to support a transmutation technology decision in 2007 (Figure 7.5). After key transmutation and Generation IV technology decisions have been made, Series Two will focus on fuels development to support the selected concepts and technology. The transmutation requirements will be developed through an iterative process throughout the first five years of assessment. The feasibility of meeting these requirements and resulting fuels requirements will also be developed.

Studies supporting this initiative and the Generation IV Program have previously identified several advanced fuel types that have the potential to meet performance requirements for transmutation and future power systems. Oxide, nitride and metal-based fuels support fast spectrum sodium- or lead-cooled systems for power and transmutation. Advanced TRISO fuels support the development of very high temperature gas systems for power, hydrogen, and potentially epithermal transmutation applications. A range of other advanced fuel types (cermet, dispersion, etc.) are being considered for gas-cooled fast reactors.

The Series Two fuel requirements and the Series Two Fuel Development Plan will continue to be revised and updated as new data is obtained. This activity will benefit from technical progress made by international partners in transmutation fuels and materials.

Five-year milestones include:

- Develop Series Two fuel requirements and planning and alternative testing options.
- Integrate Generation IV fuel development efforts within the Series Two Fuel Development Plan.
- Provide fuels data to transmutation technology selection studies.

4.5.1 Objective and Scope for Series Two Fuel Design, Specifications and Analyses

This activity involves evaluating various fuel concepts within the framework of transmutation objectives. Detailed development plans for each fuel concept and testing requirements until the technology selection also covered by this activity.

The major FY 2003 objectives for Generation IV Transmutation Fuels are as follows:

- Evaluate alternative options for Curium-bearing fuels.
- Conduct Fuels and Materials Modeling Workshop.
- Revise Series Two fuels functions and requirements.
- Revise the Five-Year Fuel Development Plan.
- Revise the International Series Two Fuels Handbook.
- Conduct initial safety assessment report on low-conversion ratio fast reactors.

4.5.2 Highlights for Series Two Fuel Design, Specifications and Analyses

The following is the major highlight for the first quarter:

- The FY02 milestone report on fast reactor-based transmutation was completed and posted to the AFCI program IMS system; the report title was "Development of Low Conversion Ratio Fast Reactor for Transmutation," with number ANL-501-1-DDP-000224. In this work, design options to achieve low conversion ratio (CR=0.5-0.0) were explored and preliminary safety studies were conducted. The results demonstrate neutronic feasibility and high transmutation rates; furthermore, favorable transient safety behavior was retained throughout.

4.5.3 Technical summary for Series Two Fuel Design, Specifications and Analyses

Technical summaries are provided for the low-conversion ratio fast reactor analyses and the modeling workshop.

Low-Conversion Ratio Fast Reactor Analysis. The high leakage configurations employed to achieve low conversion pose difficulties for conventional fast reactor physics methods. Consequently, a detailed examination of reactivity coefficient predictions for the low conversion ratio fast reactor systems has been initiated. First, the transport effect associated with voiding the sodium in the core and upper plenum was investigated. The VARIANT nodal variational transport code was used to obtain P_1-P_5 spherical harmonics solutions for flooded and voided sodium conditions. For the pancaked core with a 0.5 CR, the VARIANT calculations yielded a void worth significantly more positive (>\$1) than the diffusion results. This result appeared to conflict with previous fast reactor benchmarks where the transport effect was observed to be minor (<\$0.10). To confirm this result, the hexagonal configuration was converted to R-Z geometry and transport theory calculations were performed with the TWODANT discrete ordinates code. In this case, a \$2 void worth difference was observed between transport and diffusion results indicating a large transport effect. Nearly identical results were obtained for both 230 group and 33 group structures.

This transport effect is attributed to the inability of diffusion theory to accurately predict the leakage rate. The core leakage is overpredicted by diffusion theory leading to a more negative sodium leakage component, particularly in the above core plenum region. Thus, the diffusion results are not conservative for scenarios where the reactivity increase associated with reduced sodium density will be more positive than predicted. Based on this result, a complete set of reactivity coefficients was evaluated to ascertain possible transport effects on other leakage based reactivity feedback parameters.

Results for the CR=0.5 pancaked geometry core design are summarized in Table 2; the diffusion theory results are compared to VARIANT transport results using a P_3 spherical harmonics expansion. The sodium void worth increases by \$1.2 when transport theory is used. To verify the void worth results, an independent Monte Carlo model was performed using the VIM code; the void worth result of \$3.33±0.18 is in excellent agreement with the VARIANT result.

Significant variations are also observed in the GEM reactivity worth which decreases by ~\$0.30. Once again, diffusion theory overpredicts the negative reactivity change associated with an increase in core leakage. By contrast, the geometric expansion results are similar between

diffusion and transport theory predictions. Thus, the diffusion theory problems appear to be caused by large perturbations in the local leakage effects. In addition, streaming effects may be important in these zones, particularly for the emptied GEM assemblies.

2. Table. Comparison of Diffusion and Transport Reactivity Coefficients for CR=0.5 Core

	Beginning of Cycle		End of Cycle	
	Diffusion	Transport	Diffusion	Transport
Beta	0.0032		0.0032	
Sodium Void ($)	2.03	3.20	2.21	3.35
Sodium Density (cents/K)	0.06	0.07	0.07	0.08
Radial Expansion Coefficient (cents/K)	-0.36	-0.34	-0.35	-0.33
Axial Expansion ($) (1% expansion of fuel & clad)	-0.34	-0.35	-0.28	-0.28
Axial Expansion ($) (1% expansion of fuel)	-0.46	-0.49	-0.41	-0.43
Voided GEM Worth ($)	-0.74	-0.46	-0.68	-0.44

Reactivity coefficients trends caused by refinement of the energy group structure or cross section generation technique were also evaluated. In particular, cross section variations within the plenum region were investigated in detail. In the FY02 study, radial reflector cross sections were utilized for the axial reflecting lower shield and plenum zones. A refined approach was employed to generate cross sections specifically for the plenum composition. A $0.60 decrease in the sodium void worth of the plenum region (axial reflector) was observed when the refined cross sections are utilized. The reduced plenum worth is attributed to changes in the iron cross section, with the sodium cross-section giving a minor effect. A detailed cross section comparison of the radial reflector iron cross-section and axial reflector cross-section showed that there were significant differences in the capture cross section in the iron resonance range. These results indicate that the precise treatment of self-shielding in the axial reflector regions is important and utilization of radial reflector cross sections (which are generated with a much higher structural volume fraction) are not adequate.

It is noted that the transport and cross section effects observed for the CR=0.5 configuration will be more severe for the lower conversion ratio designs where the leakage is enhanced. Thus, a similar study is being pursued to generate accurate reactivity coefficients for the CR=0.0 design. In addition, the impact of the refined reactivity coefficients on the passive safety performance will be assessed using the simplified models employed for the FY02 study.

Modeling Workshop. Much progress is being made in the area of fuel material modeling and a lot of interested not only in the US but in the international community as well. In order to bring this community of scientists together a workshop has been organized. The workshop is titled "Modeling and Simulations of Materials' Properties for Nuclear Fuels Applications" and will be held on June 9-10, 2003 in Santa Fe, New Mexico. A call for papers will be going out in early February to the US and international material scientists and a web page is being constructed to handle registration, paper submission, and general workshop information.

4.6 Series Two Nitride Fuel Development

Nitride fuel is one of the fuel forms that are being pursued for transmutation applications. Such fuel types can be used in the sodium or lead alloy cooled fast reactors and accelerator driven systems. The development of nitride fuels to support Generation IV and higher actinide transmutation presents many technical challenges. These fuels must be capable of high burnup to minimize the number of recycles required, be compatible with low-loss separations processing, be easily fabricated in a remote environment, and behave in a benign manner during core steady-state and off-normal events. Because the Generation IV/transmutation system architecture has not yet been defined, the five-year fuel development program concentrates on developing a technology base common to most applications.

For fast reactors, the fuel composition of interest includes fertile materials mixed with plutonium and minor actinides. However, for potential heterogeneous core design scenarios, fertile free fuels are also of interest. If accelerator-driven systems are chosen in conjunction with fast reactors to achieve the transmutation goals, fertile-free fuels are of primary interest.

4.6.1 Objective and Scope of the Series Two Nitride Fuel Development

The FY03 objectives for the nitride fuel development covers process improvements in parallel to fuel pellet fabrication and characterization for ATR irradiation. The specific activities include:

- Continue to investigate enhanced nitride synthesis, blending, pressing and sintering techniques;
- Develop process parameters to fabricate actinide fuel with depleted UN as a diluent;
- Characterize fertile-free and fertile nitride test batches for physical and chemical composition and property measurements; and
- Fabricate cylindrical pellets from each composition for the ATR fertile actinide nitride irradiation test. Ship completed fuel pellets to ANL for loading into test fuel capsules.

4.6.2 Highlights of the Series Two Nitride Fuel Development

The following are the major highlights for the nitride fuel development during the first quarter of FY03:

- Fertile-free nitride pellets for the AFC-1 tests in the ATR were shipped to Idaho. Isotopic and chemical analyses (except oxygen) for these nitride pellets were completed.
- Upgrades to the oxygen-to-metal ratio analyzer have been completed, and a purchase order for LECO nitrogen/oxygen and carbon/sulfur analyzers has been issued.
- Detailed characterization of the unirradiated and high-dose irradiated ZrN samples were performed with interesting observations (see technical details below).
- Quantum Mechanical (QM) calculations of fundamental properties of nitrides, such as lattice parameters, bulk modulus, Young's modulus, and Poisson's ratio, have been performed to assist the atomistic and continuum level modeling.

- First principles calculations of the electronic structure of Am predicted the energy versus volume functions for several possible crystal structures. The results will allow for the optimization of the Modified Embedded Atom parameters, with impact on the modeling of thermo-mechanical properties of Am and AmN.

4.6.3 Technical Progress of the Series Two Nitride Fuel Development

The first quarter progress for the nitride fuel development is reported for the following sub-tasks:

- Nitride pellet fabrication;
- Assessment of radiation tolerance of ZrN, NbN and TiN;
- Crystallographic Texture and Mechanical Behavior Anisotropy in Sintered ZrN Pellets;
- Atomistic simulations of the Fundamental Properties of Nitrides; and
- First principle calculations of americium (Am).

Nitride Pellet Fabrication. Nitride pellets for the ATR insertion scheduled for FY03 were completed in late summer. Approximately 40 pellets for each of the six compositions were fabricated. Various sintering temperatures were used to sinter the pellets, depending on the Am content of the compositions. Some compositions had the full 40 pellets available, while others had less than 40, because a number of pellets were rejected due to cracks, chips, etc. Final pellets for compositions 1, 2, 5, and 6 are shown in Fig. 5.9. The pellets for each of the compositions were welded into a total of 17 stainless steel shipping containers (see Fig. 5.10).

Isotopic composition for the plutonium used in the pellets is given in Table 3. The PuN used for each of the compositions came from the same PuO_2 feedstock. The isotopic composition has a fairly high Pu-239 content, ~93.9% with the other major constituent being Pu-240 at about 5.97%.

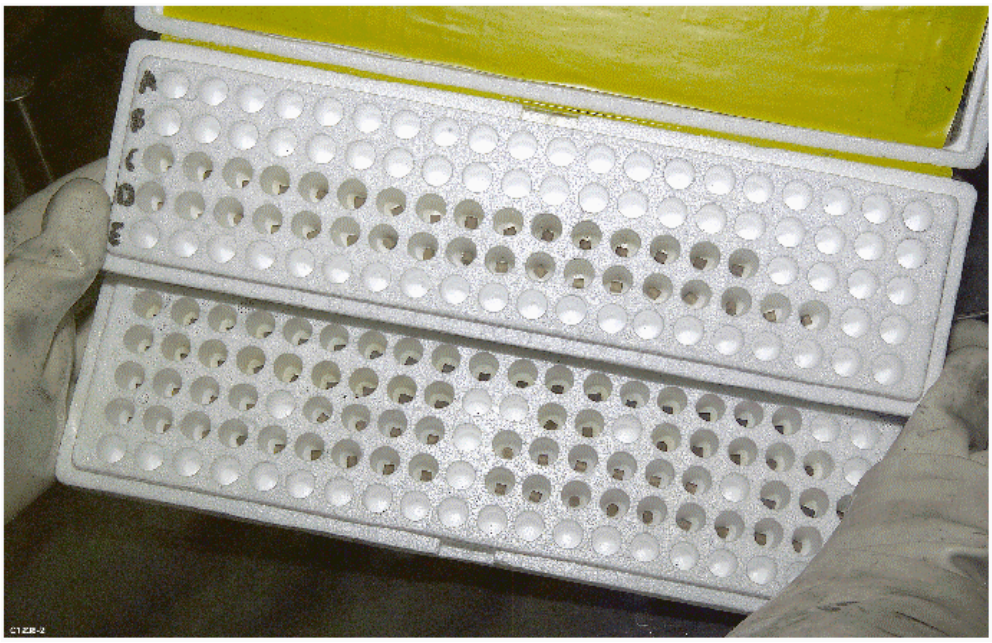

Figure 4-9. Nitride pellets for compositions 1, 2, 5, and 6.

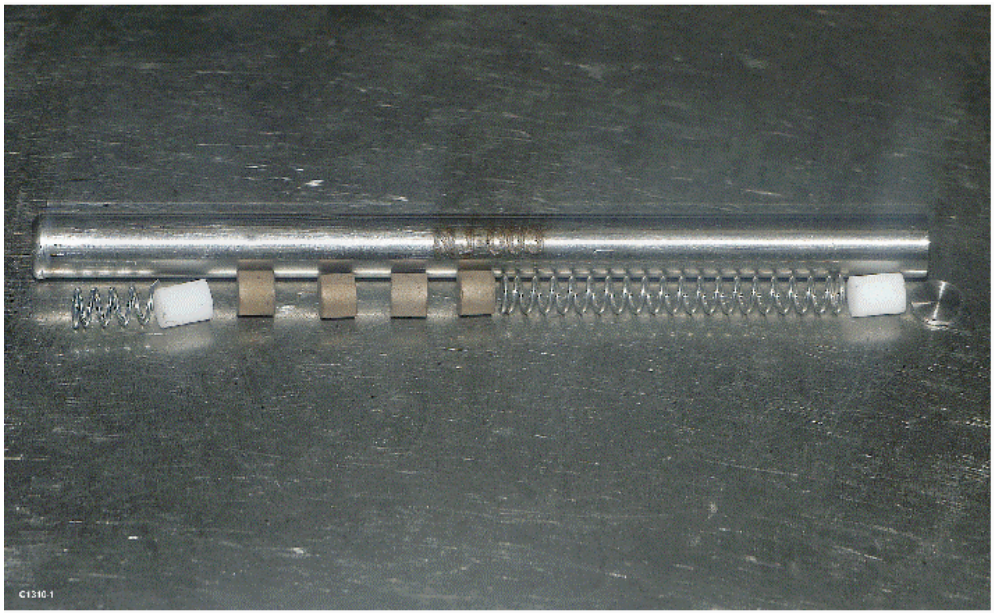

Figure 4-10. Nitrides packaged for shipment.

3. Table – Isotopic Composition (wt%) of ATR Actinide Nitrides

Isotope	Comp1	Comp2	Comp3	Comp4	Comp5	Comp6	Average	Feed stock value
Pu 238	0.0101	0.0095	0.0118	0.0099	0.0107	0.0100	0.010	0.009
Pu 239	93.7975	93.8662	93.8843	93.8729	93.8717	93.8746	93.861	93.902
Pu 240	6.0569	5.9905	5.9725	5.9845	5.9833	5.9820	5.995	5.969
Pu 241	0.1057	0.1051	0.1035	0.1048	0.1057	0.1050	0.105	0.096
Pu 242	0.03	0.0286	0.0278	0.0278	0.0286	0.0284	0.029	0.024
Pu 242	n/a	n/a	n/a	n/a	n/a	n/a	n/a	n/a

The chemical content for each of the six compositions is given in Fig. 5-11. The weight percent of the constituent is given against the composition. The solid red lines are the measured chemical composition while the dashed blue lines are the targeted composition. The large error bars for the Am and Np indicate a large uncertainly in the measure; they were measured as impurities, requiring several thousand-fold dilutions, which introduces dilution error. For those compositions where the measured value is less than targeted composition, an actinide component boiled off. For those compositions where the measured value is greater than the target composition, constituents (most likely actinides) other than that constituent boiled off.

Of greatest concern regarding actinide boil off was americium. The amount of Am that boiled off was actually less than anticipated. This was in part because the sintering temperature was adjusted to account for Am content; the high Am content pellets were sintered at a lower temperature than those that had low or no Am content.

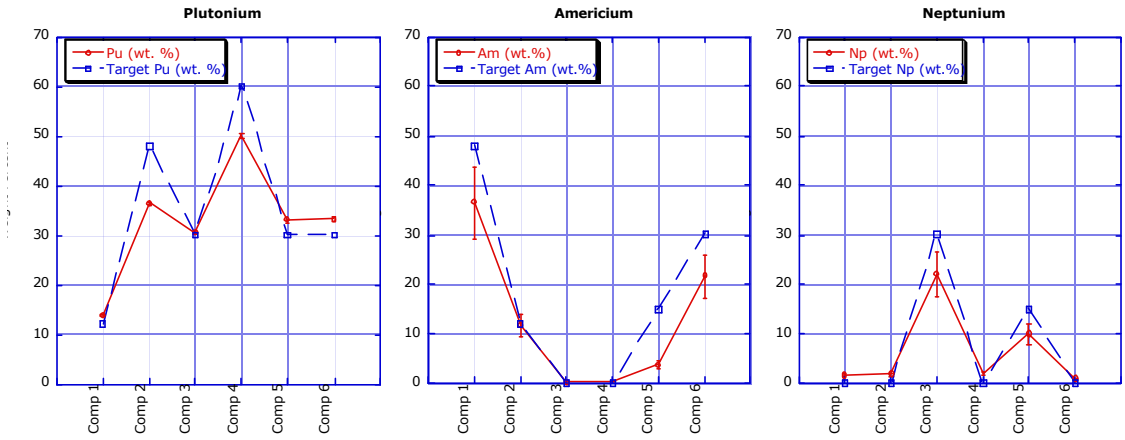

Figure 4-11. Chemical compositions for the actinides in the six nitride compositions.

The weight percents for the Zr, N, and C are given in Fig. 5-12. The large error in the Zr is also due to dilution error. Unlike the actinides, it is unlikely that much, if any, ZrN boiled off. This is seen from the compositions 3 and 4, where a sintering temperature of 1700°C was used and no Am was present. The measured value is very close to the target value. For compositions 1, 2, 5, and 6, where Am is present and lower sintering temperatures were used, actinides boiled off, leaving a higher weight percent of ZrN.

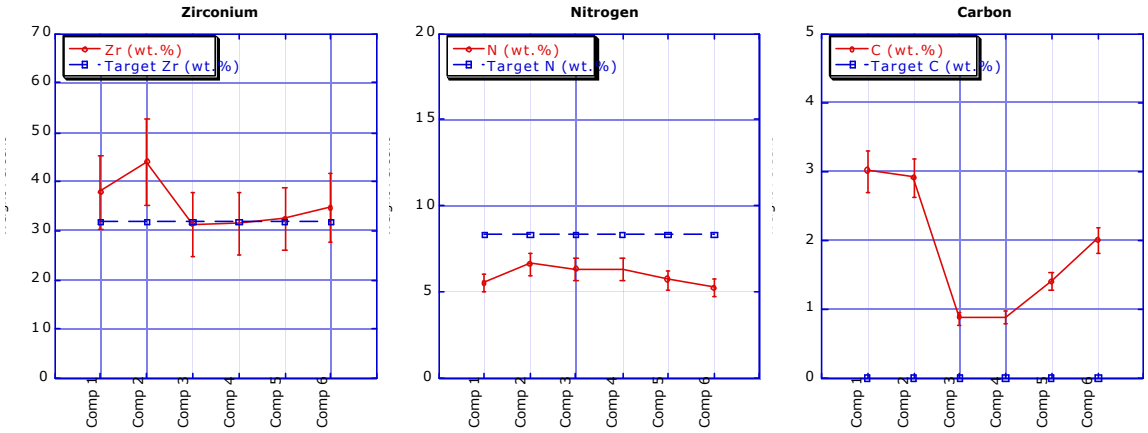

Figure 4-12. Chemical compositions for the Zr, N, and C in the six nitride compositions.

The measured concentration of nitrogen is lower than the target value, however, the amount of nitrogen present is relatively constant, despite the higher sintering temperatures for compositions 3 and 4. This can be due to a number of reasons. During chemical analysis, because some of the handling of the nitrides samples was done in air, some of the nitrides converted back to oxide; analysis for oxygen is currently being pursued. The high residual carbon content suggests that not all the carbide converted to nitride. However, x-ray diffraction (not shown) revealed no significant amount of carbide or oxide present in these materials. Furthermore, the carbon content appears to be dramatically affected by composition, where compositions 3 and 4 have significantly lower C content than the others. This could be due to two causes; 1) if the residual

C content was the same for all PuN, AmN, and NpN, then the higher sintering temperature for compositions 3 and 4 burned off more C; or 2) what seems more likely, the lower oxide-to-carbide-to-nitride conversion temperature used to produce AmN left higher residual amounts of C in the AmN feedstock material. The issues of low nitrogen and high carbon contents are currently being investigated.

Part of the problems associated with nitrogen and carbon analyses will be alleviated with the purchase two pieces of analytical equipment to be installed in-line (i.e., in the same glovebox line) with the fuel fabrication equipment: nitrogen/oxygen and carbon/sulfur impurity analysis equipment. This should allow for very rapid turn around and high precision measurement of these elements. Upgrades to another piece of equipment, the oxygen-to-metal-ratio analysis equipment, have been made. This equipment will aid in the optimization of the amount of graphite needed to reduce the oxide to nitride.

For additional information on this topic, please contact Bob Margevicius at margevicius@lanl.gov .

Assessment of Radiation Tolerance of Zirconium, Niobium, and Titanium Nitrides. We continued to experiment with various techniques to evaluate radiation damage evolution in ZrN following irradiation with heavy ions. The heavy ions employed in our experiments were Xe ions, in order to simulate fission product damage. This quarter, we used cross-sectional transmission electron microscopy (XTEM) and micro-diffraction (μD) to examine samples irradiated with 450 keV Xe^{3+} ions.

Figure 5-13 shows an XTEM bright-field micrograph obtained from a polycrystalline sample of ZrN irradiated with 450 keV Xe^{3+} ions at cryogenic temperature (~100K). The fluence used in this irradiation was $2 \cdot 10^{16}$ Xe/cm^2. Figure 5-14 shows results from a Monte Carlo simulation (performed using the Transport of Ions in Matter or TRIM code) of displacement damage and ion stopping for 450 keV Xe^{3+} ions into ZrN. At the ion fluence of interest, $2 \cdot 10^{16}$ Xe/cm^2, results in Fig. 5-14 indicate that the peak displacement damage level is nearly 80 displacements per atom (dpa). This peak displacement damage occurs at a sample depth of about 50 nm. (The computer simulation was performed assuming ions are incident normal to the surface of the ZrN target. This was also the experimental condition used for the results shown in Fig. 5-13.) The peak Xe concentration at $2 \cdot 10^{16}$ Xe/cm^2 fluence is slightly greater than 3 atomic percent, according to the simulation results shown in Fig. 5-14. This peak concentration occurs at a depth of ~ 90 nm, i.e., slightly deeper than the peak in the displacement damage.

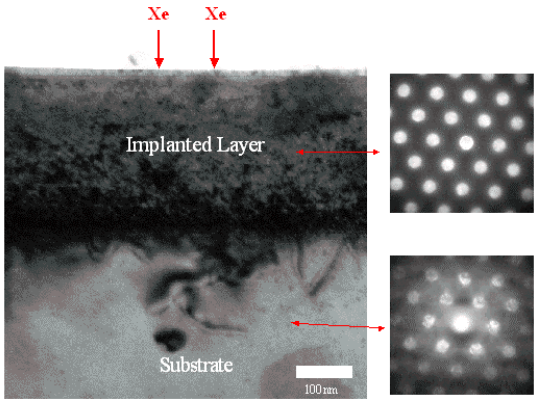

Figure 4-13. Bright-field, cross-sectional TEM micrograph of the irradiated microstructure of a ZrN sample implanted at 100K with 450 KeVXe^{3+} ions to a fluence of $2*10^{16}$ Xe/cm^2. the surface of the ZrN sample is at the top of

the micrograph. At rignt are microdiffraction patterns obtained from the implanted layer (top) and the substrate (bottom). Both patterns can be indexed as (011)-oriented d cubic ZrN, and are consistent with the rocksalt crystal structure.

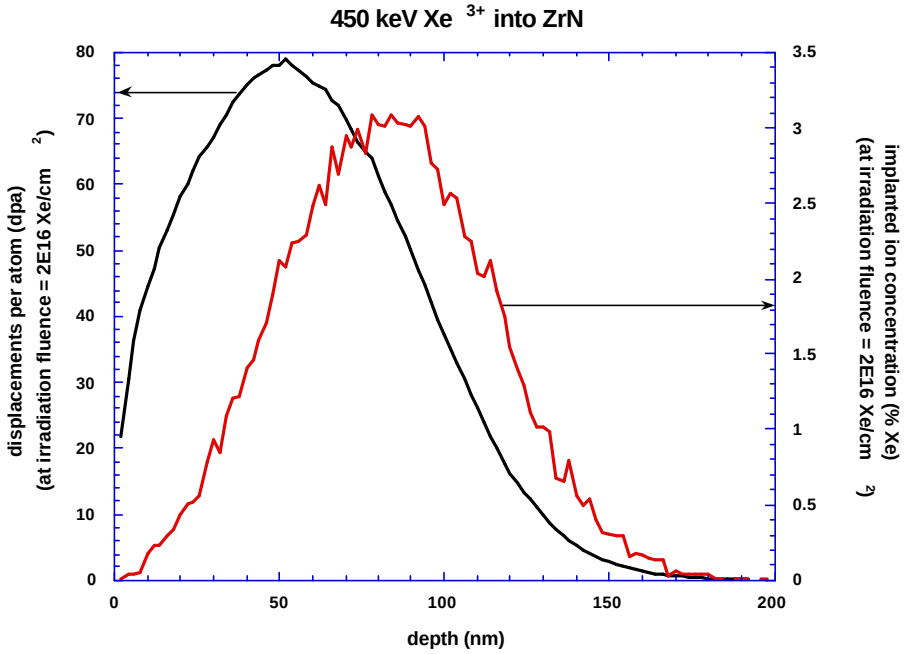

Figure 4-14. Monte Carlo simulation results for displacement damage (black curve) and implanted Xe concentration (red curve) as a function of target depth ofr 450 KeV Xe^{3+} ions implanted into Zr.N to a fluence of $2*10^{16}$ Xe/Cm^2.

The inset μD patterns in Fig. 5-14 reveal that the implanted layer is isostructural with the substrate, and that the irradiated layer maintains an epitaxial relationship with the substrate throughout the implantation. No evidence for amorphization of ZrN was found in these cryogenic irradiation conditions, to the peak test dose of 80 dpa.

The defects in the implanted microstructure appear to be small (~nm diameter), cluster-like defects. Defect density is greatest near the end of range of the Xe. Also, the thickness of the damage layer, approximately 250 nm, is significantly greater than the thickness predicted by TRIM. This has been observed before in other ceramic materials such as ZrO_2.[9] Apparently, point defects are fairly mobile, even under the cryogenic irradiation conditions used here. As stress in the implanted layer increases with increasing ion fluence, defects migrate down the stress gradient within the target material.

Evidence for small voids, microtwinning, and nano-dimensional recrystallization, as were observed in past irradiation experiments on ZrN using 300 keV Xe^{++} ions (see quarterly report 04/2002), were not found in these experiments. Experiments are in progress to reconcile these different results.

[9] N. Yu, K. E. Sickafus, P. Kodali and M. Nastasi, J. Nucl. Mater. 244 (1997) 266-272.

In order to assess possible differences between the irradiation damage properties of different nitrides, we initiated experiments during this quarter on the radiation damage behavior of niobium nitride. We intend to compare the behavior of NbN to ZrN to determine the similarities and differences in behavior between nitrides of different composition, but with essentially the same crystal structure. The niobium nitride we chose for the irradiation experiments described here was provided by Kurt J. Lesker Co. (Clairton, PA). Specifically, these were hot-pressed, polycrystalline NbN sputtering targets, 99.5% purity. X-ray diffraction experiments performed by us revealed that the niobium nitride is tetragonal rather than cubic, as is ZrN. The tetragonal structure is best described as an approximate doubling of the periodicity along the c-axis, such that the a and b dimensions are equal (approximately given by 0.4386 nm), while the c dimension is roughly given by c = 2a (experimentally given by 0.8693 nm). In the literature, this tetragonal distortion of the rocksalt crystal structure is ascribed to a significant deficiency of nitrogen in the compound. According to Kim et al.[10], the compound responsible for the tetragonal nitride structure is best described as NbN_{1-x}, where x is approximately 0.42. This phase of niobium nitride is called the gamma (γ) phase, while the cubic phase is called the delta (δ) phase. According to Heger and Baumgartner, x ranges from 0.15 to 0.3 in γ-NbN_{1-x}.[11] Clearly, there is some debate as to the range of non-stoichiometry in γ-NbN_{1-x}. The tetragonally-distorted sodium chloride structure of γ-NbN_{1-x} is generally attributed to ordering of nitrogen vacancies.

In our experiments, bulk samples of NbN_{1-x} were irradiated at cryogenic temperature (~100K) with 300 keV Xe^{++} ions to fluences of $1 \cdot 10^{16}$ and $2 \cdot 10^{16}$ Xe/cm^2, and with 120 keV N_2^+ ions to a fluence of $1 \cdot 10^{18}$ N/cm^2. In the latter case, N ions were used to intentionally increase the nitrogen concentration in the irradiated layer towards the equimolar, NbN composition. Grazing incidence X-ray diffraction (GIXRD) measurements revealed that under all irradiation conditions tested, the NbN_{1-x} transforms from a tetragonally-distorted NbN_{1-x} phase to a cubic, δ-NbN_{1-x} phase (though the transformation is not complete in any specific experiment). Figure 5-15 shows GIXRD results obtained from pristine versus irradiated NbN_{1-x} samples. The tetragonal splitting present in the diffraction from the unirradiated NbN_{1-x} diminishes slightly upon irradiation, especially for the sample irradiated with Xe^{++} ions. Apparently, the ordering of nitrogen vacancies is disrupted by the displacement damage associated with the Xe ion irradiation. In the case of the N_2^+ irradiation, the structure would be expected to evolve towards a cubic structure, since the concentration of nitrogen vacancies should decrease linearly with increasing dose. However, little change in structure is observed following the N_2^+ ion irradiation. For Xe, it is not clear whether there are domains of tetragonal and cubic phase NbN_{1-x} mixed within the implanted layers, or whether the tetragonal distortion is simply disappearing in a continuous fashion with increasing ion fluence.

[10] S.-J. Kim, H. R. Franzen and W. Lengauer, J. Less-Common Met. 160 (1990) 193-196.
[11] G. Heger and O. Baumgartner, J. Phys. C: Solid State Phys. 13 (1980) 5833-5841.

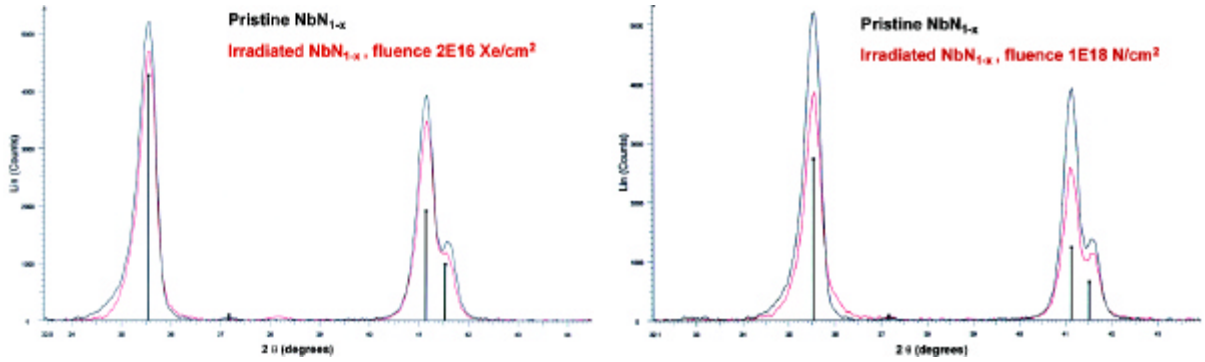

(a) (b)

Figure 4-15. Grazing incidence X-ray diffraction (GIXRD) patterns obtained from pristine (black curves) versus irradiated (red curves) NbN_{1-x} samples: **(a)** 300keV Xe^{++} ions to fluence $2*10^{16}$ Xe/Cm^2, **(b)** 120keV n_2^+ ions to a fluence of $1*10^{18}$ N/cm^2.

As with NbN in this report, in order to assess possible differences between the irradiation damage properties of different nitrides, we initiated experiments during this quarter to synthesize titanium nitride samples, in preparation for radiation damage experiments. We intend to compare the behavior of TiN to our observations on NbN to ZrN, in order to determine the similarities and differences in behavior between nitrides of different composition, but with essentially the same crystal structure.

This quarter, 130 nm thick films of TiN were successfully deposited on Al_2O_3 single crystal substrates by sputter deposition of a sintered TiN target in an N_2 atmosphere (target at ambient temperature). X-ray diffraction measurements shown in Fig. 5-16 revealed that the samples contain crystalline TiN grains with the cubic, NaCl structure. These samples are currently being annealed to improve the crystallinity of the TiN thin films. These samples will be used for future radiation damage experiments.

For additional information on this topic, please contact Kurt Sickafus at kurt@lanl.gov .

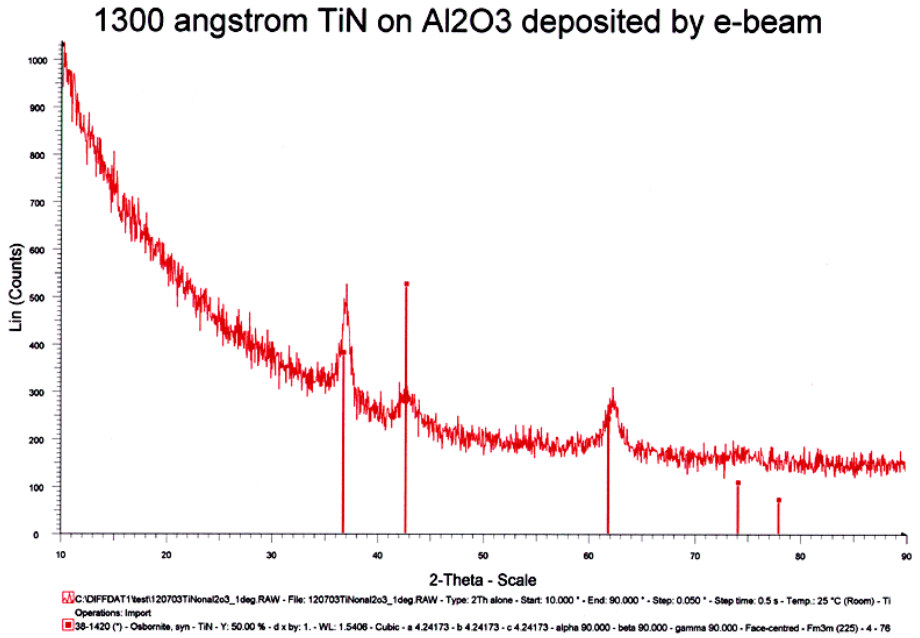

Figure 4-16. Grazing incidence X-ray diffraction (GIXRD) patterns obtained from pristine TiN_x thin film deposited on a single crystal sapphire (Al_2O_3) substrate.

Crystallographic Texture and Mechanical Behavior Anisotropy in Sintered ZrN Pellets (Arizona State University). The crystallographic texture and variation of mechanical properties with respect to characteristic sample directions were studied and measured in sintered ZrN to evaluate the mechanisms that can compromise the structural stability of fuels during transmutation. The initial assessment on anisotropy of the mechanical properties placed emphasis on texture characterization and analysis, hardness variations and fracture toughness. The crystallographic texture was measured first to determine the characteristic directions of the samples. Then, Vickers hardness (H_v) and Fracture Toughness (K_{Ic}) were measured using samples from pure ZrN pellets. These pellets were prepared with an improved sintering process, with respect to that used to sinter the material evaluated initially.

Cylindrical ZrN pellets, 12 mm in diameter and approximately 12 mm in height were sintered at LANL using an improved process. Samples for texture, metallographic characterization and microhardness testing were cut from these pellets using Wire Electro-Discharge Machining (WEDM). These samples were first polished with SiC paper (600, 800 and 1200 grit) and then finished with 1 µm diamond paste. The samples for texture analysis were disks perpendicular to the axis of the pellets and were also used to obtain the hardness on the longitudinal plane. Slices parallel to the longitudinal direction were also cut to obtain hardness values on the radial plane. Samples for fracture toughness were also cut using WEDM, in the form of micro-beams with height and thickness of approximately 1 mm and lengths of about 6-7 mm. The axes of some of these beams were cut parallel to the axis of the cylinder (longitudinal fracture plane) whereas another set of beams had their lengths cut parallel to the radial direction (radial fracture plane). Notches with lengths of approximately one half of the height were also made using WEDM. The surfaces of these beams were polished with SiC paper only up to 1200 grit.

Texture analysis was carried out in a Rigaku RU200 rotating anode X-ray diffractometer equipped with a pole figure goniometer. The diffractometer was operated at 50 kV and 100 mA

with a 0.5° slit. Data collection was carried out at 5° intervals between 0 and 75° tilt angle and full rotations for the twist angle.

Hardness testing was carried out in a standard microhardness testing apparatus using a Vickers indenter (four-sided pyramidal diamond tip) with a load of 500 g. Five indents were made per sample, in order to obtain average values of the hardness. Fracture toughness testing was performed using a screw-driven loading stage under displacement control following the procedures specified by the standard ASTM E-399. The load resulting in fracture was measured using a 500 lb load cell.

Microstructural characterization, hardness determination and fractographic observations were carried using Optical Microscopy. The results from the microhardness testing for the new material compared to hardness of material prepared with the old sintering process are shown in Fig. 5-17.

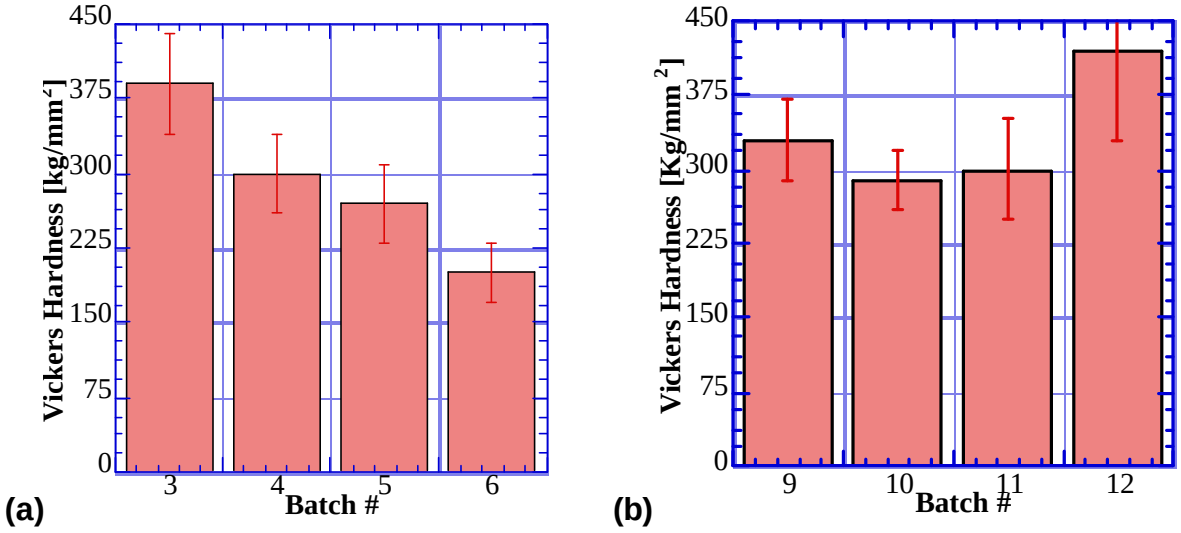

Figure 4-17. Vickers hardness (a) old material (b) new material.

Note that there is a measurable increase in the average mechanical properties of the material produced with the new sintering process and that the variations on the hardness are less pronounced from batch to batch, which indicates that the improved sintering process results in better and more uniform properties. This, in turn, makes material characterization to estimate reliability easier to carry out, while increasing the confidence on the results. The raw pole figures collected for the texture characterization are shown in Fig. 5-18. It is evident from these figures that the sample has a strong {200}-{111} fiber texture, given the axisymmetric nature of the pole figures. Further analysis was carried out to extract the strength of the texture components as multiples of the intensity of a random sample (see Figs. 5-19 and 5-20).

Note that the maximum intensity in the two pole figures corresponds to the center, which is the direction parallel to the axis of the cylindrical pellets, and that the maximum intensity

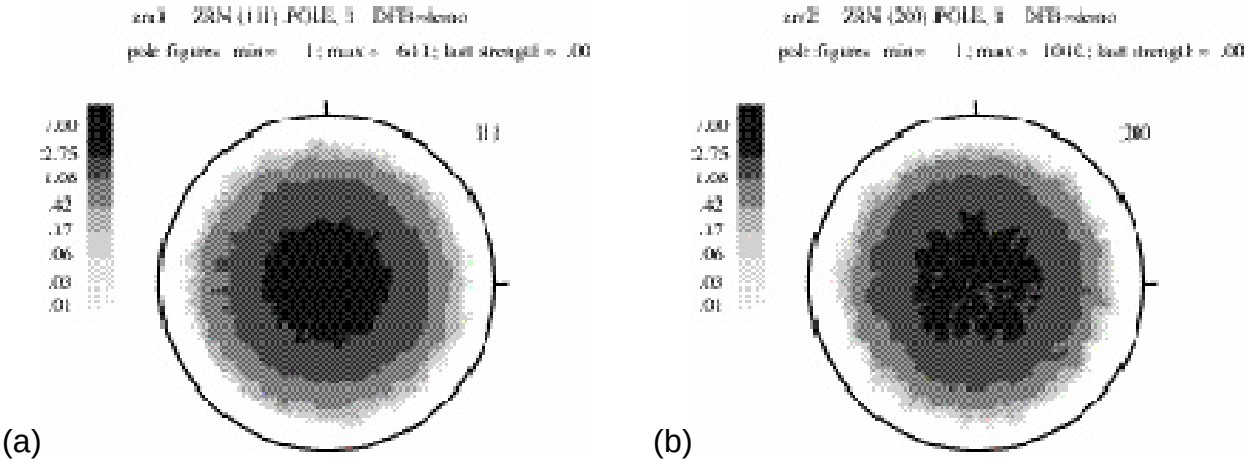

Figure 4-18. (a) {111} pole figure; (b) {200} pole figure. The axis of the cylindrical pellets corresponds to the center (axis 3).

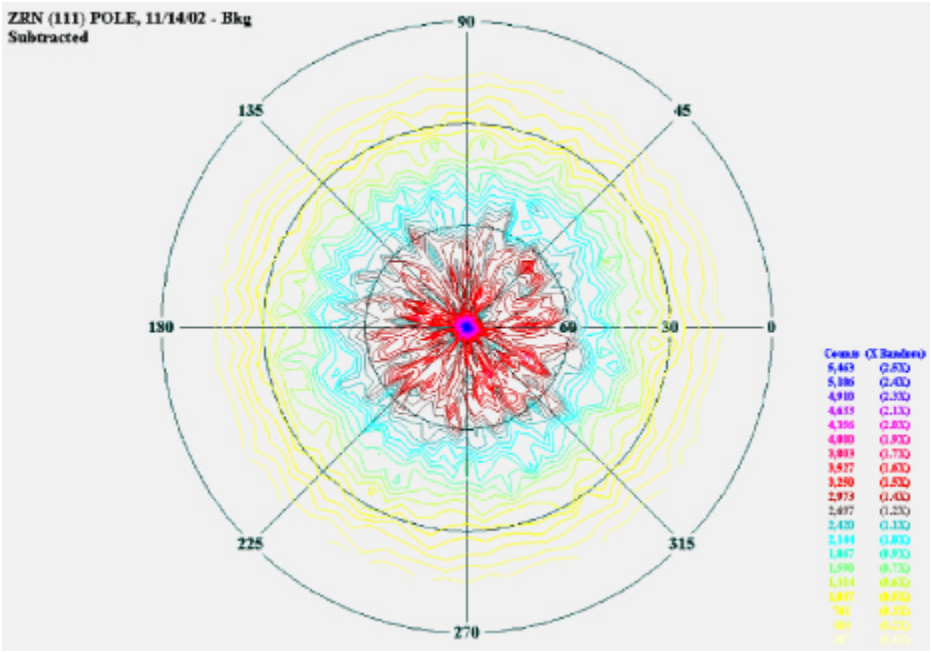

Figure 4-19. Redefined {111} pole figure after background subtraction and defocusing correction.

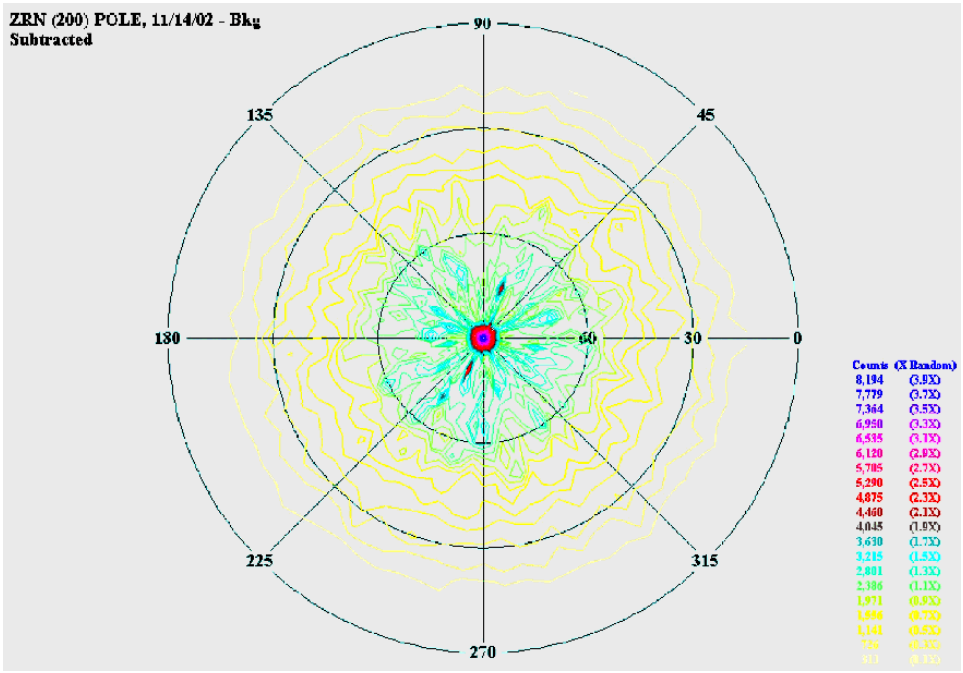

Figure 4-20. Redefined {200} pole figure after background subtraction and defocusing correction.

of the {200} figure is about 4 m.r.d whereas the maximum intensity of the {111} pole figure is 2.5 m.r.d. Fiber textures with {200}-{111} components are common in cubic metals, particularly after recrystallization.[12,13] However, ZrN has the rock salt structure and the mechanisms by which texture develops in ceramics are not that well understood. Two or three mechanisms may be responsible for the development of this texture, as follows:

- Particle rotation during powder compaction: this mechanism could play a significant role if the powder particles used to prepare the material have facets due to cleavage or can cleave easily during compression. Once the cleavage facets are present the compression will tend to align the crystallographic facets perpendicular to the applied stress, i.e., the compression direction. No references regarding the existence of cleavage planes in ZrN were located in a preliminary survey of the literature.
- Inelastic deformation during sintering: it is well know in metals that compressive deformation tends to produce texture components parallel to the vector normal to the slip plane of the active dislocations, i.e., {111} in fcc and {110} in bcc. Ionic materials with the rock salt structure tend to slip on {110} planes, whereas rock salt materials with more covalent bonding tend to slip on either {110} or {100}[8]. The slip behavior of ZrN does not seem to be well characterized, since a thorough literature search did not result in any published results on this regard.
- Recrystallization during sintering: recrystallization textures result from the preferred crystallographic orientation of grains nucleating during the recrystallization process. This

[12] Kocks, U.F., C.N. Tomé, and H.-R. Wenk, Texture and Anisotropy, Cambridge University Press, Cambridge, 1998.
[13] Llanes, L., et al., Acta metall. mater., 1993. 41(9): p. 2667-2679
[13] From NIST ceramic database: http://www.ceramics.nist.gov/srd/scd/Z00220.htm#M6P1
[13] Note that the value of toughness for monolithic ZrN is between 5 and 7 MPa.m1/2 according to the NIST

phenomenon is not well understood in metals and that is even more the case for ceramics due to the large number of parameters involved.

Further analysis of the texture was carried out using popLA (Preferred Orientation Package, Los Alamos) to look at the distribution of orientations on lateral directions. Inverse pole figures were created after performing a harmonic analysis of the measured pole figures, which allowed the simulation of the distribution of orientations along any direction. The resulting inverse pole figures are shown in Fig. 5-21.

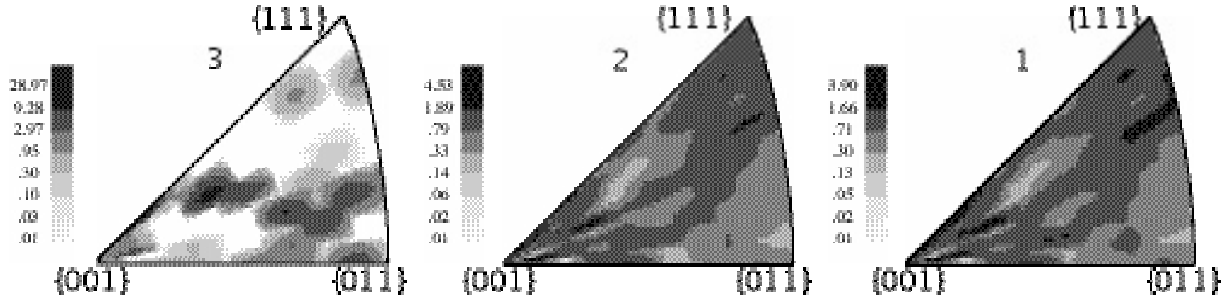

Figure 4-21. Inverse pole figures for sintered ZrN. (a) longitudinal axis ("3); (b) and (c) lateral axes (2 and 1)

These inverse pole figures represent the crystallographic orientations that are parallel to certain physical direction in the sample. One can see from Fig. 5-21(a) that the texture component close to {001} is indeed stronger than that parallel to {111}. Furthermore, the distribution of orientations along the two lateral directions is almost identical on both shape and intensity, confirming the existence of a true fiber texture in this material. A detailed knowledge of the slip behavior of ZrN would allow the simulation of the deformation processes leading to this result. This, in turn, is important because texture in polycrystalline materials usually leads to anisotropic properties. This anisotropy can be used advantageously in structural applications by careful manipulation of the geometry of components according to the applied loads and material properties, e.g., the direction with the highest strength should be parallel to the largest applied stress. It would be worthwhile to investigate the mechanisms that lead to texture development in this material, since that will provide an opportunity to tailor the manufacturing to increase the structural reliability of the materials being considered. In this sense, hardness and fracture toughness were used to evaluate the anisotropy on mechanical properties, which will be discussed next.

Results of the hardness tests on both radial and longitudinal planes of the sintered pellets showed that the material had similar values of hardness for the two orientations. The distribution of hardness for the radial plane was quite close to that shown in Fig. 5-17b, which was obtained for the longitudinal direction. Note that the Vickers hardness of monolithic ZrN has been reported to be between 13 and 16 GPa (1300 to 1600 Kg/mm^2)[14], whereas the average value obtained here is approximately 340 Kg/mm^2, about four times lower. As discussed in previous reports, hardness is controlled by porosity, the distribution of which does not seem to be affected significantly by the existence of a preferred crystallographic texture. The fracture toughness, on the other hand, is more likely to be affected by the texture, since the strength of particles along the crack path will certainly depend on the orientation. This is discussed in the next section.

[14] From NIST ceramic database: http://www.ceramics.nist.gov/srd/scd/Z00220.htm#M6P1

The fracture toughness measured on the two principal material directions first showed a small difference between the radial and the longitudinal (compression) planes, with the values on the radial plane higher by about 10%. However, further analysis has shown that the sample used has too many internal cracks to be reliable and the measurement was carried out again. The second experiment revealed the same trend, i.e., the toughness on the radial plane was higher than the toughness on the longitudinal plane but the difference between the two directions was much higher, about 50% (1.5±0.3 Mpa.$m^{1/2}$ for the radial direction and 1.0±0.1 MPa.$m^{1/2}$ for the longitudinal direction[15]). It was also found that the crack path for the radial direction tended to be less tortuous than for the longitudinal direction, as shown in Fig. 5-22.

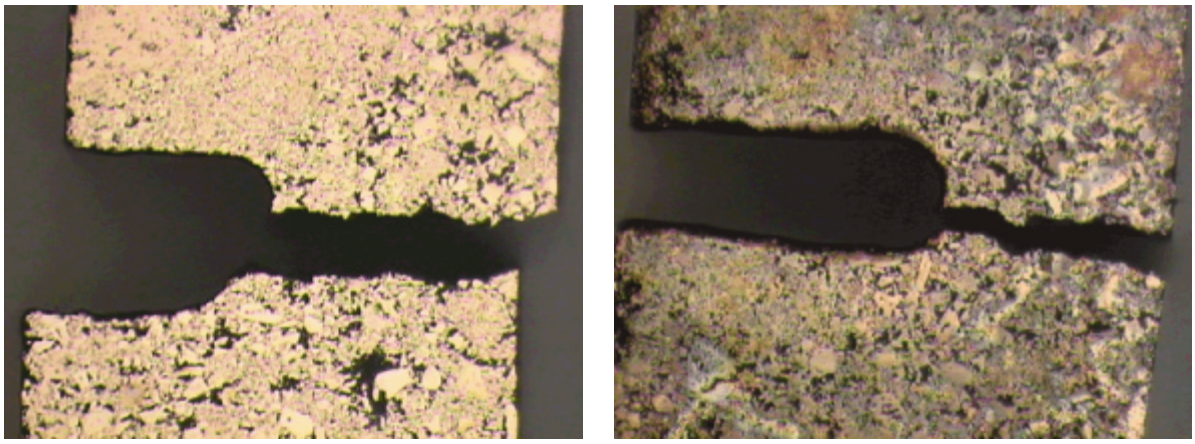

Figure 4-22. Crack paths for different crack planes. (a) Crack on the radial plane, (b) Crack on the longitudinal plane.

This result is interesting because crack deflections are usually associated to higher fracture toughness in brittle materials. However, the lower value of toughness obtained for the case with the tortuous path indicates that cracks probably tend to propagate around particles, and that this path is weaker on the longitudinal plane. The crack on the radial plane probably goes more through particles, which may have an orientation that renders them more resistant to fracture in this particular case. A better understanding of the basic fracture mechanisms of monolithic ZrN is needed in order to fully explain these results. More testing and fracture surface characterization are being carried out to confirm this behavior and gather more statistics. In addition, experiments will also be carried out after heat-treating the specimens under nitrogen.

For additional information on this topic, please contact Pedro Peralta (Arizona State University) at pperalta@asu.edu.

Atomistic Simulations of the fundamental properties of Nitrides. With the procurement of a Quantum Mechanical Code (QM) at the end of the last quarter, much of the effort in this period has concentrated on QM calculations. These calculations have been targeted towards predicting fundamental properties and the ongoing investigation of non-stochiometry in TiN and ZrN. Alongside the QM calculations Energy Minimization (EM) calculations have also been performed to evaluate the incorporation of the fission product Xe in important nitride materials. In parallel to earlier energy minimization calculations the QM technique has been used to predict

[15] Note that the value of toughness for monolithic ZrN is between 5 and 7 MPa.$m^{1/2}$ according to the NIST database.

basic structure and elastic properties of some important nitrides. Predicted elastic properties for TiN and ZrN are given in Table 4.

4. **Table –** Predicted Elastic Properties for ZrN and TiN, from QM.

Material	Bulk Modulus (GPa)	Young's Modulus (GPa)	Poisson's Ratio
ZrN	222(260[14])	351(380[14])	0.236(0.256[14])
TiN	254(318[15])	573	0.124

In addition the QM technique allows us to predict electronic properties, such as Mulliken population and density of states. From Table 5 it is clear that the observed structures and predicted ionic character of ZrN and UN are very similar. However, the predicted densities of states (compare Fig. 5-23 and 5-24) show that there are distinct electronic structure differences. As a consequence there will be differences between ZrN and UN in terms of their bond energies and possibly associated physical/electronic properties. This merits further investigation.

5. **Table .** Predicted Lattice Parameters and Mulliken Population for UN, ZrN and TiN, from QM.

Material	Experimental Lattice Parameter(Å)	Predicted Lattice Parameter(Å)	Mulliken Population
UN	4.890[16]	4.86	0.76
ZrN	4.585[17]	4.588	0.86
TiN	4.238[18]	4.234	0.79

These calculations are presently being extended to model the solid solutions ZrN/UN by forming supercells incorporating two cations. The intention is that these results will feed directly into the thermodynamic calculations being undertaken by M. Stan and co-workers.

It is also critical to understand the atomic scale mechanisms by which fission products are accommodated in the fuel lattice. In this regard we have calculated the incorporation energy for Xe into a range of nitride materials – CmN, UN, ZrN and TiN. In these lattice structures we have considered three possible trap sites; isolated cation and nitrogen vacancies and the neutral di-vacancy, which is composed of one cation and one nitrogen vacancy. This is analogous to previous work done by Grimes and Caltow[16] on fission products accommodation on UO_2. Results are given in table 6. Incorporation energies assume that the trap site is available for the fission product to occupy. As such it is not surprising that for all four materials studied the di-vacancy trap is energetically favored since this trap site provides the largest lattice space for Xe which is a large atom.

[16] R.R. Grimes and C.R.A. Catlow, Phil. Trans. R. Soc. Lond. A, 335, 609 (1991).

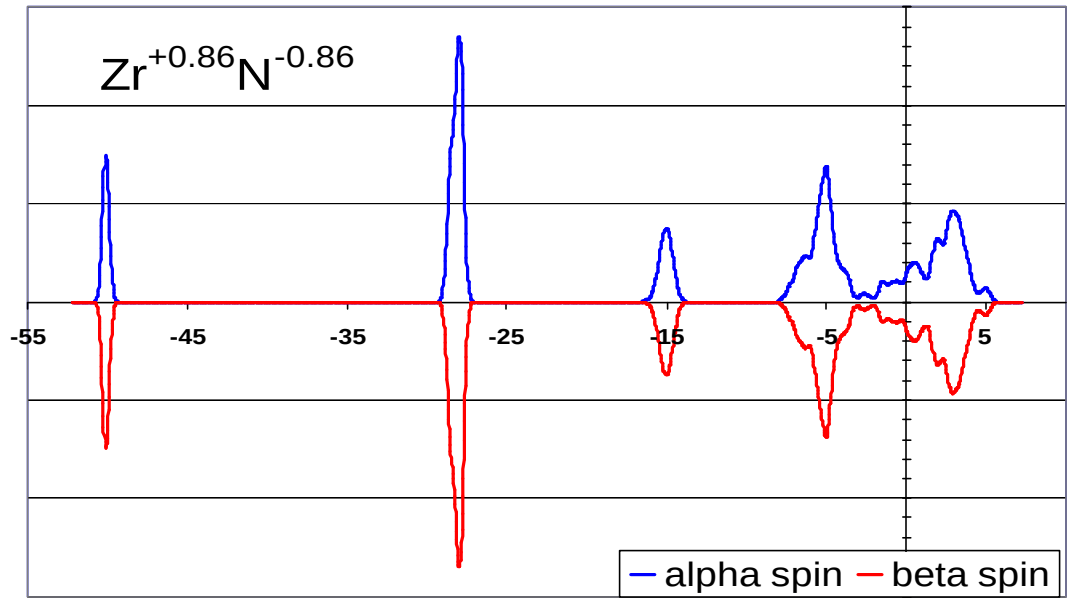

Figure 4-23. Predicted density of states for ZrN.

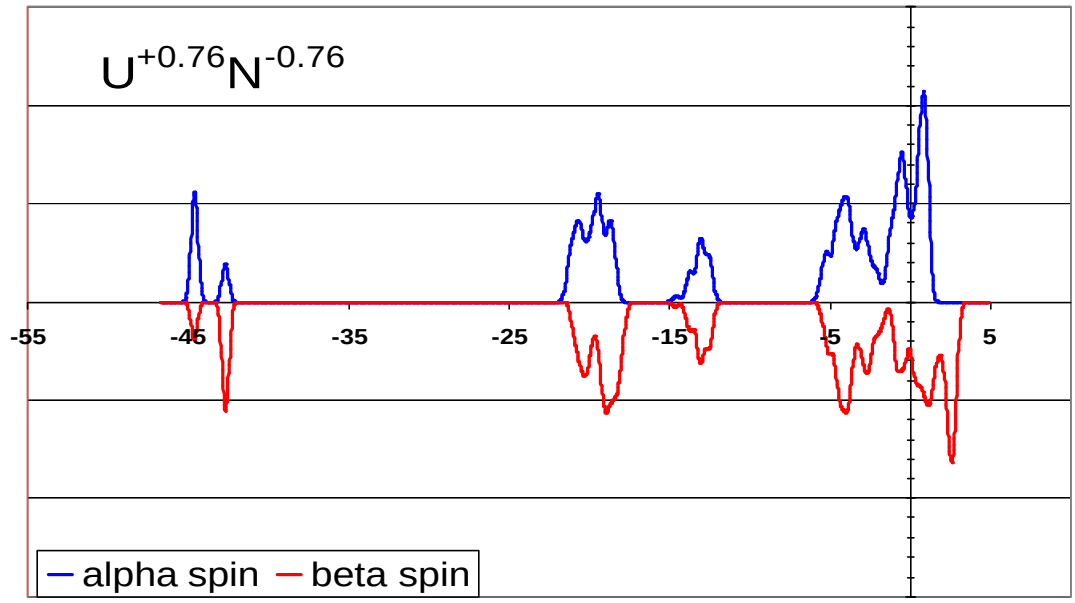

Figure 4-24. Predicted density of states for UN.

As the concentration of fission products increases there are no longer sufficient intrinsic trap sites for the fission product ions to occupy. Since we have previously shown that the intrinsic defect concentrations will be very low in these materials this will be the situation after a very short time. Thus, the fission product will occupy a trap site that must be formed specifically through the majority defect process, which for these materials is the Schottky reaction. We have therefore also calculated the internal energy for solution, which incorporates the trap formation. These are also presented in Table 6. Interestingly we now observe that the di-vacancy is no longer the favorable trap site but in all cases, it is the nitrogen vacancy. Nevertheless, the solution energies are high indicating that solution of Xe is a very unfavorable process

thermodynamically. Nevertheless, Xe may still be trapped due to a large kinetic barrier to migration (i.e. a high migration activation energy).

6. **Table** Incorporation and Equilibrium Solution Energy for Xe accommodation on CmN, UN, ZrN and TiN, from EM.

		Incorporation energy at pre existing site			Solution energy in equilibrium		
Material	**Lattice Parameter (Å)**	**Cation vacancy**	**Nitrogen vacancy**	**Di vacancy trap**	**Cation vacancy**	**Nitrogen vacancy**	**Di vacancy trap**
CmN	5.027 [17]	2.35	0.87	0.70	11.15	9.66	12.63
UN	4.98 [18]	2.40	0.92	0.74	9.75	8.27	11.14
ZrN	4.585 [19]	3.99	1.70	1.41	11.61	9.32	12.52
TiN	4.238 [20]	5.49	2.53	2.13	13.26	10.31	13.65

Having predicted the lattice structure and energy of TiN, calculations of non-stochiometric compositions have been initiated. These involve not only single unit cell and 1x1x2 repeat units (also mentioned in the last quarterly report) but the more computationally demanding 2x2x1 and 2x2x2 supercells. A parallel set of calculations has also been initiated for ZrN. These calculations are still ongoing and will be completed in the next quarter at which point we should be able to contrast changes in electronic structure with varying non-stochiometry in TiN (for which experimental data is available) and the diluant ZrN.

For additional information on this topic, please contact Robin W. Grimes (Imperial College of London) at

First principles calculations of Americium. Earlier, we had used results from state-of-the-art ab initio electronic structure calculations to develop a many-body modified embedded atom model (MEAM) potential. This is because there is limited amount of reliable experimental data for Am and the heavier actinides. Pure theoretical considerations based on state-of-the-art ab initio electronic structure calculations are therefore most desirable. This is a difficult task due to the strong 5-f electron correlation in the actinides, especially the later actinides as Am where the 5f electrons are believed to be localized.

In the present study we have incorporated the 5-f localization in Am via spin-exchange modeling, which, despite its unphysical long range magnetic ordering, can be seen as an approximation describing the main features of energetics such as bulk modulus and equilibrium volume. In order to impose the exchange split and localization, an external magnetic field was applied. However, during the refining of the MEAM potential, we realized that this applied field led to a small shift in the total energy that was slightly different for the different structures. This did not affect properties like the elastic constants and equilibrium volumes, but made the comparison in total energy between the different crystal symmetries uncertain. During this quarter we corrected this systemic problem and the erroneous data was recalculated. Table 7

[17] Y. Akimoto, J. Inorg. Nucl. Chem., 29, 2650-2652 (1967).
[18] H. Hollek, E. Smailos and F. Thuemmler, J. Nucl. Mat. 32, 281-289, (1969).
[19] N. Schoenberg, Acta Chem Scan. 8, 213-220 (1954).
[20] A.N. Christensen, Acta Chem. Scan. A. 29, 56-568 (1975).

shows the properties computed for bcc, fcc, and hcp Am structures, and Fig. 5-25 shows the energy versus volume curves for the same structures. Calculation of the dhcp structure is underway. We have to re-determine the MEAM parameters.

During this period we have also developed and debugged a new optimization code to determine MEAM parameters for a two-component Am-N and other systems for the next phase of this project. Our earlier code could only fit a one-component MEAM potential.

For additional information on this topic, please contact Anders M. Niklasson at amn@lanl.gov.

7. **Table** – Properties computed using ab initio method . The units are eV/atom, Angstrom, and GPa respectively for the cohesive energy, lattice constant and modulii.

	E_c	Lattice Constant	Bulk Modulus	$(C_{11}-C_{12})$	C_{44}	Vacancy Energy
bcc	6.282	3.798	40.52	--	--	1.27
fcc	6.301	4.802	32.62	17.55	0.033	--
hcp	6.313	a = 3.399, c/a = 1.611	--	--	--	--

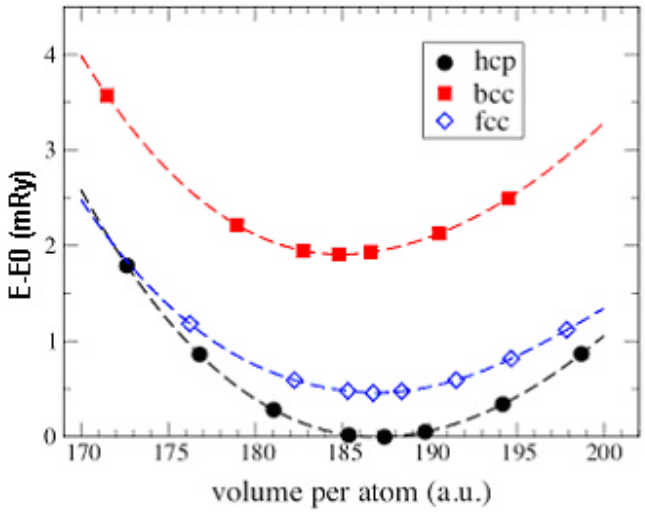

Figure 4-25. The energy, relative to the ground state EO, versus volume for bcc, fcc, and hcp Americium.

4.7 Series Two Metallic Fuel Development

The objective of the Metallic Fuel Development activities is the establishment of a metal alloy fuel option for transmutation in a series-two-type fast spectrum reactor or ADS. The metal fuel development activities involve fabrication and fabrication process development, characterization, and modeling. Non-fertile and Low-U compositions are being addressed, per the direction of the larger program.

Fabrication activities described in the five-year plan address two primary needs for the AFC and Generation IV programs: (1) development of fabrication processes that can be deployed for large-scale transmutation fuel manufacturing, and (2) fabrication of specimens suitable for irradiation testing, characterization and property measurement.

Characterization activities are intended to gather a working knowledge of the metal fuel alloy, and include studies of phase equilibria and melting temperatures, fuel/cladding interdiffusion behavior, and measurement of thermophysical properties.

Modeling activities will develop models and codes that predict fuel properties and behavior and collect property information into the AFC Fuels Handbook

4.7.1 Metallic Fuel Development Objective and Scope

Initial efforts, including those in FY 2003, are concentrated on providing small samples of metal fuels with well-characterized microstructures for irradiation testing. Experience gained in fabricating small samples will provide a basis for developing large-scale fuel manufacturing processes in subsequent years.

FY 2003 activities are narrowly focused on obtaining the information necessary for safety analysis of the AFC-1 and FUTURIX irradiation experiments. Specific objectives and milestones for FY 2003 are to complete fabrication of metallic fuel slugs and metallic and nitride test capsules for AFC-1 tests (fertile and non-fertile fuel).

4.7.2 Metallic Fuel Development Highlights

- Differential thermal analysis for samples of all compositions to be used in the AFC-1 irradiation test was performed. Most indicated phase transitions would be expected from assessment of relevant binary phase diagrams.
- Assessment of the microstructure of as-cast Pu-10Np-10Np-40Zr was conducted and compared with similar analysis results for as-cast Pu-40Zr, Pu-10Np-40Zr and Pu-12Am-40Zr. It appears that addition of Np to the Pu-Zr or Pu-Am-Zr alloys leads to formation of a second phase, of an MZr_2 type, in the (Pu,Zr) matrix phase.

4.7.3 Metallic Fuel Development Technical Summary

The metallic fuel development is primarily performed at ANL-W. The work in the first quarter primarily consisted of characterization activities on non-fertile fuel samples, as summarized below. For additional information contact douglas.crawford@anlw.anl.gov.

Thermal analysis runs on all AFC-1 fuel alloys were completed. Table 8 summarizes data from differential thermal analysis. Oxidation of the fuel alloys during the test prevented interpretation of mass change data.

8. **Table** – Summary of differential thermal analysis (DTA) data for AFC-1 fuel specimens.

Alloy	Event*	Assignment
Pu-40Zr	625°C	δ -> ε
Pu-12Am-40Zr	700°C	δ -> ε
Pu-10Np-40Zr		unknown
Pu-10Np-10Am-40Zr	500°C, 630°C	unknown
Pu-60Zr	600°C	α->ε

*average event temperature heating/cooling

Thermal analysis of Pu-40Zr and Pu-12Am-40Zr showed a single endothermic transformation on heating, corresponding to the transformation from the face-centered cubic δ-Pu solid solution to the body-centered cubic ε-Pu solid solution. This transformation was reversed on cooling and repeatable over a series of runs. The transformation was shifted to higher temperatures for the Am-bearing alloy. This behavior would be consistent with expansion of the δ-Pu phase field by Am stabilization, although this has not been experimentally verified. The Pu-60Zr alloy exhibited one exothermic transformation on heating, consistent with a transformation from the as-cast structure to the ε-(Pu,Zr) phase field. The Np-bearing alloys each exhibit two exothermic transformations on heating. Due to the complexity of the ternary and quaternary alloys system, it is not currently possible to identify the nature of these transformations; further investigations are under way.

Chemical and isotopic analysis necessary for reactor insertion was completed. Summary data are reported here in Table 9. These data represent averaged analysis for all specimens of a given composition.

9. **Table** – Summary chemical analyses data for AFC-1 fuel specimens

	Pu-60Zr	Pu-40Zr	Pu-12Am -40Zr	Pu-10Np -40Zr	Pu-10Am -10Np-40Zr
Total Pu	39.7	59.2	48.7	50.1	40.1
Zr	60.2	40.3	40.5	41	41.0
Np-237	-	<40	0.25	8.4	9.5
Am-241	-	0.3	11.9	0.23	10.8

Neptunium-bearing specimens experienced loss of neptunium due to 'sooting'. The high oxygen content of the only available metallic Np apparently resulted in oxide soot being deposited on the arc melter internals. Mass loss and chemical analysis data indicate that loss of americium was minimal during arc melting. Early on in the project, metallic fuel specimens were prepared by using powder metallurgical processing in an attempt to maintain low processing temperatures and prevent americium volatilization, since previous work with melt-casting for the X501 irradiation had resulted in high Am loss. This technique did not produce specimens with the desired low impurity content, and was abandoned in favor of arc casting for fabrication of AFC-1 test specimens. A macroscopic view of specimens produced by arc-casting are shown in Fig. 5-

26. The arc casting process uses a high current, low voltage arc to rapidly melt the sample charge; melt times are on the order of 10 seconds. A series of melts is used to homogenize the metallic alloy and to drop cast into a mold held below the arc melter hearth. Although melt temperatures are high, the short total melt times resulted in low losses of americium, based on measured mass losses during melting and chemical analysis of the cast fuel specimens.

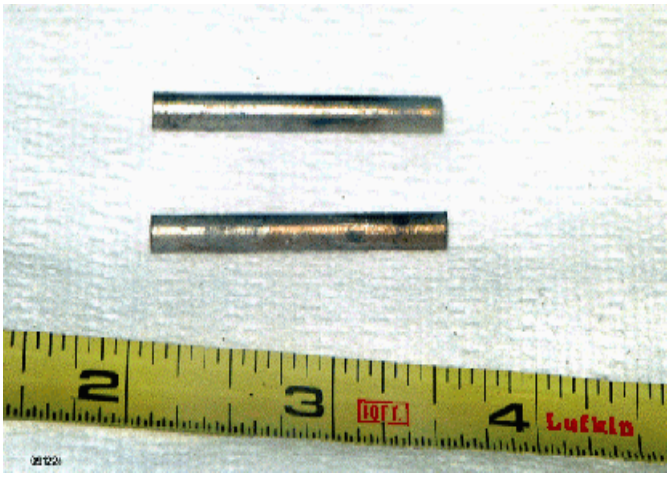

Figure 4-26. AFC-1 TRU fuel specimens fabricated by arc casting.

Figure 5-27 shows batched vs. analyzed americium content in Pu-Am-Zr fuel specimens. In all cases, the analyzed Am content is within the analysis error of the batched americium content for Pu-12Am-40Zr alloys. In the case of Pu-10Am-10Np-40Zr specimens, analysis results are skewed toward higher than batched Am contents. Work is continuing in an effort to reduce the measurement uncertainty in analysis of americium, which will be necessary to develop a fabrication process capable of the very low TRU losses required by transmutation objectives.

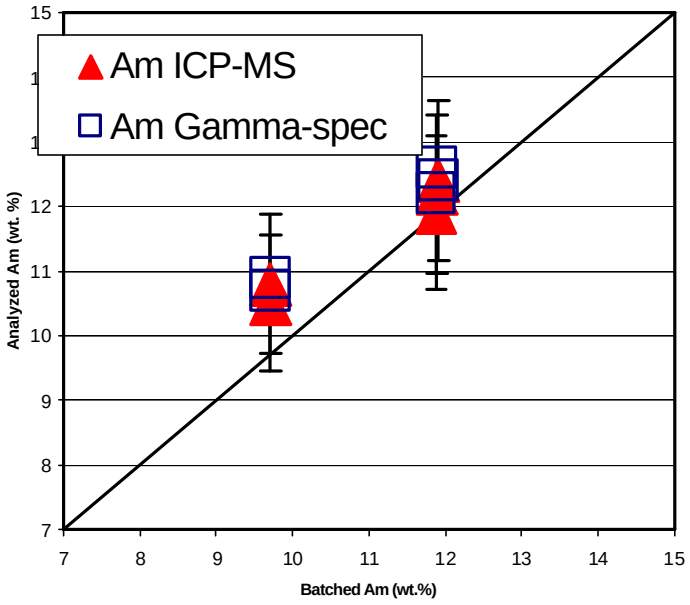

Figure 4-27. Am-loss data for Pu-12Am-40Zr fuel specimens.

Microstructural analysis of the AFC-1 Pu-10Am-10Np-40Zr alloy conducted late in FY02 is presented here. Two specimens have been analyzed using scanning electron microscopy (SEM) with energy-dispersive and wavelength-dispersive spectrometry (EDS/WDS). X-ray diffraction patterns have also been collected. The two samples that were analyzed are labeled MD21SEM1 and MD23SEM2. The charge materials for both fuel pins were melted using an arc-melting process, and the final rods were cast using quartz molds. The samples were transversely sliced from the as-cast rods.

Samples MD21SEM1 and MD23SEM2 exhibited some porosity, as shown in Fig. 5-28. Small pores were observed in the center of the samples, and larger voids were present along the circumference. The sample microstructures were comprised of a gray-contrast matrix phase and globular precipitates (see Fig. 5-29). This microstructure was observed throughout most of both samples. A few areas were found that were slightly enriched in actinides (see Fig. 5-29). An approximately 75-micron-wide band, along the outer edge of the samples, was observed to have a different microstructure, compared to the majority of the sample areas. In this region (see Fig. 5-30), a surface layer is present, along with a two-phase layer.

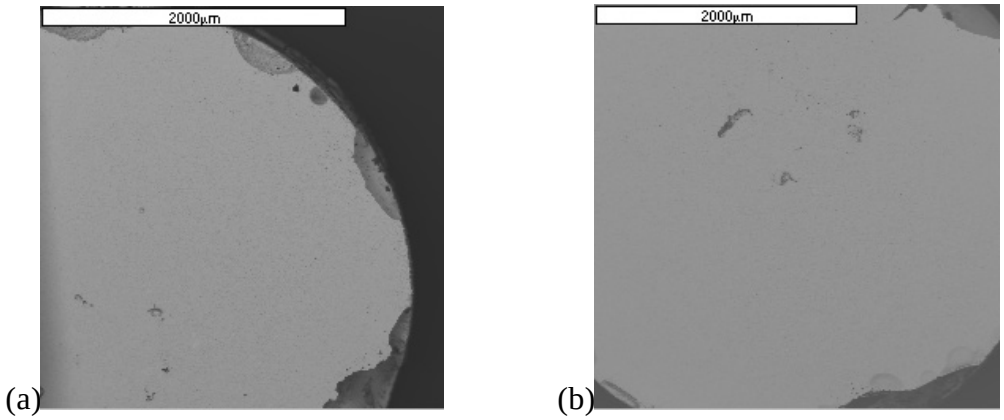

Figure 4-28. Backscattered electron micrographs (a) MD21SEM1; (b) MD23SEM2.

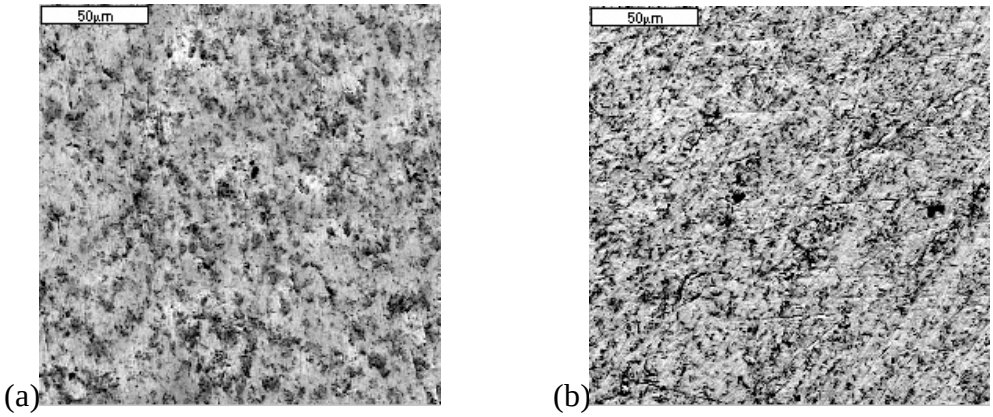

Figure 4-29. SEM micrographs of the microstructures (a) MD21SEM1 and (b) MDSEM2. The bright contrast areas are slightly enriched in actinides.

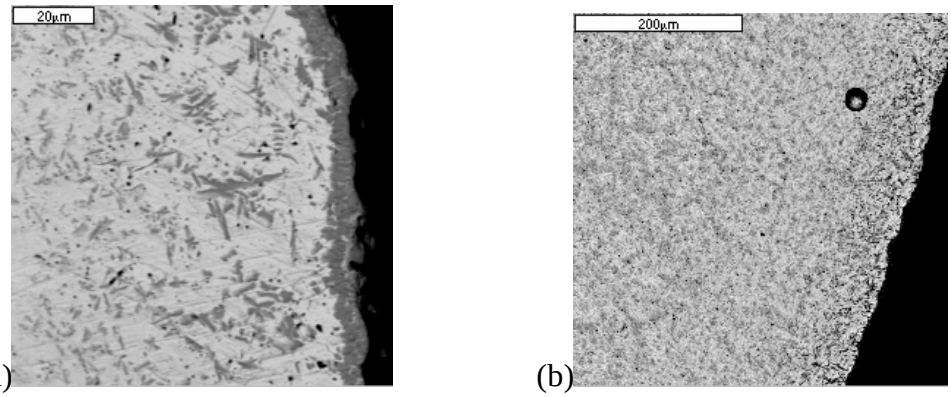

(a) (b)

Figure 4-30. SEM micrograph of the microstructure observed in the outer region of samples (a) MD21SEM1 and (b) MD23SEM2.

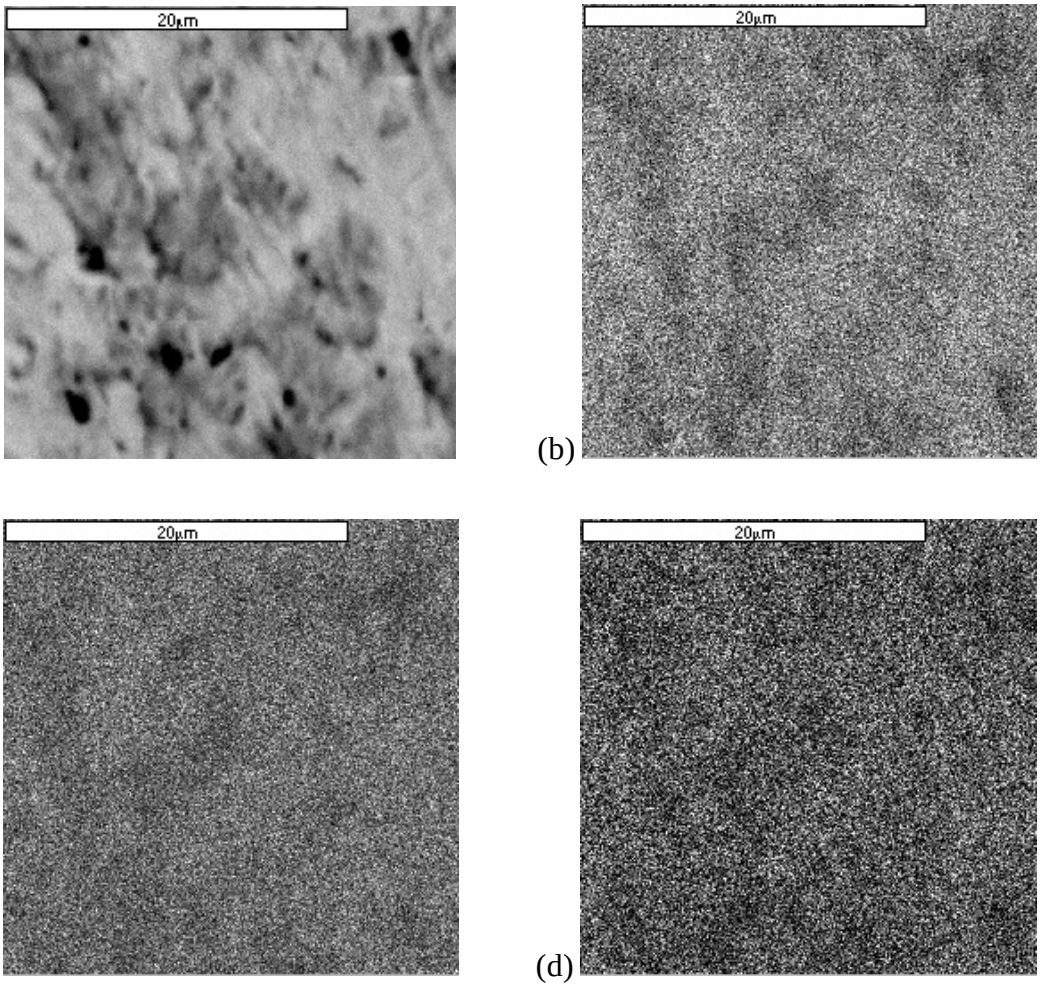

(a) (b)

(c) (d)

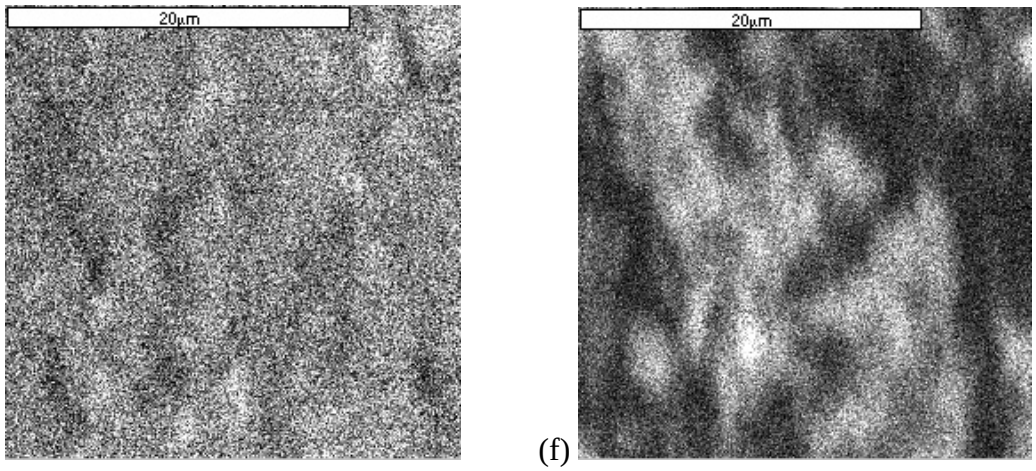

Figure 4-31. (a) A backscattered electron image of sample MD23SEM2 along with X-ray maps for (b) Pu; (c) Np; (d) Am; (e) Zr and; (f) O. Pu, Np, Am, and Zr are generally well distributed throughout the alloy. Some oxygen- and zirconium-enriched phases are observed. Some of the dark areas in (a) are pores.

X-ray maps were taken of different regions of the alloy microstructure. Figure 5-31 shows X-ray maps for the general microstructure for sample MD23SEM2. This same microstructure and elemental distribution was observed for sample MD21SEM1. Figure 5-32 shows X-ray maps taken in the outer region of sample MD21SEM1.

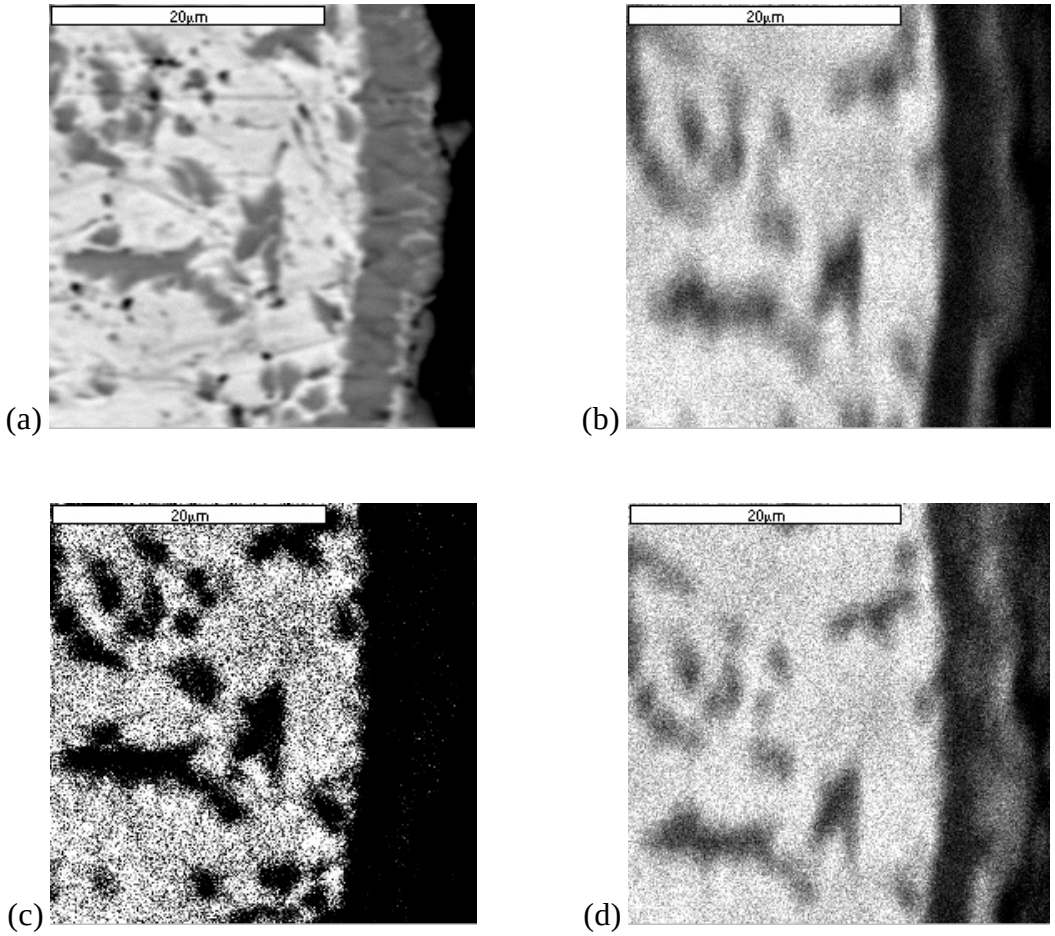

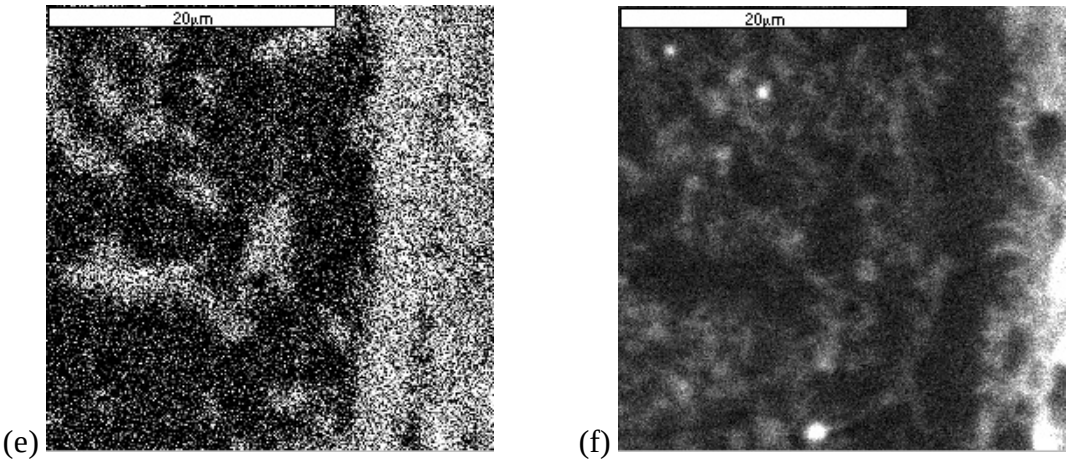

(e) (f)

Figure 4-32. (a) A backscattered electron image taken at the outer surface of sample MD21SEM1 along with X-ray maps for (b) Pu; (c) Np; (d) Am; (e) Zr; and (f) O.

The alloy constituents were generally distributed uniformly throughout both samples. A few areas were found that were slightly enriched in actinides and zirconium. Some oxygen-enriched phases were observed in the sample microstructures. The oxygen-enriched phases most likely developed as a result of the oxygen that is present as an impurity in some of the charge materials. The Zr-enrichment observed in the X-ray maps suggests the possible presence of a precipitate phase that is enriched in Zr, along with a matrix phase that contains less Zr. This observation agrees with the X-ray diffraction data. Based on these data, the microstructure of a Pu-40 Zr-10 Np-10 Am alloy appears to consist of Pu and an MZr_2-type phase.

The microstructure of a Pu-40 Zr-10 Np-10 Am alloy is most similar to the one observed for a Pu-40 Zr-10 Np alloy. Both matrix and precipitate phases can be identified in each of these alloys, whereas in as-cast Pu-40 Zr and Pu-40 Zr-12 Am alloys, only a single phase comprises the alloy microstructure.

Summary x-ray diffraction (XRD) data for all AFC-1 metal fuel alloys in the as-cast state is presented in Fig. 5-33. Data for AFC-1 alloys based on microscopy and XRD is summarized in Table 10. Pu-40Zr and Pu-12Am-40Zr alloys contained only a face-centered cubic δ-phase Pu-Zr solid solution. This is to be expected, as both Am and Zr are known to be strong δ -Pu stabilizers. Pu-60Zr alloys contained the α-(Zr,Pu) hexagonal solid solution phase in the as-cast condition, indicating that the rapid cooling conditions resulted in a non-equilibrium microstructure. Pu-10Np-40Zr alloys and Pu-10Am-10Np-40Zr alloys were found by x-ray diffraction to contain both a δ-phase solid solution phase and an MZr_2 phase.

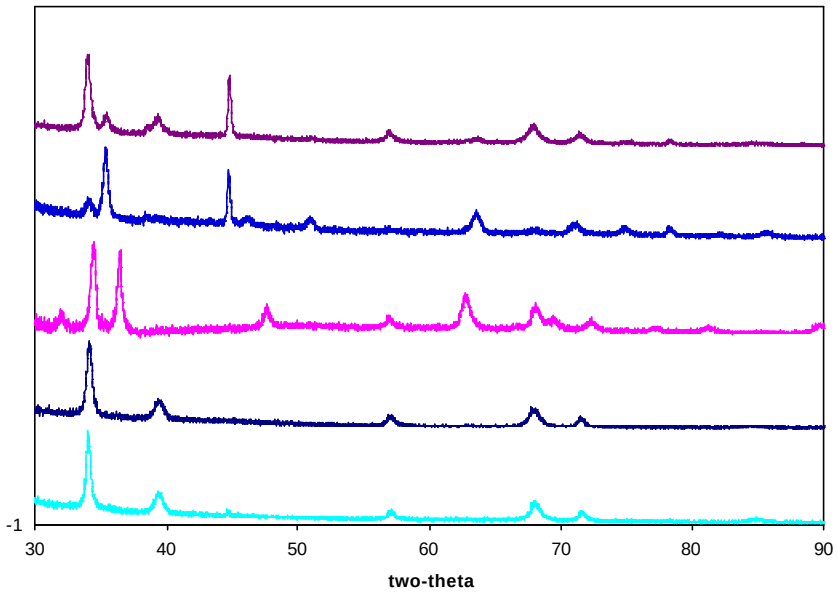

Figure 4-33. Metal alloy XRD patterns. Top to bottom; Pu-10Am-10Np-40Zr, Pu-10Np-40Zr, Pu-60Zr, Pu-12Am-40Zr, Pu-40Zr.

10. **Table** – Summary characterization data for AFC-1 metallic fuel alloys.

Alloy	SEM (phases)	XRD	Density (g/cm^3)
Pu-40Zr	1	δ-(Pu,Zr)	10.1
Pu-12Am-40Zr	1	δ-(Pu,Zr)	9.9
Pu-10Np-40Zr	2	δ-(Pu,Zr) + MZr_2	10.3
Pu-10Np-10Am-40Zr	2	δ-(Pu,Zr) + MZr_2	10.1
Pu-60Zr	2-3	α-Zr	8.5

Assembly and annealing of diffusion couples composed of 422 stainless steel (representative of HT-9 cladding alloy) against AFCI fuel compositions have been assembled and annealed and are awaiting microstructural characterization.

4.8 Series Two TRISO Fuel Development

Advanced TRISO fuels can be used in gas-cooled systems. They are of interest for a deep burn application, especially for fuels containing plutonium. Inclusion of minor actinides in this fuel type may also have practical transmutation implications if used in gas-cooled epithermal or fast reactors, which are being considered as part of the transmutation strategy in Series Two. TRISO fuel particles are also of interest for the Very High Temperature Gas-Cooled reactors (VHTGR).

Zirconium carbide-based coating systems have the potential for operation at higher temperatures and for more effective retention of silver and palladium fission products. These characteristics make ZrC of interest to both the VHTR and to transmutation fuels with Pu and other transuranic elements in the kernel. Titanium nitride coating systems have potential application to gas-cooled fast-spectrum reactors, and may have applications to the VHTR and transmutation systems. Advanced kernel chemistries such as oxycarbides and carbides offer potential performance advantages while high-density nitride and oxide kernel formulations are of interest to fast spectrum gas–cooled reactors. Irradiation testing of advanced TRISO fuels will provide scoping evaluations of the irradiated performance of advanced coating/kernel uranium fuels with testing for fission product release at temperatures above 1600°C in existing fuel testing apparatus. Advanced coated particles will be fabricated, compacted, and shipped to INEEL for irradiation in ATR (AFC-2). TRISO coated particles with kernels containing Pu and Np, and no U, are of interest for fast spectrum gas-cooled reactors and for deep-burn transmutation designs of thermal gas-cooled reactors. Such coated particles have never been fabricated, nor characterized, and may require dimensional modifications to the kernel, the buffer layer, and the coating layers for optimal performance. This series of activities would establish kernel fabrication and coating equipment in a plutonium glovebox facility, develop and demonstrate the chemistry of the gelation process for Pu/Np kernel fabrication, design and fabricate Pu/Np fuel (with either advanced or standard coatings systems) and perform out-of-core characterization and testing of the fuel by 2007.

The major milestone is to develop a performance package by FY 2007 to support the technology selection. Intermediate milestones include:

Start the Pu kernel development.	FY 2005
Start the fuel irradiation tests.	FY 2005
Perform out-of-core characterization and testing of fuel (AFC-2)	FY 2007

4.8.1 Objective and Scope for Series Two TRISO Fuel Development

In FY 2003, kernel fabrication and advanced coating technologies will continue to be developed. As part of the kernel fabrication task, uranium oxide kernel fabrication will be performed for support of research tasks on advanced coating and advanced characterization methods. The evaluation and testing of the advanced kernel fabrication methods include (a) microwave methods that eliminate the use of solvents, and (b) materials to produce oxy-carbide, carbide and nitride kernels for evaluation as candidates for Generation IV reactors.

For coating technologies, this activity includes completion of a coating laboratory at ORNL, and fabrication of uranium oxide particles for use as a reference fuel for quality control (QC) and characterization studies. These particles will also be used for defining reference coating conditions for dense kernels. The FY 2003 scope also includes the installation of auxiliary equipment and development of process techniques for applying advanced coating zirconium carbide titanium nitride (ZrC, TiN) in existing labs with existing coatings.

The above fabrication tasks are performed primarily by ORNL. In addition, General Atomics (GA) will support the TRISO fuel work by preparing a test specifications document for the initial irradiation of coated TRISO fuels and developing ZrC coatings. GA will continue the technology transfer for fuel design and fabrication to ORNL.

The major FY 2003 milestones include:

- Fabrication of 1 kg of UO_2 kernels.
- Fabrication of 100 g of UO_2 particles with reference coating.
- Fabrication of coated particles with advanced coating system.
- Design methods, analyses and test specifications for the TRISO fuel.
- Fabrication of advanced oxycarbide, carbide and nitride kernels.
- Characterization for Series Two advanced coatings
- Formulation of an accident evaluation model.

4.8.2 Highlights for Series Two TRISO Fuel Development

The following are the major first quarter highlights for the Series Two TRISO fuel development activities:

- 750g of dried and calcined uranium oxide gel-spheres was made for use in fuel development.
- The laboratory for coating uranium-containing fuel was operated with surrogate materials until coordinated experimental plans for uranium coating are established. Work on nitride coating in support of GENIV and I-NERI activities continued in the surrogate laboratory.
- ORNL has developed draft plan for TRISO fuel development that makes optimum use of existing capabilities to support a 2007 downselect. The Deep Burn Fuel Development Plan was issued by General Atomics to the AFC program.

4.8.3 Technical Summary for Series Two TRISO Fuel Development

Technical summaries are provided below for the following activities:

- Uranium Kernel Laboratory;
- Coating Laboratory and Development; and
- Fuel Design and Development

For additional information on these activities, contact David Williams (ORNL) at williamsdf2@ornl.gov .

Uranium Kernel Laboratory. The scope of the Uranium Kernels Lab activity is to establish uranium-kernel fabrication by internal gelation in existing facilities by minor modifications and additions to existing equipment. This activity will produce limited amounts of uranium kernels for programmatic purposes. Additional depleted uranium oxide gel-sphere runs were conducted. The gelation apparatus and dried kernel product is shown in Fig. 5-34. Improved operation was achieved with more precise capillaries used for drop formation.

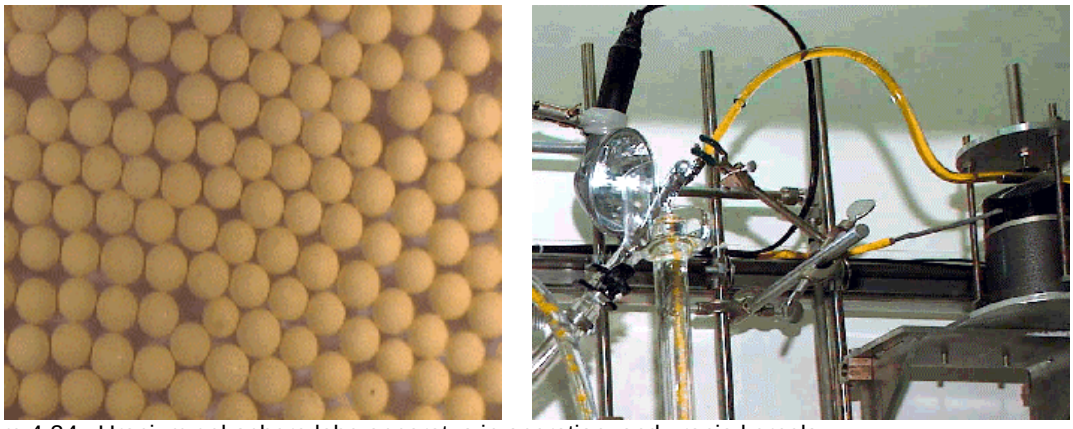

Figure 4-34. Uranium gel-sphere labe apparatus in operation, and urania kernels.

Coating Laboratory and Development. The scope of the Coating Lab activity is to establish a laboratory for sintering, coating, and primary characterization of uranium-bearing TRISO-coated particles. The scope of the coating development is to support process optimization, advanced coating studies, and materials characterization in existing equipment that is limited to analysis of non-radioactive surrogate particles. The coating in the uranium coating lab was used to benchmark and shakedown these new systems. New coating development work was focused on nitride coatings in the surrogate coating lab. A photograph of TiN coated particles is displayed in Fig. 5-35. The details of this work are reported in the I-NERI project. The AFCI program has established the capability and primary equipment to pursue the nitride coating development.

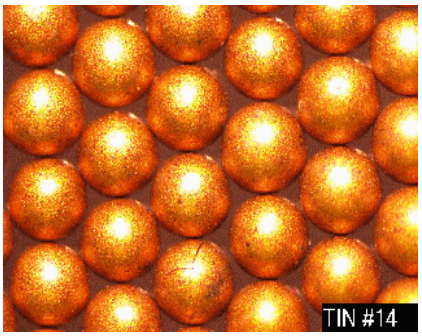

$$2\ TiCl_4 + N_2 + \text{excess } H_2 \rightarrow$$

$$2\ TiN + 8\ HCl + \text{excess } H_2$$

Figure 4-35. 500 micron TiN coated particles made in the surrogate coating lab.

Fuel Design and Development. A re-planning activity was performed. A basis for future work assumes the ongoing kernels glovebox lab (including sintering) can be completed within current budget constraints, and additional high-alpha capability can be added as needed in a stagewise approach. Activities are also based on using a high-alpha glovebox capability for making kernels

in conjunction with normal radiochemical labs for coating (e.g., hoods), in an optimal fashion. Optimal coordination with other DOE programs is also assumed. The development of advanced fuel coatings (e.g., ZrC) for very high-temperature service and transmutation applications that require improved noble metal retention/resistance is to be supported by the AFC program. Conventional SiC -TRISO will be fabricated as a baseline for comparison.

A technical strategy was developed based on the following arguments:

1. Oxygen release from high-burnup TRU fuels is significantly higher than in U-fuels. Oxygen control strategies, such as the UO_2* design (Journal of Nuclear Materials 115, p.69) will be tested for suitability in TRISO-based transmutation. These fuel designs are attractive for high burnup applications, and apply to most all oxide kernels, regardless of actinide composition. This greatly simplifies the kernel chemistry requirements and development needs. Similar stratetgies using SiC dispersed in low-density carbon layers have been evaluated for chemical trapping of the corrosive Pd fission product (Journal of Nuclear Materials 246, p.215).
2. The demands of developing a getter-layer for oxygen (or Pd) are expected to be less than development of a very high performance ZrC barrier layer to replace SiC. The infrastructure needed to pursue getter and barrier layer development is about the same. Therefore the development of ZrC as a getter layer will be pursued first. Out-of-pile testing of unirradiated fuel will be used to supplement the evaluation of advanced coatings.
3. Because of the limitations imposed by safe handling of radiotoxic materials, it is expected low-activity diluents (e.g., Zr, U, U-235, Th) will be used in this work. These constituents will be used as necessary to best approximate the transmutation fuel requirements. Representative amounts of Np-237 can be used in the smallest coating batches (25 grams heavy metal) and smallest compacting batch (~ 1 gram heavy metal). A limited amount of Pu- and Am-bearing kernels can be blended in with less hazardous kernels to permit a “seeded”, or sparse, coating fabrication. Sorting out the minor actinide bearing TRISO will permit unbonded irradiations of small amounts of fuel for basic screening of high-burnup designs. Further consultation with ORNL safety experts are needed to establish the limits of this type of operation. This strategy is depicted in Figure 5-36.

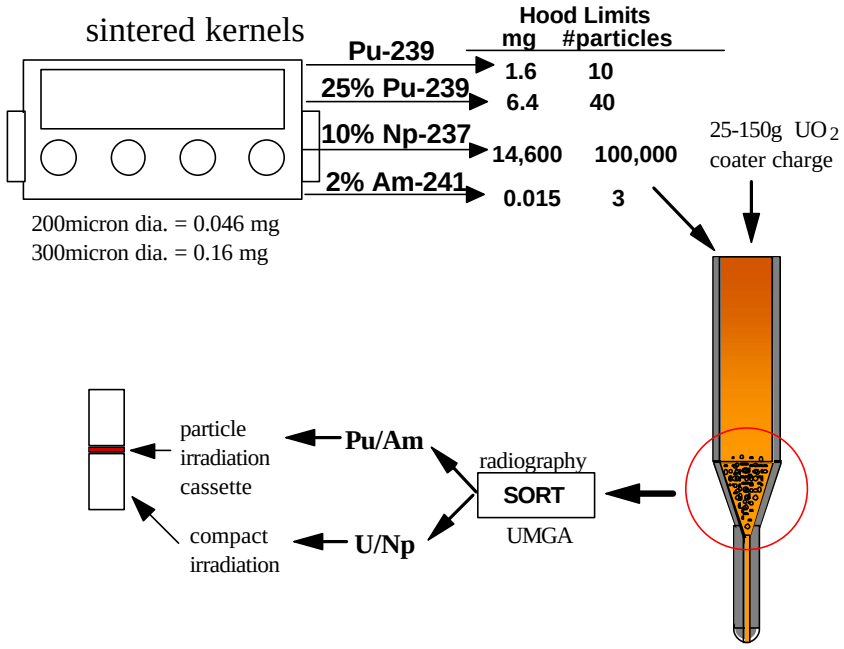

Figure 4-36. Sparse TRISO Fabrication Strategy.

4.9 Series Two Advanced Fuel Forms

Fuel forms will be assessed and feasibility studies will be conducted for the most promising candidates. Dispersion fuels of several metallic and ceramic matrix materials and a few solid solution materials will be evaluated. The goal is to narrow the list of candidates to two and perform initial scoping studies by the end of FY 2003.

Subsequent efforts will be focused on a few selected forms and will require some initial scoping tests. Special tests may be designed and fuel samples may be included in the AFC-1 through AFC-5 test series discussed previously. The development of advanced fuel concepts will be performed in collaboration with international partners. U.S. efforts in selected fuel forms will likely complement and supplement similar international efforts in order to maximize the benefits of mutual research and reduce the development time period.

As Generation IV fuel development needs are defined, they will be developed within the framework for this activity.

The major milestones for this activity include:

Develop advanced fuels testing plan.	FY 2004
Identify and develop (to the point of proof-of-principle) high-risk but large payback innovative fuel concepts.	FY 2007

4.9.1 Objectives and Scope for Series Two Advanced Fuel Form Development

Work under this activity includes an assessment of innovative fuel forms which hold the potential for increased efficiency and reduced overall cost in processing, transmutation, and recovery.

For the case of micro-structured fuels, a more detailed assessment will be performed. This task will investigate fuels manufactured to contain micron-sized fissile material structures (e.g., spheres or cylinders) spaced uniformly in matrix materials. Such structures will allow most fission product fragments to escape from the fissile material and come to rest in the matrix material. After a period of irradiation, separation of the fissile material from the matrix containing the embedded fission products will allow an efficient partitioning of the bulk of the fissile material from the fission products. The fissile material could then be reused by incorporating it into new micro-structured fuel. Efficient separation of the fissile materials from the fission products using this technology could greatly reduce costs for an advanced fuel cycle as compared to aqueous or pyrochemical separation methods.

4.9.2 Highlights for Series Two Advanced Fuel Form Development

The following are the major highlights for the first quarter advanced fuel form development activities:

- A patent disclosure on the microstructured fuels concept was submitted to the Laboratory's Patent Committee. The DOE has decided to pursue a patent application and this task is in progress.

- NiAl single crystal irradiation studies using RBS/C showed no amorphization under cryogenic temperatures up to 10^{14} Xe/cm^2. At higher fluences the rate of damage accumulation decreased dramatically.

4.9.3 Technical Summary for Series Two Advanced Fuel Form Development

The technical summary for advanced fuel form development is provided for the following two activities:

- Microstructured fuels
- Radiation Damage Evolution in NiAl Single Crystal

Microstructured Fuels. Fuel structures are under investigation that would allow some separation of fission products from the fissile material during burn-up. This could allow a much cheaper separation of the fission products and fissile material after the fuel is removed from the power system and allowed to cool. A patent disclosure on the microstructured fuels concept was submitted to the Laboratory's Patent Committee. The DOE has decided to pursue a patent application and this task is in progress.

Preliminary neutronics calculations were done on one of microstructured fuel concepts using the MCNPX code. The results confirmed the viability of the fuel concept, but also identified a number of deficiencies in the code for modeling fission products. Future work will look at modifications to the MCNPX code to improve the fission product modeling and give a more complete simulation of the microstructured fuels.

Because the patent application is under review, further technical data cannot be disclosed in this quarterly report. For additional information, the reader is referred to Gordon Jarvenin at gjarvenin@lanl.gov .

Radiation Damage Evolution in NiAl Single Crystal. This quarter, radiation damage studies were initiated on NiAl, a proposed matrix for dispersion fuels. Our goal was to assess radiation damage accumulation and the propensity for amorphization in this matrix material.

A single crystal NiAl sample was irradiated under cryogenic conditions (~100K) with 450 keV Xe^{++} ions to fluences of $1•10^{13}$, $5•10^{13}$, and $1•10^{14}$ Xe/cm^2. The (110)-oriented single crystal NiAl target was tilted 7° from normal incidence with respect to the Xe^{++} ion beam, in order to avoid channeling effects during implantation. Figure 1-37 shows Rutherford backscattering/ ion channeling (RBS/C) spectra obtained from unirradiated NiAl (in a channel-oriented and random geometry with respect to a 2 MeV He^+ beam) and from Xe^{++} ion irradiated NiAl to the fluences described above. The results reveal (1) that single crystal NiAl is not amorphized under cryogenic Xe^{++} ion irradiation conditions, at least to a fluence of $1•10^{14}$ Xe/cm^2 (otherwise, the damage peak, beneath the surface scattering position for Ni, would have reached the "random" level (the blue curve)); and (2) the rate of damage accumulation was observed to decrease dramatically with increasing fluence. With regard to the latter finding, the damage remained almost unchanged between fluences $5•10^{13}$ and $1•10^{14}$ Xe/cm^2. In other words, retained damage remained constant even though the ion dose was doubled. This result is very unusual, though it was observed in earlier ion irradiation damage studies on single crystal NiAl by Thomé et al.[21]

[21] L. Thomé, C. Jaouen, J. P. 'Rivière and J. Delafond, Nucl. Instr. and Meth. B 19/20 (1987) 554-558.

Our results to date are in very good agreement with the results published by Thomé et al., as illustrated in Fig. 5-38. However, the reasons for the deceleration of radiation damage accumulation and even the decrease in damage observed by Thomé et al. is not understood at this time. Experiments using TEM are planned to elucidate these effects.

For additional information on this topic please contact Kurt Sickafus at kurt@lanl.gov .

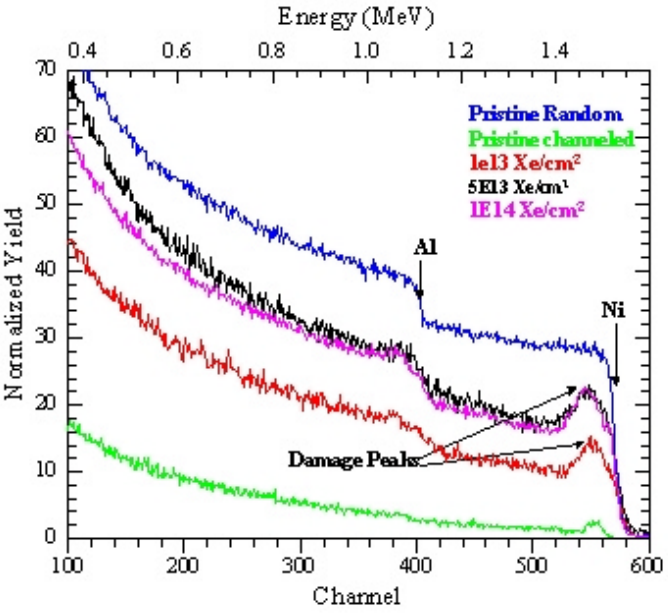

Figure 4-37. 2 MeV He^{+} Rutherford backscattering/ion channeling (RBS/C) spectra obtained from unirradiated single crystal NiAl in a random orientation (blue spectrum) and in an (110) channel orientation (green spectrum), and from channel-oriented Xe^{++} ion irradiated NiAl to the fluences $1*10^{13}$ (red) $5*10^{13}$ (black) and $1*10^{14}$ Xe/Cm^{2} (pink).

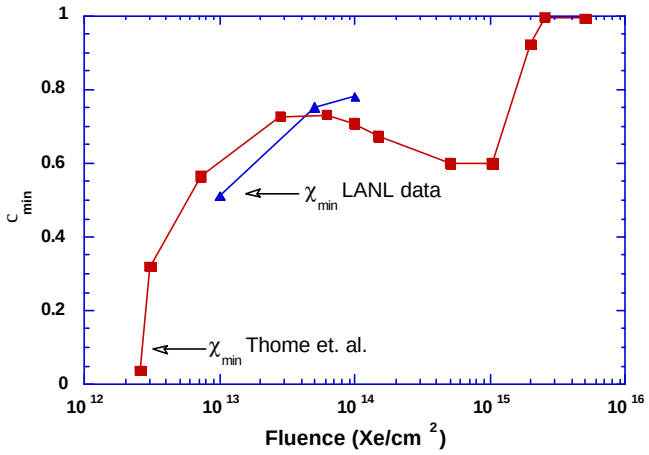

Figure 4-38. Comparison between the damage accumulation factor, cmin, for RBS/C data obtained by Thomé et al. on 360 keV Xe^{++} ion irradiated NiAl at 90 K versus our (LANL) data obtained following irradiation with 450 keV Xe^{++} at 100K (LANL χ_{min} values obtained from the RBS/C data in (a) χ_{min} is defined as the ratio between the RBS/C peak height at the peak damage backscattered energy position (for the backscattered He^{+} ions), versus the RBS peak height in the random orientation for the same backscattered He^{+} energy position.

4.10 Series Two ATR Irradiation Experiments

With the exception of TRISO fuel (which has applications in deep burn epithermal gas cooled reactor), all other Series Two transmutation fuel types are developed for fast spectrum systems. At present, the U.S. emphasis on metal and nitride fuels which are either fertile-free or with low-fertile content. Because, there is no fast spectrum irradiation capability in the U.S., initial screening tests for these fuels will be performed in thermal reactors (ATR). Such thermal spectrum irradiation will not only provide some initial data for fuel behavior but is also a pre-requisite for subsequent fast spectrum irradiation.

4.10.1 Objectives and Scope for Series Two ATR Irradiation Experiments

Tests of metal and nitride fuels (in ATR) are required in order to assess fuel performance. Series Two fuels for Generation IV transmutation applications will be subject to high burnup irradiation testing to assess the transmutation potential. Developing a database of irradiation behavior is therefore the key component of the near–term fuel development program. Irradiation performance data will be combined with physical, thermal, and chemical property data to develop models leading to a better understanding of the complex behavior of these fuels.

The AFC-1 test series will include samples of metal and nitride fuels containing plutonium, americium, and neptunium. Uranium contents in the test fuel will reflect the range of uranium contents being considered for different transmutation scenarios. This initial series of screening tests will provide initial fuel behavior information and identify potential life-limiting phenomena to be addressed with further design and performance assessment. The Series Two tests are expected to continue through FY 2007 as additional fuel design parameters and compositions and notable performance phenomena are evaluated. It is likely that some of the AFC-1 test capsules will be irradiated to provide irradiated test samples for later safety-related transient testing. The specific FY03 milestones are given below:

Complete fabrication of fuel capsules for AFC-1 (a-d) tests (non-fertile metallic and nitride fuel).	March 2003
Initiate AFC-1 irradiation test in ATR.	April 2003
Complete fabrication of fuel capsules for AFC-1 (e-f) tests (fertile metallic and nitride fuel).	September 2003
Complete safety documentation and approval for the AFC-1 (e&f) tests	September 2003

4.10.2 Highlights for Series Two ATR Irradiation Experiments

The following are the major highlights for the Series Two ATR irradiation experiments:

- Twelve plutonium and minor actinide-bearing metal fuel slugs were encapsulated and welded in HT-9 cladding for the AFC-1 fuel irradiation test in the ATR.
- The AFC-1 Experiment Fabrication Control Plan was reviewed and revised.
- Construction of the AFC-1 irradiation test outer capsule welding station was completed. The AFC-1 capsule weld process specification was qualified and approved by the INEEL welding engineer for insertion in the ATR. The process and equipment used to fill the

AFC-1 outer containment with helium was validated. All process trials resulted in > 99.5% helium gas purity within the capsule, exceeding the capsule specification of 97%.

- The neutronic analyses were completed with the final pellet compositions to assure the design linear heat generation rates could be provided.
- The experiment safety assurance package (ESAP) was drafted and will be completed when final analysis information is available.
- Material was procured for fabrication of the thermal neutron shield that will surround the test capsules. These materials are borated aluminum, cadmium, and aluminum alloy. The preliminary designs for utilization of these materials were completed for the ATR and the ATRC.
- The 6M drum for shipment of the rodlets from ANL-W to ATR was delivered to ANL-W.
- The experiment capsule handling tool and transfer buckets were fabricated. Operator training for using the handling tool has been completed.
- The physics analysis required to specify enrichment for the fertile fuel pellets to be used in the capsules AFC-1E and AFC-1F, as well as other tasks necessary for insertion of the capsules in the ATR are delayed until funding is available.

4.10.3 Technical summary for Series Two ATR Irradiation Experiments

The technical summary for the Series Two fuel irradiation experiments activities in the first quarter are provided for the following sub-tasks:

- Test Capsule Fabrication for AFC-1; and
- AFC-1 test analyses and preparations.

Test Capsule Fabrication for AFC-1. The fuel rods and the test capsule are fabricated at ANL. For additional further please contact douglas.crawford@anl.gov .

- Twelve plutonium and minor actinide-bearing metal fuel rodlets were encapsulated in HT-9 cladding for the AFC-1 (formerly ATW-1) fuel irradiation test in the ATR. The fuel specimens were successfully decontaminated and transferred out of the Casting Laboratory glovebox into the Fuel Manufacturing Facility for radiography and encapsulation into outer capsules.
- Radiography of AFC-1 metal fuel specimens was completed following resumption of operations in the Fuel Manufacturing Facility (Bldg. 704). Radiographs revealed two fuel specimens with defects in the top endplug welds. These specimens were returned to the Casting Laboratory glovebox for rework.
- Fuel rodlet welding process qualification trials in the Casting Laboratory (CL) plutonium glovebox revealed that inconsistent welds resulted after moving the equipment into the CL glovebox. A new parameter set for fuel closure welding was developed in the CL glovebox. A qualification set was welded and destructively examined, verifying that weld parameters are now acceptable. The Welding Procedure Specification was updated and personnel requalified on the new procedure.

- Construction of the AFC-1 irradiation test outer capsule welding station was completed. The AFC-1 capsule weld process specification was qualified and approved by the INEEL welding engineer for insertion in the ATR. The procedure used to fill the AFC-1 outer containment capsule with helium was validated. All process trials using this procedure resulted in >99.5% helium fill gas purity within the capsule, exceeding the capsule specification of 97%.
- The AFC-1 Fabrication Control Plan was revised and updated. This document serves as the primary vehicle for communicating fabrication process details and QA controls to the ATR.
- Review of LANL's QA plan for AFC-1 rodlet fabrication continued. The ANL QA plan for fabrication of AFC-1 test fuel is the QA plan that is approved by the ATR organization, and it calls for ANL approval of the LANL QA plan for fabrication of the nitride test pellets.

AFC-1 test analyses and preparations. The following tasks are performed at INEEL. For additional information, please contact Richard Ambrosek at rga@inel.gov .

- Two approaches are being pursued in the fabrication of baskets for the AFC-1 irradiation program, one using borated aluminum, and one using a cadmium shield in an aluminum sleeve.
- Following unsuccessful attempts by the vendor to extrude the borated aluminum basket/neutron shield, a decision was made to extrude solid rods and then drill the rods to form the basket/shield. The rods were successfully extruded, and following initial unsuccessful by the vendor to drill the borated aluminum (the material fractured), a different drill bit was procured and the vendor was able to successfully complete a demonstration fabrication. The task is currently on hold pending final cost estimates and receipt of funding.
- To insure against delays in fabrication of the borated aluminum basket/shield, a second path to basket/shield fabrication is being pursued in parallel. Alternative materials for the neutron shield were evaluated while attempts to fabricate the borated aluminum were in progress. Physics evaluations indicated that an aluminum-sheathed cadmium sleeve would provide the performance required by the test. A preliminary design was generated and materials were procured. The preliminary design for the ATRC (ATR critical facility) and ATR cadmium baskets is shown in Figures 5-39 and 5-40.
- The fission heating rates for the pellet compositions and irradiation axial position are shown in Table 11 and Table 12. The isotopics for the analysis are shown in Table 13 and Table 14.
- Approval of the ESAP (Experiment Safety Assurance Package) will require that a plan be in place identifying cadmium disposition from start to finish (irradiated cadmium is a mixed hazardous waste). Preliminary evaluations of activity level have been performed and the evaluations for identifying a waste stream are in progress.
- A test plan for the ATRC measurements was prepared. The plan incorporates the required measurements for AFC-1 in the ATRC facility. The delays in the fabrication of the basket/shield resulted in the delay of the ATRC tests. Because of this, the required

data for the ESAP to support a March insertion in the ATR will not be available early enough, and insertion in the ATR was postponed until May 2003 (the next scheduled ATR shutdown after March). The analyses show that the desired burn-up for the low burn-up capsules (AFC-1A and AFC-1B), can be obtained in two ATR nominal power cycles; the low burn-up tests support the scheduled Phénix irradiation. A May insertion in the ATR ensures that the low burn-up tests will be completed prior to the ATR core internals changeout (CIC) currently scheduled for February 2004. The desired high burn-up levels will require five nominal power cycles; these data will support fuel development efforts, but are not needed in support of the Phénix irradiation. A delay of one cycle to the scheduled CIC is being pursued to allow completion of the high burn-up tests prior to CIC.

11. Table –The linear fission heat rate and burnup distribution of the proposed AFC-1 fuel at the East flux trap position at the begin of irradiation (Cadmium Filter)

ID		Liner heat rate (w/cm)	Fission heat rate (w/g)
AFC-1B (Metal)	Rodlet 1	151.12	123.92
	Rodlet 2	167.30	135.92
	Rodlet 3	248.93	206.88
	Rodlet 4	194.38	165.11
	Rodlet 5	213.84	172.14
	Rodlet 6	158.01	152.70
AFC-1D (Metal)	Rodlet 1	132.67	110.76
	Rodlet 2	136.87	112.49
	Rodlet 3	228.18	189.39
	Rodlet 4	168.25	140.62
	Rodlet 5	210.44	170.29
	Rodlet 6	133.35	129.74
AFC-1A (Nitride)	Rodlet 1	55.57	62.28
	Rodlet 2	167.41	160.29
	Rodlet 3	156.16	149.41
	Rodlet 4	253.10	232.01
	Rodlet 5	150.75	166.81
	Rodlet 6	143.76	181.28
AFC-1C (Nitride)	Rodlet 1	54.98	62.22
	Rodlet 2	184.61	149.43
	Rodlet 3	174.53	165.55
	Rodlet 4	246.70	231.51
	Rodlet 5	166.13	184.11
	Rodlet 6	149.17	190.03

12. Table – The linear fission heat rate and burnup distribution of the proposed AFC-1 fuel at the East flux trap position at the end of 100 EFPDs irradiation (Cadmium shroud)

ID		Liner heat rate (w/cm)	Fission heat rate (w/g)	Pu depletion (atom%)	Heavy metals depletion (atom%)	Am depletion (atom%)
AFC-1B (Metal)	Rodlet 1	157.58	131.19	5.12%	2.48%	6.47%
	Rodlet 2	180.47	149.13	7.11%	2.87%	9.09%
	Rodlet 3	273.96	233.17	6.16%	3.45%	9.02%
	Rodlet 4	213.02	184.71	7.66%	3.56%	11.78%
	Rodlet 5	226.95	186.37	7.29%	3.57%	11.19%
	Rodlet 6	174.74	171.88	7.84%	4.27%	0.00%
AFC-1D (Metal)	Rodlet 1	139.60	118.13	3.66%	1.79%	7.53%
	Rodlet 2	151.23	126.04	6.38%	2.59%	9.04%
	Rodlet 3	248.15	210.46	5.81%	3.20%	9.38%
	Rodlet 4	186.28	158.45	6.18%	2.99%	9.30%
	Rodlet 5	222.86	183.91	6.08%	2.92%	8.65%
	Rodlet 6	149.20	147.35	6.59%	3.44%	0.00%
AFC-1A (Nitride)	Rodlet 1	59.05	66.88	5.77%	1.55%	5.66%
	Rodlet 2	169.44	165.36	5.68%	2.83%	8.85%
	Rodlet 3	165.96	161.57	7.10%	2.62%	9.24%
	Rodlet 4	274.00	258.04	6.76%	3.96%	10.23%
	Rodlet 5	162.43	183.34	7.54%	3.42%	11.28%
	Rodlet 6	151.04	195.06	5.37%	2.37%	7.17%
AFC-1C (Nitride)	Rodlet 1	56.26	64.37	6.44%	1.76%	6.39%
	Rodlet 2	196.01	161.62	6.84%	3.38%	8.77%
	Rodlet 3	194.01	187.71	9.71%	3.64%	11.41%
	Rodlet 4	290.12	279.83	7.35%	4.29%	12.97%
	Rodlet 5	188.23	213.30	9.89%	4.53%	13.08%
	Rodlet 6	156.05	203.76	6.95%	3.01%	8.38%

13. Table – Experiment metal fuel composition for AFC-B and AFC-D at the beginning of irradiation

Capsule ID	-1B	1/D	2/B	2/D	3/B	3/D	4/B	4/D	5/B	5/D	6/B	6/D
Am (%)	11.96%	11.96%	10.80%	10.50%	0.32%	0.31%	12.40%	11.90%	0.23%	0.24%		
Np (%)	0.27%	0.27%	9.50%	10.10%	0.00%	0.00%	0.23%	0.25%	8.76%	7.86%		
Pu 238 (%)	0.05%	0.05%	0.05%	0.05%	0.06%	0.06%	0.05%	0.05%	0.06%	0.06%	0.06%	0.06%
Pu 239 (%)	82.58%	82.58%	82.60%	82.59%	82.83%	82.84%	82.57%	82.57%	82.83%	82.83%	82.83%	82.83%
Pu 240 (%)	16.51%	16.51%	16.48%	16.49%	16.22%	16.22%	16.51%	16.51%	16.21%	16.21%	16.21%	16.21%
Pu 241 (%)	0.52%	0.52%	0.52%	0.52%	0.55%	0.54%	0.52%	0.52%	0.56%	0.56%	0.56%	0.56%
Pu 242 (%)	0.34%	0.34%	0.34%	0.34%	0.35%	0.35%	0.34%	0.34%	0.35%	0.35%	0.35%	0.35%
Total Pu by assay (%)	48.48%	48.48%	40.13%	39.75%	59.11%	59.34%	48.83%	48.36%	49.79%	50.30%	39.67%	39.72%
Zirconium	40.45%	40.45%	41.00%	38.90%	41.00%	39.00%	41.00%	40.00%	40.40%	41.60%	60.70%	59.60%
Carbon	0.00%	0.00%			0.008%	0.020%			0.006%		0.194%	0.013%
Oxygen (est)	0.00%	0.00%			0.069%	0.303%			0.105%		0.020%	0.006%
Other	0.00%	0.00%										
Sum	0.83900	0.83900	0.88700	0.88700	0.83600	0.83600	0.83200	0.83200	0.75100	0.75100	0.93700	0.93700
	0.16200	0.16200	0.11300	0.11300	0.16400	0.16400	0.16800	0.16800	0.24900	0.24900	0.06300	0.06300
	3.999	3.911	5.315	5.195	6.111	5.724	2.581	2.079	5.281	5.678	2.452	2.223
Am (g)	0.545		0.491	0.472	0.014	0.014	0.532	0.529	0.011	0.01	0	0
Np (g)	0.012		0.432	0.454	0	0	0.01	0.011	0.401	0.34	0	0
Pu 238 (g)	0.001		0.001	0.001	0.002	0.002	0.001	0.001	0.001	0.001	0.001	0.001
Pu 239 (g)	1.823		1.507	1.476	2.208	2.221	1.73	1.775	1.887	1.804	0.844	0.839
Pu 240 (g)	0.364		0.301	0.295	0.432	0.435	0.346	0.355	0.369	0.353	0.165	0.164
Pu 241 (g)	0.011		0.01	0.009	0.015	0.015	0.011	0.011	0.013	0.012	0.006	0.006
Pu 242 (g)	0.008		0.006	0.006	0.009	0.009	0.007	0.007	0.008	0.008	0.004	0.004
Total Pu by assay(g)	2.207		1.824	1.788	2.666	2.682	2.096	2.149	2.278	2.178	1.02	1.013
Total TRU by assay(g)	2.764		2.747	2.714	2.68	2.696	2.638	2.689	2.69	2.529	1.02	1.013
Zr(g)	1.842		1.864	1.749	1.849	1.762	1.76	1.778	1.849	1.802	1.56	1.52
Carbon (g)	0		0	0	0	0.001	0	0	0	0	0.001	0
Oxygen (g)	0		0	0	0.003	0.014	0	0	0.005	0	0	0
Other (g)	0		0	0	0	0	0	0	0	0	2.585	2.533
Total	4.606		4.611	4.463	4.533	4.473	4.398	4.467	4.544	4.331		
inches	1.482	1.447	1.484	1.494	1.483	1.488	1.5	1.488	1.506	1.428	0.99	1.002
cm	3.765	3.675	3.77	3.795	3.766	3.78	3.81	3.78	3.824	3.627	2.515	2.544
Vol	0.47625	0.46487	0.47688	0.48005	0.47638	0.47815	0.48194	0.47815	0.48371	0.45880	0.31813	0.32180
Density	8.39682	8.41316	11.14527	10.82187	12.82805	11.97116	5.35540	4.34802	10.91759	12.37589	7.70745	6.90798

14. Table – Experiment nitride fuel composition for AFC-A and AFC-C at the beginning of irradiation

AFC-1 rodlet ID#		-1C	-2A	-2C	-3A	-3C	-4A	-4C	-5A	-5C	-6A	-6C
Am (%)	0.36500	0.36500	0.11700	0.11700	0.00130	0.00130	0.00210	0.00210	0.03670	0.03670	0.21500	0.21500
Np (%)	0.01550	0.01550	0.01830	0.01830	0.22000	0.22000	0.02000	0.02000	0.10000	0.10000	0.00850	0.00850
Pu 238 (%)	0.00010	0.00010	0.00010	0.00010	0.00010	0.00010	0.00010	0.00010	0.00010	0.00010	0.00010	0.00010
Pu 239 (%)	0.93800	0.93800	0.93870	0.93870	0.93880	0.93880	0.93870	0.93870	0.93870	0.93870	0.93870	0.93870
Pu 240 (%)	0.06060	0.06060	0.05990	0.05990	0.05970	0.05970	0.05980	0.05980	0.05980	0.05980	0.05980	0.05980
Pu 241 (%)	0.00110	0.00110	0.00110	0.00110	0.00100	0.00100	0.00100	0.00100	0.00110	0.00110	0.00110	0.00110
Pu 242 (%)	0.00030	0.00030	0.00030	0.00030	0.00030	0.00030	0.00030	0.00030	0.00030	0.00030	0.00030	0.00030
Total Pu by assay (%)	0.13800	0.13800	0.36300	0.36300	0.30600	0.30600	0.50100	0.50100	0.33000	0.33000	0.33300	0.33300
Zirconium	0.27000	0.27000	0.34000	0.34000	0.28000	0.28000	0.28000	0.28000	0.25000	0.25000	0.34000	0.34000
Carbon	0.03000	0.03000	0.02900	0.02900	0.00870	0.00870	0.00880	0.00880	0.01400	0.01400	0.02000	0.02000
Oxygen (estimate)	0.02000	0.02000	0.02000	0.02000	0.02000	0.02000	0.02000	0.02000	0.02000	0.02000	0.02000	0.02000
Other												
Sum	0.83900	0.83900	0.88700	0.88700	0.83600	0.83600	0.83200	0.83200	0.75100	0.75100	0.93700	0.93700
Nitrogen by difference	0.16200	0.16200	0.11300	0.11300	0.16400	0.16400	0.16800	0.16800	0.24900	0.24900	0.06300	0.06300
	3.999	3.911	5.315	5.195	6.111	5.724	2.581	2.079	5.281	5.678	2.452	2.223
Am (g)	1.46	1.428	0.622	0.608	0.008	0.007	0.005	0.004	0.194	0.208	0.527	0.478
Np (g)	0.062	0.061	0.097	0.095	1.344	1.259	0.052	0.042	0.528	0.568	0.021	0.019
Pu 238 (g)	0	0	0	0	0	0	0	0	0	0	0	0
Pu 239 (g)	0.518	0.506	1.811	1.77	1.756	1.644	1.214	0.978	1.636	1.759	0.767	0.695
Pu 240 (g)	0.033	0.033	0.116	0.113	0.112	0.105	0.077	0.062	0.104	0.112	0.049	0.044
Pu 241 (g)	0.001	0.001	0.002	0.002	0.002	0.002	0.001	0.001	0.002	0.002	0.001	0.001
Pu 242 (g)	0	0	0.001	0.001	0.001	0	0	0	0	0.001	0	0
Total Pu by assay(g)	0.552	0.54	1.929	1.886	1.87	1.752	1.293	1.042	1.743	1.874	0.817	0.74
Total Pu by sum (g)	0.552	0.54	1.929	1.886	1.87	1.752	1.293	1.042	1.743	1.874	0.817	0.74
Total TRU by assay(g)	2.073	2.028	2.648	2.589	3.222	3.018	1.35	1.088	2.465	2.65	1.365	1.237
Zr(g)	1.08	1.056	1.807	1.766	1.711	1.603	0.723	0.582	1.32	1.42	0.834	0.756
Carbon (g)	0.12	0.117	0.154	0.151	0.053	0.05	0.023	0.018	0.074	0.079	0.049	0.044
Oxygen (g)	0.08	0.078	0.106	0.104	0.122	0.114	0.052	0.042	0.106	0.114	0.049	0.044
Other (g)	0	0	0	0	0	0	0	0	0	0	0	0
Nitrogen by diff. (g)	0.646	0.632	0.599	0.585	1.002	0.939	0.434	0.35	1.317	1.416	0.156	0.141
inches	1.501	1.487	1.796	1.484	1.956	1.819	0.78	0.644	1.772	1.918	0.873	0.801
cm	3.813	3.777	4.562	3.769	4.968	4.62	1.981	1.636	4.501	4.872	2.217	2.035
Vol	0.54531	0.54016	0.65243	0.53902	0.71049	0.66072	0.28331	0.23397	0.64370	0.69676	0.31706	0.29103
Density	7.33346	7.24044	8.14652	9.63792	8.60112	8.66327	9.11019	8.88577	8.20411	8.14915	7.73355	7.63834

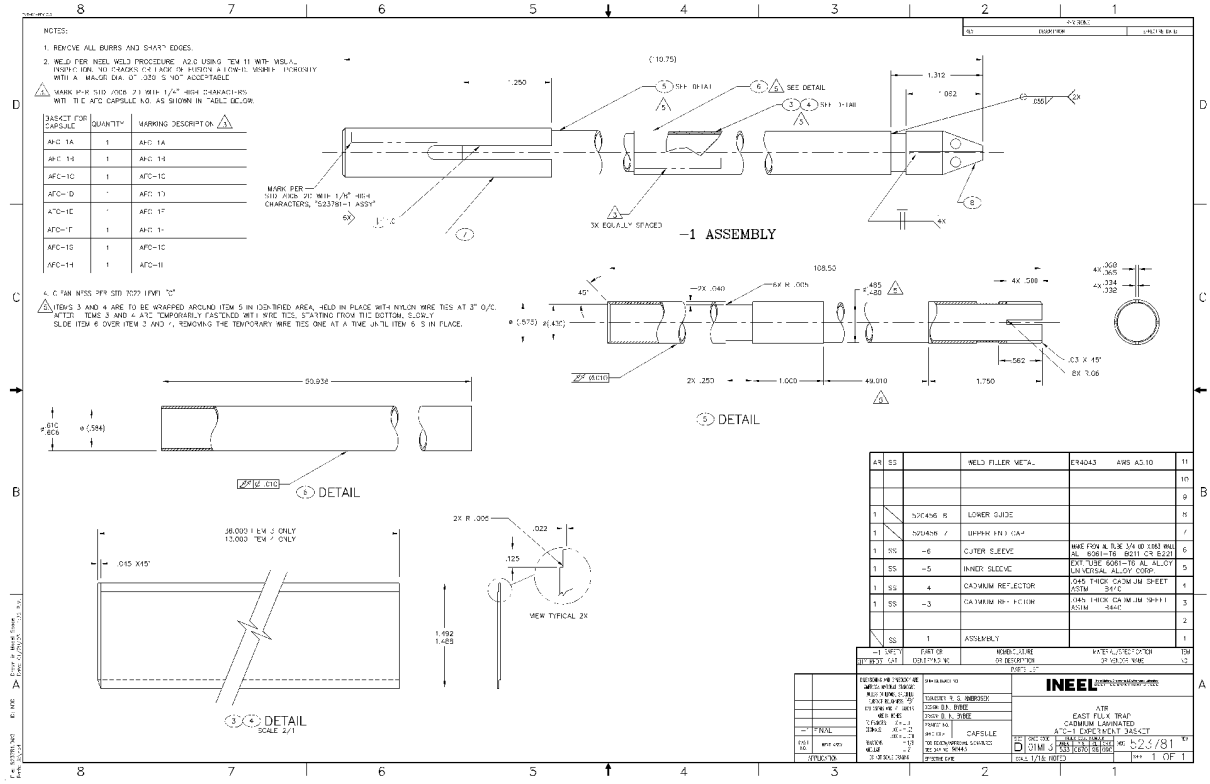

Figure 4-39. Preliminary ATR Cadmium Basket.

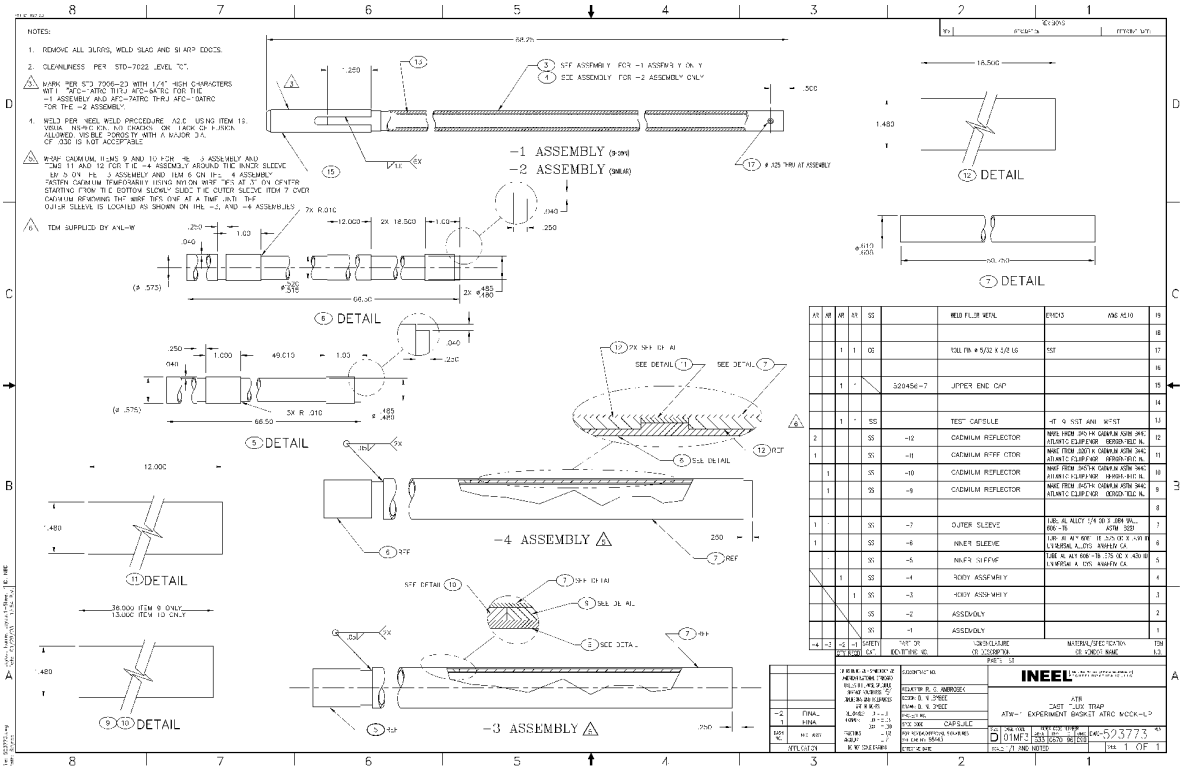

Figure 4-40. Preliminary ATRC Cadmium Basket.

4.11 Series Two FUTURIX Irradiation

FUTURIX is the international name of the irradiation test designated as AFC-3 in the AFCI 5-Year Program Plan. It is a collaborative irradiation experiment with the French CEA, with significant participation by ITU. This experiment will test 10-cm-long experimental fuel pins in the Phénix fast-spectrum reactor located in France. The US program will provide fuels for four of the experimental fuel pins. Plutonium, neptunium, and americium transmutation fuels will be fabricated in the US and transported to ITU for encapsulation in standard Phénix cladding. Reactor insertion of this experiment is scheduled to occur in April 2006. The experiment is scheduled for two irradiation cycles (240 EFPDs) before the shutdown of the Phénix reactor and should achieve heavy metal burnups in the range of 5-10 at.%, with americium transmutation as high as 20 at.%. The irradiated fuels will be shipped back to the US for post-irradiation examination (PIE) and separations testing.

4.11.1 Objective and Scope for Series Two FUTURIX Irradiation

The FY03 efforts are primarily focused on providing the technical data to CEA about the fuels that are being fabricated in the U.S. Part of the technical data will be compiled the Transmutation Fuels handbook with oxide fuel input from CEA. The second revision of the International handbook will be published at the end of FY03. Also, the fabrication process qualification and quality control reviews will be performed at the U.S. sites.

4.11.2 Highlights for Series Two FUTURIX Irradiation

The following is the major highlight for the FUTURIX Irradiation in the first quarter of FY03:

- The first edition of the AFC Fuels Handbook, issued within the program at the end of FY-02, was transmitted to the CEA for use in analyzing the performance of the US experimental pins. Best-estimate thermo-physical properties and/or property correlations for both metallic alloy and nitride transmutation fuels were included.

4.11.3 Technical Summary for Series Two FUTURIX Irradiation

No formal agreement between the US-DOE and the French-CEA has been reached, and no money has been transferred to the CEA by the DOE to support in earnest the design and analysis of the proposed experiment; thus, progress on the experiment has been minimal. The Presentation Report, which formally proposes the irradiation experiment to the Phénix reactor operators, was planned to be completed by the end of FY02. It remains incomplete, but it should be completed and submitted during the 2nd quarter of FY-03.

An agenda was formalized with the CEA to discuss FUTURIX during the upcoming DOE/CEA Coordination Meeting to be held in Washington, DC in January. The US will propose that the compositions originally proposed for the four US-supplied fuels be revised to include one non-fertile and one low-fertile composition for both the metallic alloy and nitride fuel types, consistent with the AFCI program change this year to include low-conversion ratio fast reactors for actinide transmutation.

For additional information on the status of the FUTURIX collaboration please contact Steve Hayes steven.hayes@anl.gov .

4.12 ATR Fast Flux Booster Design

Earlier studies have shown that fast spectrum transmutation is most effective to meet the transmutation objectives of reducing the minor actinide inventories in spent nuclear fuel. Therefore, it is important that fast spectrum test capabilities are readily available for the fuel developers as the proof-of-principle experiments continue and transition into proof-of-performance testing with a more prototypic neutron spectrum. Unfortunately, all fast reactors in the U.S. are shut down and fast spectrum irradiation capabilities are currently only available outside the U.S. Conducting experiments overseas will likely be slow and expensive. Therefore, the U.S. must develop some small scale fast-spectrum irradiation capabilities in this country. A leading option at this time is the installation of a fast neutron flux booster (FNFB) in the ATR.

The five-year milestones include:

Complete fuel specifications.	FY 2004
Complete preliminary design.	FY 2004
Complete final design.	FY 2005
Complete fabrication, assembly, and installation.	FY 2005
Begin operation.	FY 2006

4.12.1 Objectives and Scope for ATR Fast Flux Booster Design

An initial project will be to design, fabricate, and install a FNFB ATR. The FNFB will convert thermal neutrons in the flux trap into fast neutrons and create an environment representative of the fast flux spectrum in a fast reactor. The FNFB would boost the fast flux in the ATR South flux trap by a factor between 2 and 3, produce a fast flux greater than 6.0×10^{14} n/cm^2-sec, and have a volume large enough to accommodate the fuel test samples. In FY 2003, INEEL will define the requirements, begin developing the specifications for the FNFB fuel, complete the pre-conceptual design, and conceptual design.

4.12.2 Highlights for ATR Fast Flux Booster Design

There are no highlights for the first quarter because the work did not start.

4.12.3 Technical summary for ATR Fast Flux Booster Design

The activities are expected to begin in the second quarter of FY03.

5 TRANSMUTATION ENGINEERING

5.1 Introduction

The top-level objective for Transmutation Engineering is to develop the engineering basis for the transmutation of minor actinides (MA) and long-lived fission products (LLFP) so that informed decisions can be made in the next five years concerning transmutation technologies, and a path forward can be developed for implementation in support of that objective. Proof-of-principle information is being developed in areas not supported in the fuels, separations, Generation IV research or other DOE-NE research programs. In the near term five-year period, transmutation engineering activities are focused in the areas of physics, nuclear data and codes, coolants and corrosion, structural materials and accelerator-based transmutation. Subsequent to the decision on transmutation technology and a successful proof-of-principle phase, engineering development and demonstration will be performed to provide proof-of-performance in preparation for deployment of a transmuter technology. In the next five years, information provided by transmutation engineering and other advanced fuel cycle activities will provide support for key decisions.

Five-Year Plan

We completed the Transmutation Engineering Section of the AFCI Five-Year Program Plan, providing the input to the Technical Integrator. Follow-on efforts incorporated DOE comments, resulting in the AFCI Program Plan (Rev. C).

Work Packages

The first draft of the Transmutation Engineering Work Packages were prepared and reviewed, and, following resolution of comments, a complete set of the work packages for Transmutation Engineering was submitted to DOE.

CEA Collaboration

The Transmutation Engineering Team participated in a DOE-CEA (Commissariat à l'Energie Atomique in France) collaboration meeting in Washington DC, revising the WP3 on transmutation and developing a path forward for future Accelerator collaborations. It was also recognized that material irradiations are possible in Phenix during the same irradiation planned for Futurix.

5.2 Transmutation Physics (Series Two)

5.2.1 Transmutation Physics Objectives and Scope

Transmutation engineering physics will provide nuclear cross-section data in the thermal, epithermal and fast neutron spectra. This data will allow the accurate prediction of transmutation rates and reduce calculation uncertainties. Coefficients of reactivity will be obtained in all three spectra to support licensing and safety analyses. Analysis codes will be developed validated and benchmarked so that design calculations can be made with confidence.

The major objective of high-energy physics activities is to improve and maintain the computer codes used in the analyses of transmutation systems. As part of the improvement, the nuclear data accuracy is reevaluated to match desired objectives.

5.2.2 Transmutation Physics Technical Summary

Cross Section Evaluations

New Evaluations of n+^{238}U and n+^{239}Pu up to 150 MeV Incident Energies. We have completed our new evaluations of neutron-induced reactions on ^{238}U and ^{239}Pu for incident neutron energies up to 150 MeV. These evaluations are now added to the LA150 library, which did not previously include any study on actinides.

In the present evaluations, GNASH nuclear model calculations were extended up to 150 MeV incident energy, which required including up to 50 compound excited nuclei. A double-humped barrier-fission model was used, and the fission barriers for these excited nuclei were calculated by using Z,A trends from Sierk's rotating nucleus model. These barriers were then normalized to known barrier heights near stability.

The channels transmission coefficients entering into the Hauser-Feshbach formalism as implemented in GNASH were obtained by using the high-energy relativistic optical model developed by Young. The reaction cross section and elastic-scattering angular distributions were also obtained in these calculations. The (n,total) cross section was adjusted to better fit (available) very accurate experimental data, and smoothed at the transition energies from the upper energy limit of our previous evaluations. In GNASH calculations, neutron, proton and gamma-ray ejectiles were allowed.

While the calculated fission cross section agrees reasonably well with measurements, the evaluated fission cross section was obtained from the experimental database alone, through a covariance analysis of all experimental data available. These were either absolute measurements or (very often) ratios to the ENDF standard ^{235}U (n,f) cross section. Yield and spectra of neutrons emitted from the fission fragments were calculated with the CEM/Furihata code by S.Mashnik (LANL). We have also started comparing these new evaluations against similar work done in Japan, France and Russia (cf. Fig.6-1).

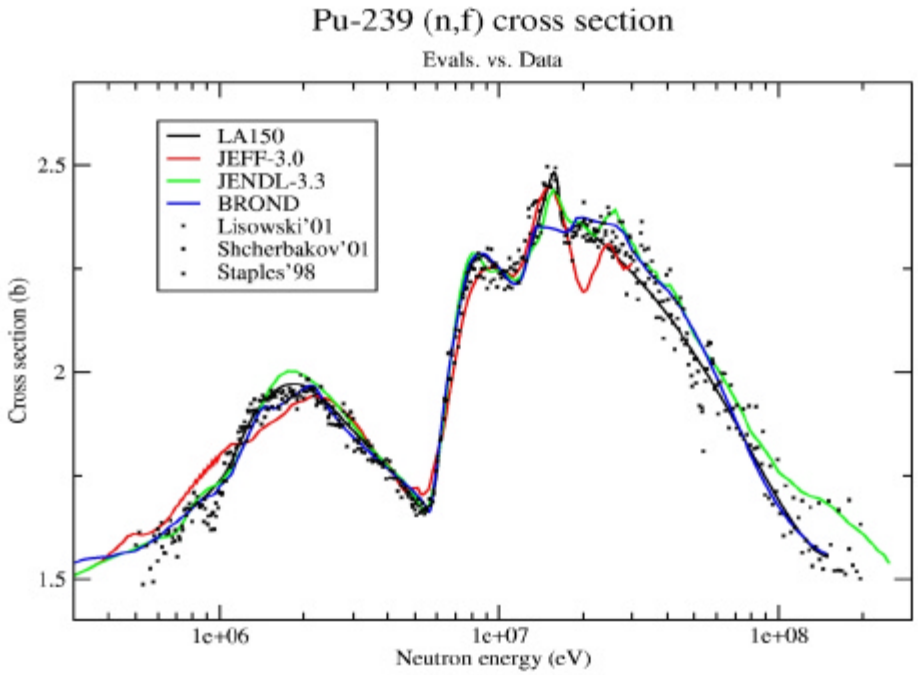

Figure 5-1. Comparison of our new Pu-239 (n,f) cross section evaluation with recent similar works.

Finally, these high-energy evaluations were ENDF-formatted and merged with extant ENDF/B-VI files for lower incident energies.

ENDF Formatting of High-Energy Evaluations. Various ENDF formatting tools were developed by P.G.Young (LANL) in the course of the LA150 program to merge new high-energy work with existing ENDF/B files which typically stopped at 20–30 MeV incident energy. However, these tools have various limitations in the number of available ENDF formatting laws, and most importantly were not designed to be used with fissile nuclei.

In the present work, we have developed a new code, written in Perl, which encapsulates the whole ENDF formatting process, making it relatively easy to follow. This code calls up most other tools developed earlier for LA150, though modified to take into account new ENDF laws and requirements for fissile nuclei. In addition, several new routines/codes have been written to incorporate fission physics (e.g., results from CEM/Furihata calculations of fission neutrons spectra). We have documented in detail this ENDF processing and the corresponding codes, which have been written in Perl and Fortran95.

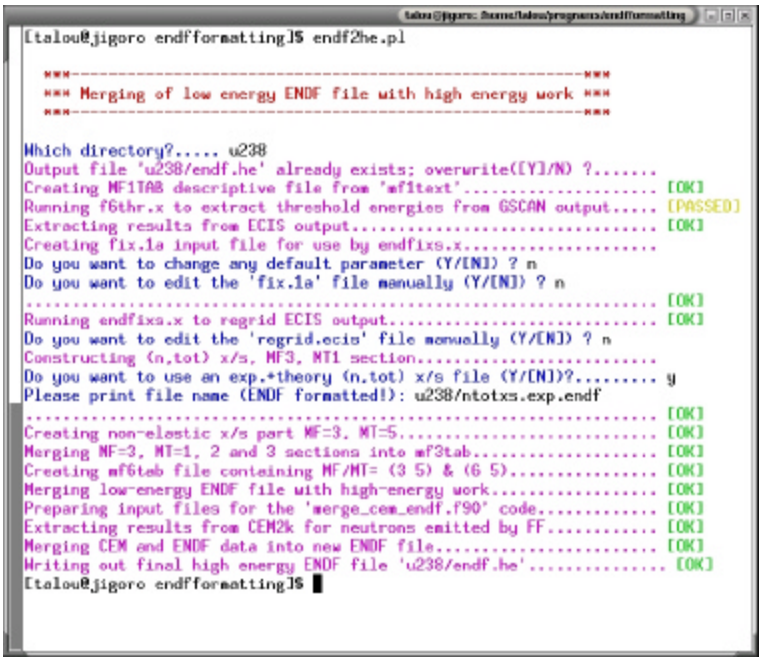

Figure 5-2. Screenshot of a typical execution of the ENDF formatting process.

New Evaluations on n+^{237}Np and n+^{241}Am. ^{237}Np and ^{241}Am are both part of a typical spent fuel composition, to be burnt into an Advanced Fuel Cycle or Accelerator-Driven system. In a recent sensitivity study by ANL,[22] it has been shown that the current uncertainties on the neutron-induced reaction cross sections on these actinides are driving up the overall uncertainties on integral parameters such as the k_{eff} criticality coefficient. Therefore, the time is ripe for new evaluations of important quantities such as the (n,f) and (n,n') cross sections, and the nu-bar fission neutron multiplicities.

We have gathered experimental data available on ^{237}Np(n,f) and ^{241}Am(n,f) cross sections, and started analyzing/formatting them in a form suitable for a covariance analysis, as was done previously for ^{239}Pu(n,f) and ^{238}U(n,f). As the importance of covariance information is rising because of newly available sensitivity tools, we intend to incorporate the (n,f) cross-section covariance information which will result from our analysis into the final ENDF file.

As a result of the LANL criticality experiment on a composite sphere of Np-U, we will be able to test our new ^{237}Np(n,f) evaluation against new integral data.

Helium and Hydrogen Production Tests. Hydrogen and helium are produced when energetic neutrons interact with materials, and these gases can lead to significant changes in materials properties such as embrittlement and swelling. Such effects have been seen in fission reactors and a significant effort has been made for the development of fusion reactors. For the Advanced Fuel Cycle Initiative, new structural materials are proposed, and the amount of gas production must be known to assess the properties of these materials under radiation damage.

[22] ANL-AAA-036, Sept. 2002.

In the first quarter of FY03, we began measurements of gas production for neutrons on three elements of structural materials. These gases are produced initially as energetic protons, deuterons and alpha particles from nuclear reactions. When these charged particles slow down and stop (with ranges of mm to cm), they acquire electrons from the material and become hydrogen (protons and deuterons) or helium (alpha particles). Our method is to measure the protons, deuterons and alpha particles that escape from thin foils as illustrated in Fig. 6-3.

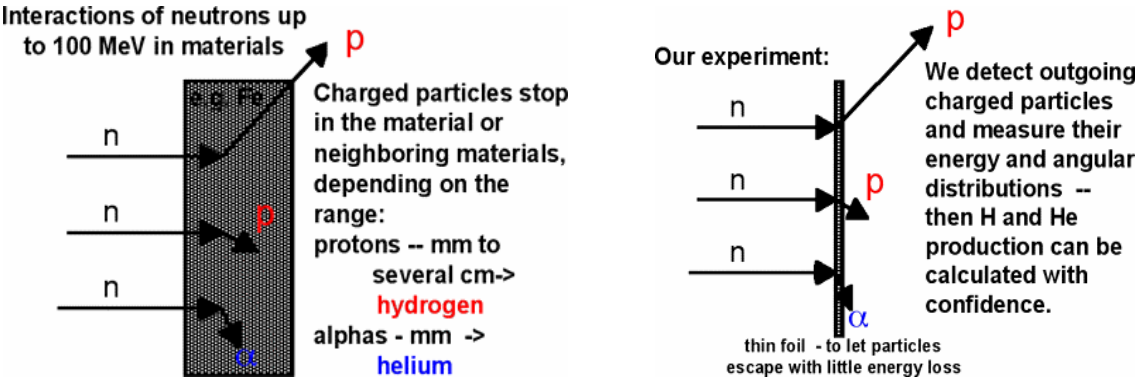

Figure 5-3. Interactions of neutrons with materials produce charged particles that stop either in the material or in neighboring materials. In our experiment, we use a thin foil of the material so that the charged particles can escape and be detected.

Fig. 6-3. Interactions of neutrons with materials produce charged particles that stop either in the material or in neighboring materials. In our experiment, we use a thin foil of the material so that the charged particles can escape and be detected.

We measure the charged particles with detector systems at four angles concurrently. Then we can move the detector systems to investigate a new set of angles. The total of 8 angles is sufficient for determining the angle-integrated production cross sections. Each detector system consists actually of 2 or 3 detectors in coincidence and arranged so that the charged particles pass through the first detector and stop in the second or third. We do this in order to identify the protons, deuterons, and alpha particles and also the small numbers of tritons and ^{3}He. An example of this identification is shown in Fig. 6-4.

Data taking began in production mode this quarter. The samples investigated included several thickness of iron, a thick chromium sample, and thin samples of the two major isotopes of nickel, ^{58}Ni and ^{60}Ni. A range of sample thicknesses is required in order to get good signal-to-background data for the different emitted particles and the different particle energies. For particles with large specific energy loss, thin samples are necessary so that the particles can escape the sample with little energy loss. On the other hand, particles with low specific energy loss (such as high energy protons) are generally much less abundant, and therefore, thicker samples are acceptable and, in fact, strongly preferred to increase the counting rate. To cover the complete range of energies for the hydrogen and helium isotopes, sample thicknesses spanning a factor of 100 from the thinnest to the thickest are often required. Consequently, we believe that the data for iron should be fairly complete whereas those for chromium and the two nickel isotopes are only partial. The data analysis is in progress with existing software. Improvements in the software to greatly speed the analysis are underway.

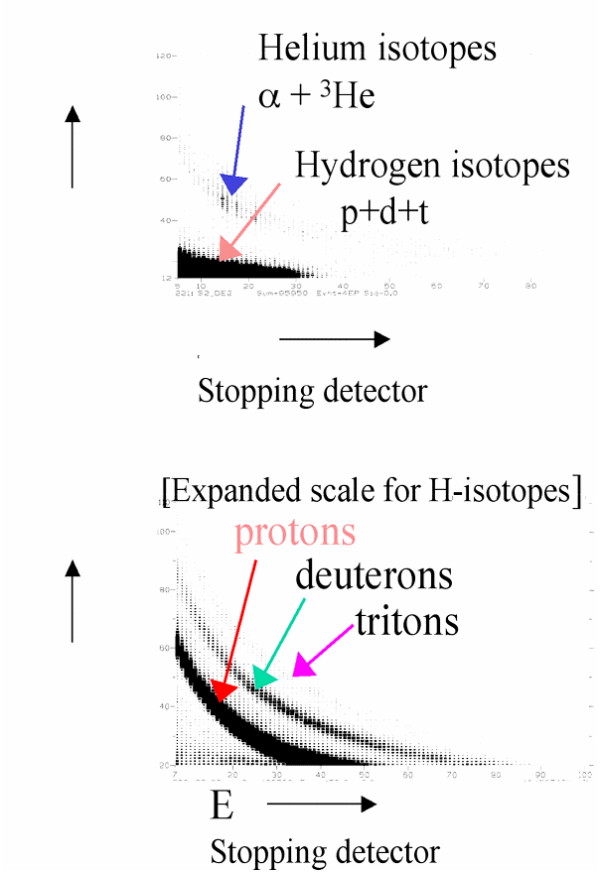

Figure 5-4. Identification of protons, deuterons, tritons, 3He and alpha particles from the commissioning experiment of neutron interactions with iron.

Minor Actinide Cross-Section Measurements**.** Work this quarter concentrated on the measurement of the ^{237}Np capture cross section using the newly-commissioned DANCE instrument at the Manuel Lujan, Jr. Neutron Scattering Center (LANSCE).

Efforts to involve UNLV in the preparation of actinide foil samples have not been successful, since the quantities involved (~1 mg) is greater than the amount permitted in the UNLV actinide laboratory. We are now investigating the possibility of having the samples manufactured at LANL. We are also looking into the possibility of having them manufactured in Russia.

Integral Experiments for Cross-Section Validation (ANL). An analysis of the TRAPU irradiation experiment using one-group cross-sections generated with the ECCO cell code and JEF2.2 nuclear data was performed. Results are generally in good agreement with previous results obtained during the analysis of PROFIL-1 experiment. A sensitivity study has also been performed. Table 1 shows the C/E values of final concentrations.

Table. C/E Values of Final Concentrations in the TRAPU Experiment Using JEF2.2 Data

U-238 = 100	TRAPU-I[23]	TRAPU-II[a]	TRAPU-III[a]
U-234	0.98 ± 2.5	1.00 ± 1.3	1.04 ± 1.0
U-235	1.00 ± 0.3	1.02 ± 0.2	1.01 ± 0.2
U-236	0.93 ± 0.5	0.95 ± 0.4	0.95 ± 0.3
Np-237	0.84 ± 6.8	0.84 ± 3.3	0.80 ± 3.2
Pu-238	1.01 ± 0.9	1.01 ± 0.4	1.04 ± 0.4
Pu-239	1.02 ± 0.4	1.00 ± 0.3	1.00 ± 0.3
Pu-240	0.99 ± 0.4	0.97 ± 0.3	0.98 ± 0.3
Pu-241	1.04 ± 0.4	1.00 ± 0.3	1.03 ± 0.3
Pu-242	1.12 ± 0.5	1.06 ± 0.4	1.03 ± 0.3
Am-241	0.96 ± 3.0	0.96 ± 3.6	0.97 ± 2.1
Am-242	1.04 ± 3.6	1.07 ± 4.0	1.04 ± 2.5
Am-243	1.10 ± 3.6	1.06 ± 4.0	1.08 ± 2.5
Cm-242	1.05 ± 2.4	1.03 ± 2.6	1.02 ± 2.1
Cm-243	-	0.76 ± 2.7	0.77 ± 2.6
Cm-244	1.05 ± 2.0	1.16 ± 2.2	1.18 ± 1.7

A preliminary analysis of the PROFIL-2 irradiation experiment using one-group cross-sections generated with the ECCO cell code and JEF2.2 nuclear data was performed. A new approach has been adopted using directly an R-Z model instead of corrective factors to be applied to an infinite medium solution. Some discrepancy has been observed with respect to the methodology used for the analysis of the PROFIL-1 experiment. An investigation is under way to explain the discrepancy

Code Development

MCNPX**.** Further testing of the MCNPX Mix-and-Match capability was completed, and documentation issued.[24] A more comprehensive report was submitted for classification review and will be issued as an LA report shortly.[25] A paper on the capability was also submitted to the ANS Math & Comp topical meeting to be held in Gatlinburg in April.

MCNPX version 2.5.b was completed and released to the beta test team in November, and documentation was issued.[26] New capabilities in MCNPX2.5.b include mix and match, photonuclear physics models, and positron sources.

[23] C/E values are in absolute values, while uncertainties are relative and given in percent.
[24] J. S. Hendricks. G. W. McKinney, F. X. Gallmeier, "Mix and Match with MCNPX," LA-UR-02-6415, October 2002.
[25] J. S. Hendricks, "MCNPX Model/Table Comparison," Los Alamos National Laboratory Report LA-UR-03-0564, 70 pp.
[26] John S. Hendricks and the MCNPX Team, "MCNPX, Version 2.5.B," Los Alamos National Laboratory Report, LA-UR-02-7086, November 2002.

The entire MCNPX beta test team was recertified in order to receive the 2.5, 2.6 and 3.0 series versions. We now have ~950 beta testers from 240 institutions internationally testing the code before official releases to Radiation Safety Information Computational Center (RSICC) and the Nuclear Energy Agency (NEA).

An MCNPX intermediate level class was held at SCK-CEN in Mol, Belgium. Twenty enthusiastic students attended, half of whom were from SCK-CEN and Belgonucleaire, and are collaborating with AFC on key experiments such as MYRRHA and TRADE.

Monte-Carlo Code Development**.** The improved Cascade-Exciton Model code CEM2k and the Los Alamos version of the Quark-Gluon String Model code LAQGSM merged with the Generalized Evaporation Model code of Furihata (GEM2) were developed further to provide reliable proton-induced fission cross sections for different applications. In collaboration, we found that by adjusting two parameters in GEM2, we were able to describe very well with CEM2k+GEM2 and LAQGSM+GEM2 all available experimental fission cross sections induced by protons with energies from 20 MeV to 10 GeV both for subactinide and actinide targets. Figure 6-5 shows a comparison of our CEM2k+GEM2 results (open circles) for proton-induced fission cross sections on subactinide and actinide targets with the approximations of Dr. Prokofiev of all available experimental data (solid lines). Similar results were obtained with our LAQGSM+GEM2 code. We started to extend our approach for reactions induced by neutrons, pions and photons, and preliminary results obtained so far are very promising.

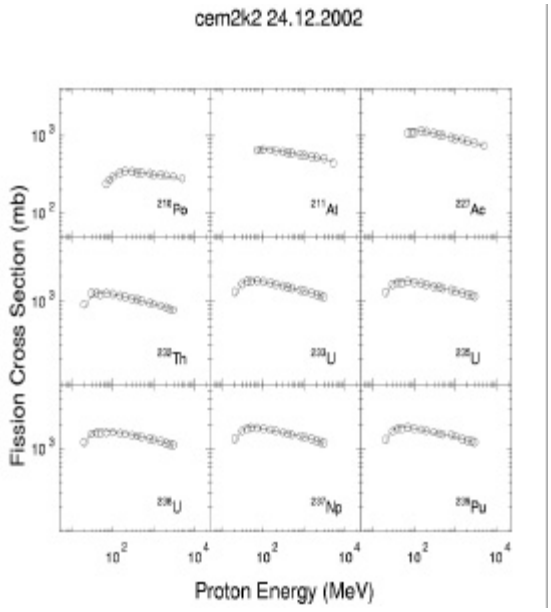

Figure 5-5. Comparison between CEM2k+GEM2 results (open circles) and Prokofiev's systematics for (p,f) cross-sections on sub-actinide and actinide targets.

MALIBU Program Support (ORNL)**.** The MALIBU (Radiochemical analysis of **M**OX **A**nd **L**EU Fuels **I**rradiated to High **BU**rnup) program is organized by Belgonucleaire to perform detailed analysis of high-burnup MOX and UOX fuel to provide experimental data on the isotopic inventory of high burnup fuel for code validation. The measurements will be performed on both MOX and LEU fuel irradiated up to 75 MWd/kg in commercial PWRs and BWRs with well-known irradiation conditions. The samples are from full MOX and LWR fuel assemblies

irradiated in the Gundremmingen BWR in Germany and the Göesgen PWR in Switzerland. Additional specifications of the fuel samples are shown in Table 2. The isotopic measurements will determine the content of major and minor actinides (^{234}U, ^{235}U, ^{236}U, ^{238}U, ^{237}Np, ^{238}Pu through ^{242}Pu, ^{241}Am, ^{242m}Am, ^{243}Am, and ^{242}Cm through ^{245}Cm) and 31 fission products. Current participants include ORNL, BNFL, PSI, Belgonucleaire, SCK·CEN, RWE NUKEM GmBh (Germany), Institute for Transuranium Elements (ITU), and Kernkraftwerk Göesgen (KKG, Switzerland). Negotiations are currently underway with the French Industry (CEA, COGEMA, and EdF). The experimental analysis will be performed at SCK·CEN, PSI, ITU, and CEA.

Table. MALIBU Program Fuel Sample Specifications

	Göesgen PWR		**Gundremmingen BWR**					
Sample	GGM1	GGU1	GRM1	GRM2	GRM3	GRU1	GRU2	GRU3
Fuel Type	MOX	UO_2	MOX	MOX	MOX	UO_2	UO_2	UO_2
Pu_{fis} (wt. %)	5.5	-	5.5	5.5	5.5	-	-	-
U235 (wt.%)	depleted	4.3	depleted	depleted	depleted	3.75	3.75	3.75
End of Irradiation	7/2001	7/2001	7/2001	7/2001	7/2001	7/2001	7/2001	7/2001
Sample Burnup (MWd/kg)	~70	~70	~60	~75	~60	~60	~75	~60
Sample Axial Position	Peak	Peak	Bottom	Peak	Top	Bottom	Peak	Top

An introductory meeting was held in Brussels in April 2002 to discuss the program. A follow-on technical meeting was to be held in December 2002, but was delayed until to ensure the participation of the reactor utilities from which the fuel is being procured. This meeting is now expected to occur in March 2003. The ORNL activities to date have focused on securing our participation in the project by meeting with Belgonucleaire representatives and providing a letter of our intentions to participate in the program. In the upcoming year, ORNL will participate in the technical meeting and will begin modeling the fuel irradiation. These calculations of the fuel irradiation will be compared with the experimental results to investigate the accuracy of our current nuclear data and analysis tools.

Malibu Program Support Highlights

- ORNL Staff met with Belgonucleaire representatives in November 2002 to discuss the scope of the MALIBU Program and ORNL's participation.
- ORNL prepared a letter, informing Belgonucleaire of our intention to participate in the MALIBU Program.

The first MALIBU technical meeting will be held in March 2003 to discuss the details of the project and to allow participants to provide technical direction.

5.3 Structural Materials

5.3.1 Structural Materials Objective and Scope

Transmutation engineering materials activities will provide detailed information on the degradation of structural materials in a fast neutron spectrum and mixed particle environment (neutrons and protons). Material limits will be established that help determine the level of burnup that can be obtained and therefore the effectiveness of the various options. Coolant technology for critical reactor and accelerator driven systems will be developed that supports the selection of technology options.

The major objective of the materials activities is to test and quantify materials properties under proton and neutron irradiation.

5.3.2 Structural Materials Highlights

- All additions to Rev. 3 of the Materials Handbook were completed, and the Handbook is scheduled to be in final form in January 2003.
- A high temperature furnace for testing to 700ºC was installed in the LANL CMR hot cells.
- Compression tests were performed on tungsten at 475ºC after proton-irradiation to up to 22 dpa.
- TRADE target workshop was held at LANL with engineers from Italy and France.

5.3.3 Structural Materials Technical Summary

Radiation-Effect Studies

LANL Hot-Cell Work. In support of obtaining data on high energy proton irradiated materials at prototypic AFCI irradiation temperatures, a furnace was installed on the mechanical testing machine in Wing 9 of the LANL hot cells in the CMR building. This set-up allows for testing in argon or nitrogen at temperatures up to 700ºC and could be modified for higher temperatures up to 1000ºC with minor changes to support testing for the GEN IV materials needs. A photo of the furnace set-up is shown in Fig. 6-6.

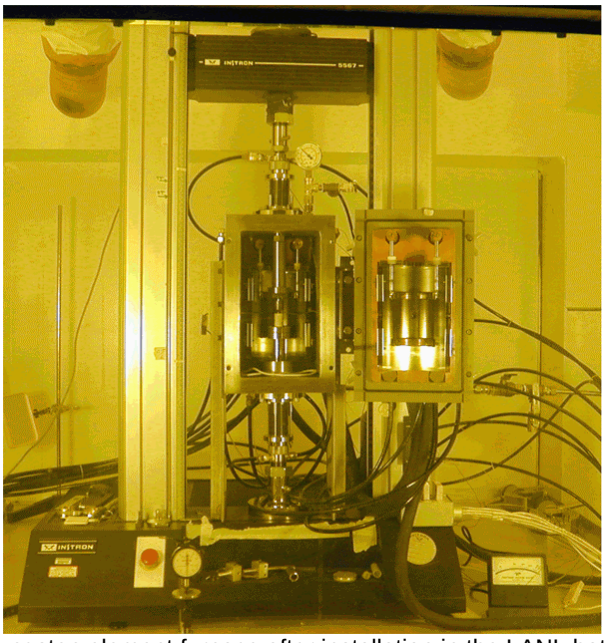

Figure 5-6. Photos showing tungsten element furnace after installation in the LANL hot cells for testing at up to 700ºC in argon or nitrogen.

One of the back-up target materials for the AFCI Program is tungsten. We have proton-irradiated tungsten, in the form of ~3 mm diameter rods, irradiated to ~22 dpa at a maximum irradiation temperature of ~270ºC. These rods were cut into compression specimens in the hot cells, polished to obtain parallel faces and tested at 475ºC. A plot of stress vs. strain for the different compression tests is shown in Fig. 6-7. This plot shows that the yield stress of unirradiated tungsten at 475ºC is much lower than it is at 25ºC and the effect of irradiation is to increase the yield stress while decreasing the ductility. Samples tested at the higher doses exhibited splintering and cracking as shown in Fig. 6-8.

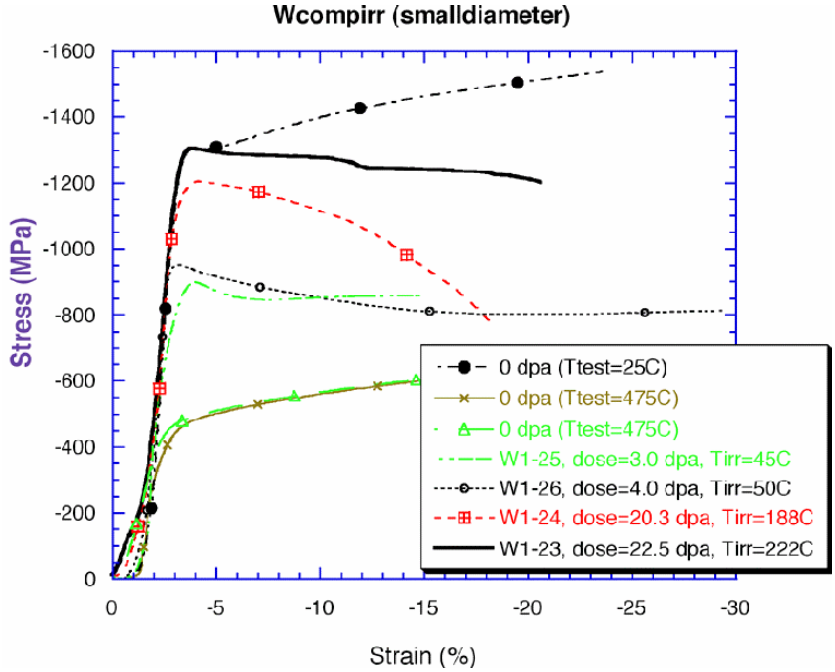

Figure 5-7. Stress/strain curves from compression tests of tungsten after irradiation to up to 22.5 dpa in a high energy proton and neutron flux.

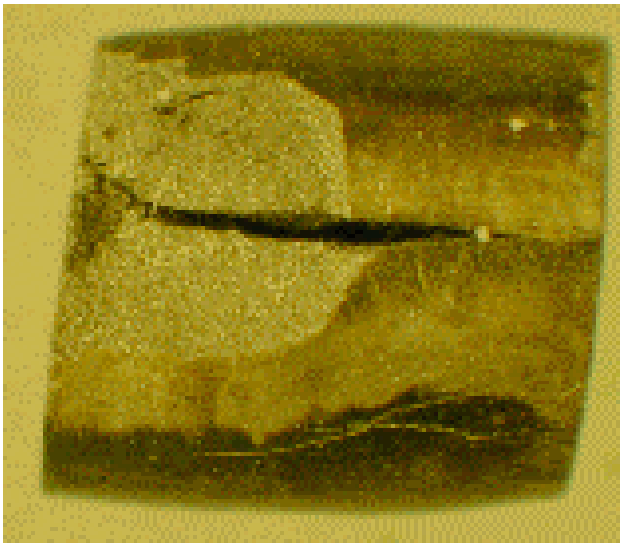

Figure 5-8. Optical photo showing cracks in irradiated tungsten specimen (22.5 dpa) after testing in compression to 20% strain. Approximate length of specimen is 3 mm.

Radiation Effects in Candidate Materials for Spallation Neutron Environments - Hardness Measurement. Analysis of irradiation-induced hardening was conducted on samples of the T-91 alloy irradiated with and without He (100 appm) to 3, 7, and 10 dpa at the Michigan Ion Beam Laboratory at the University of Michigan. Hardness was measured using a Micromet II Vickers indenter. Twenty-five indents were made on the irradiated portion of each specimen. Both 25-g and 10-g loads were utilized for analysis. Given the shallow penetration of the He implant, care

must be taken to ensure that indents made with a 25-g load do not sample material beyond the implanted layer. For a Vickers indenter, the depth of the indent is ~1/7 the diameter of the indent. Further, ASTM recommends that the indents be less than 1/3 the thickness of the implanted region so that only the implanted region is sampled. For an unirradiated hardness level of 290 kg/mm^2, indents with a 25-g load have a depth of ~2 ? m, indicating that material beyond the affected area is being influenced. The indent from a 10-g load is shallower (only 1.4 m at a hardness level of 290 kg/mm^2), but results in a larger uncertainty due to the increased difficulty of measuring smaller indents.

Hardness Results. The results of hardness measurement on the irradiated specimens (with and without 100 appm He) are listed in Table 3. The dose dependence of radiation-induced hardening for the T-91 alloy with and without He is illustrated in Fig. 6-9. For the samples without He, hardness increased with increasing dose from ~290 kg/mm^2 in the unirradiated condition to 383 kg/mm^2 at 10.0 dpa. The samples with 100 appm He increased to 395kg/mm^2 after 10.0 dpa. At all doses, except 3.0 dpa, the hardening was greater in the He-doped samples consistent with the available literature data. An analysis of the data and comparison with literature data will be presented in the next quarterly report.

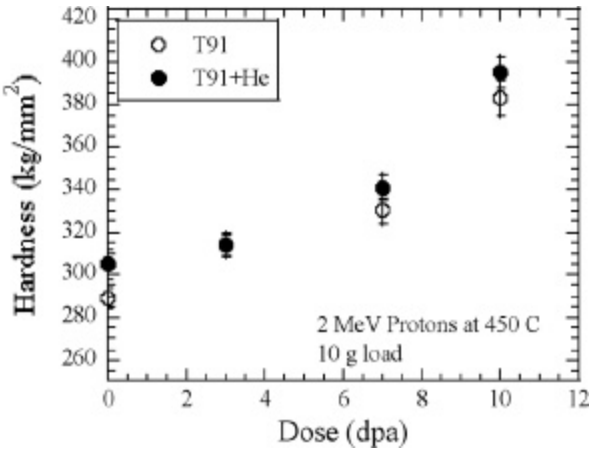

Figure 5-9. Dose dependence of hardening in T91 irradiated with protons at 450°C.

Table. Summary of Results for Hardness Measurements on He-Implanted and Proton-Irradiated T-91.

Condition	He (appm)	Indenter Load	No. of indents	Hardness	Std. Dev.	Std. Dev. Of Mean
T91-0 dpa	0	10 g	25	289.9	25.5	5.0
	0	25 g	26	289.1	16.1	3.2
T91-0 dpa	100	10 g	24	305.2	34.6	6.9
	100	25 g	25	294.2	21.2	4.3
T91-3 dpa	0	10 g	26	314.2	25.6	5.0
	100	10 g	24	314.8	29.7	6.0
T91-7 dpa	0	10 g	25	330.6	29.3	5.9
	100	10 g	24	341.3	29.8	6.1
T91-10 dpa	0	10 g	25	382.6	38.5	7.7
	100	10 g	24	394.6	32.9	6.1

Materials Handbook. The final drafts of Materials Handbook Chapters 19 (T91 [9Cr-1MoV] Ferritic/Martensitic Steel) and 22 (Pb-Bi Eutectic) were completed and reviewed in preparation for issue of Revision 3. Sections 7.5.2.4 (Effects of Irradiation on Yield Strength) and 7.4.10 (Corrosion) of the chapter on Tungsten were also finalized.

A final round of revisions and additions was made to the corrosion sections for Chapter 2 on Alloy-718 (Section 2.4.10), for Chapter 3 on SS-316L (Section 3.4.10), and for Chapter 4 on 6061-T6 aluminum (Section 4.4.10).

First and second drafts of a Handbook chapter on tantalum were received from the ESS Project at Forschungszentrum Juelich and are being reviewed. Revision 3 of the Handbook is scheduled for January 2003.

Modeling. A modeling effort is underway at LANL in collaboration with MST-8 to better understand the effect of helium and hydrogen on materials properties as well as to be able to extrapolate data to untested conditions. The modeling uses a Semi-Empirical, Many-Body Modified Embedded Atom Method (MEAM). The potentials derived from this method have been shown to describe "real" materials well.

TRADE Collaboration. A meeting was held in collaboration with researchers from Italy and France to discuss the design of a solid target and experience in using solid targets at LANL. The meeting was held at Los Alamos in November and included tours of LEDA, the LANSCE target and the DELTA loop. Presently, a matrix is being put together through e-mail communications that compares advantages and disadvantages of using either clad tungsten or tantalum for the solid target.

Coolant Technology

The major objective of LBE research activities is to develop a fundamental understanding of LBE performance parameters and measurement techniques when used as a nuclear coolant, with primary emphasis on spallation-target applications.

Coolant Technology Highlights

- Improvements were made to the DELTA Loop instrumentation for higher reliability, including the gas blow-off system for the pressure transducer and the venturi flow meter.
- We obtained the calibration curve for the venturi flow meter that agrees well with the theoretical prediction.
- Preparation of corrosion test specimens and holders were completed.
- We measured oxygen sensor dynamic range and responses, and produced more calibration data that confirmed the Nerstian behavior and uniformity.
- We expanded the corrosion model to incorporate transient behaviors, demonstrating the significant differences and source between existing models and test loops.
- TRAC modeling of DELTA was enhanced by incorporating the variable-capacity heat exchanger and loop heat losses, successfully simulating a 48-hr operation.
- Irradiation of HT-9 oxide in the Blue-room was completed. We observed changes in oxide dielectric properties through impedance spectroscopy.

DELTA Loop Operations. The first quarter of FY03 at the DELTA Loop was devoted to preparing for the first materials tests.

We conducted several runs for testing equipment. The gas blow-off system for the liquid-metal pressure transducers was installed earlier, and we operated the system directly and by inducing automatic shutdown. The pressure-transducer measurements returned to normal after restart; however, a leak through a factory weld on one of the transducers was observed. We repaired the factory defect since a replacement part would take several weeks to deliver. The part has been ordered as a backup.

We tested the cleaning-gas injection system. The automatic gas flow control was implemented via the main data acquisition and control program. Some of the mass control valves were not able to withstand pressure differentials above 40 psi. Since this system works with gases up to about 90 psig, the valves were not adequate and leaked. These valves were replaced with solenoid valves similar to the other gas valves in the system. The cleaning gas procedure was reworked, and additional hand valves were installed. The more robust system was tested and worked well.

A venturi flow meter for measurement of the liquid lead-bismuth flow rate was installed in FY02, replacing the magnetic flow meter that did not provide good measurements (Fig. 6-10). In October, the venturi flow meter was calibrated with the resulting calibration curve very similar to the theoretical prediction (Fig. 6-11).

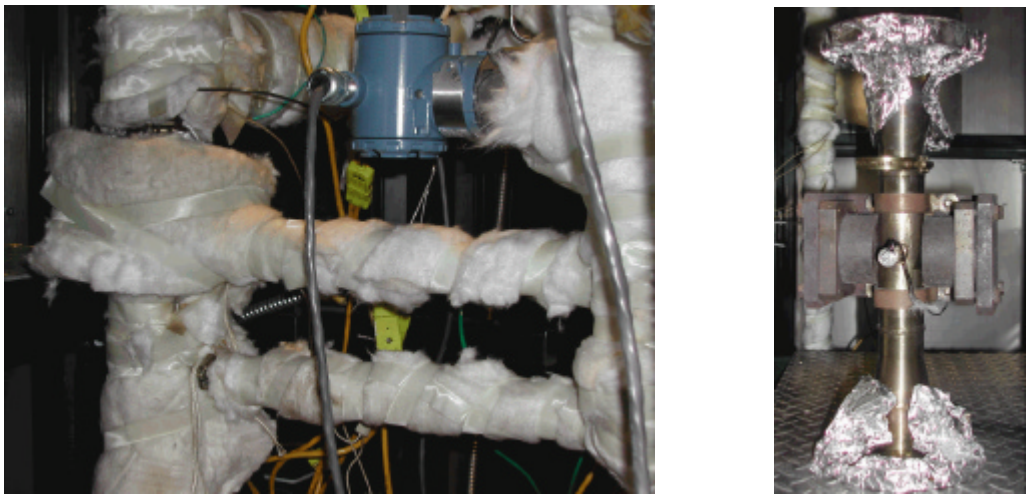

Figure 5-10. The Venturi Flow Meter and the Magnetic Flow Meter.

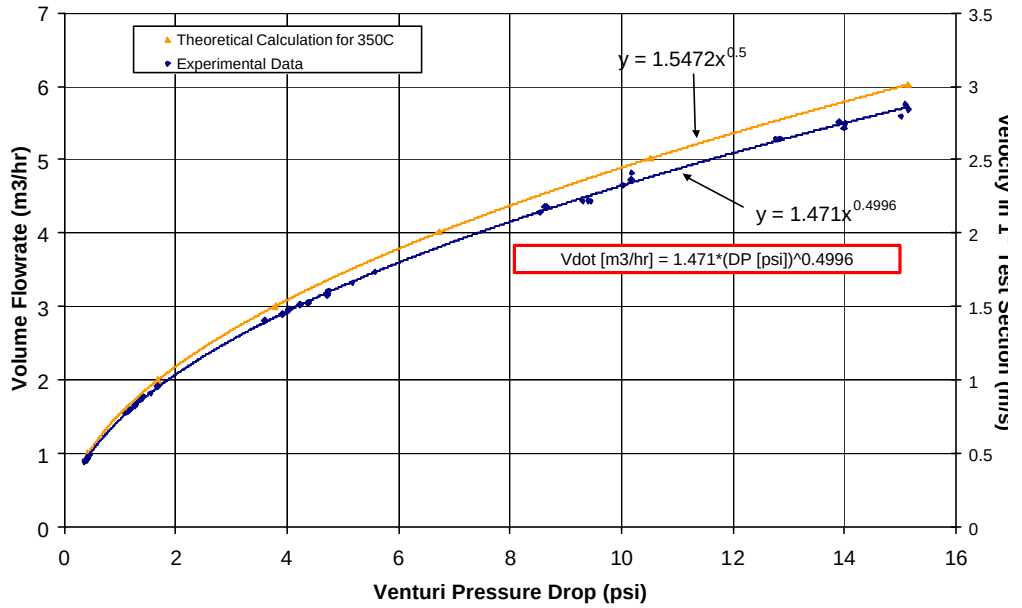

Figure 5-11. Venturi Calibration Curve.

In the course of these preparations, several problems arose that needed to be addressed: (1) the data acquisition and control system needed updating for the new instrumentation; (2) data streaming to the second computer needed to be improved and tested; and (3) a program allowing remote users to view the status of the loop needed to be implemented.

Material samples for the testing were cleaned weighed, measured and photographed and can be seen in Fig. 6-12. The holder for the samples was received; however, the aluminized SS-316 samples did not fit into the holder. A separate holder was designed and built and the rod connecting the holder cans modified to accommodate the additional holder (see Figs. 6-13 and 6-14).

Figure 5-12. Corrosion samples of 316 stainless steel, aluminized 316 stainless steel, and scale.

A replacement test section was prepared—a 2-in diameter stainless steel pipe that bolts into the long vertical leg of the loop. Three thermowells were machined and welded into the test section pipe. Thermocouples in these thermowells will measure reference temperatures for the materials test and will allow us to check flow speed in that area.

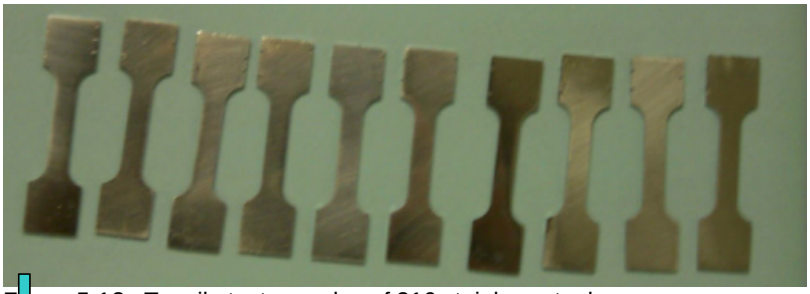

Figure 5-13. Tensile test samples of 316 stainless steel.

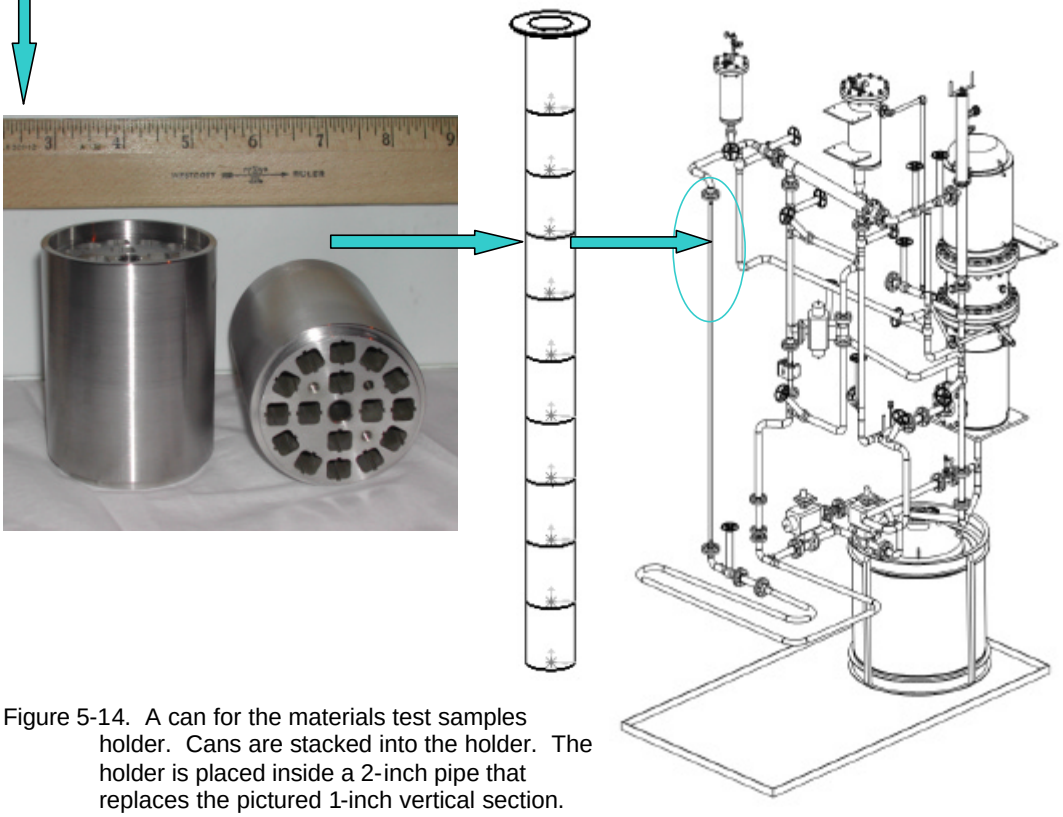

Figure 5-14. A can for the materials test samples holder. Cans are stacked into the holder. The holder is placed inside a 2-inch pipe that replaces the pictured 1-inch vertical section.

We conducted several runs to test the modified cleaning gas system, venturi flow meter, and other equipment. During these experiments, three of the four oxygen sensors failed. Examination and analysis showed that they allowed liquid lead-bismuth to leak inside the ceramic sensor element that contains the reference bismuth in equilibrium with its oxide. This effectively shorts out the sensor and makes the measurement useless. The first solution was to design a protective sheath that would protect the sensor from the static pressure inside the piping combined with transverse force due to the liquid metal flow (Fig 6-15). The sheaths were machined and installed. The oxygen sensors were assembled and installed into the loop again. Unfortunately, this procedure did not improve the seal between the ceramic element and the holding ring.

Figure 5-15. Ceramic sensor element from the oxygen sensor and its protective sheath. Graphite based sealer is visible on sensor.

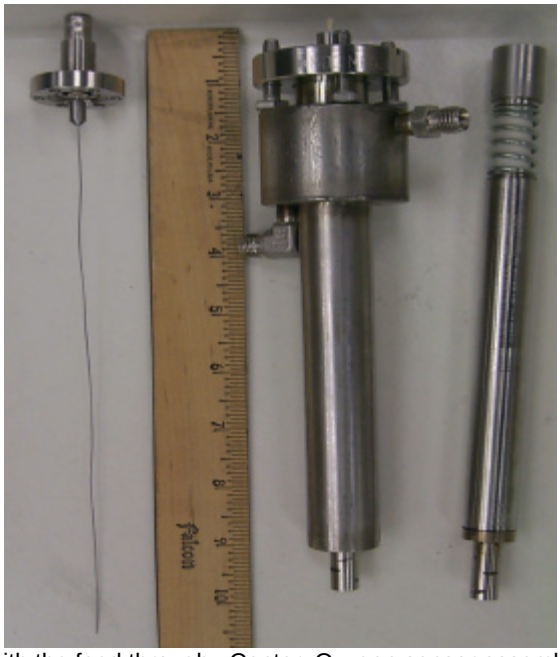

Figure 5-16. Left: sensor wire with the feed through; Center: Oxygen sensor assembled; Right: internal tube that must apply compressive load to the seal between the ceramic sensor and the retaining ring (top of sheath).

We made a decision to replace the sealing method. Graphite gaskets will be used instead of a graphite-based sealer. A formal analysis showed that a force of at least 450 lb has to be applied to the gasket surface to seal. Existing sensor design would not be able to provide such force. The sensor was redesigned with minimal changes to provide the fastest manufacturing time for the new and modified parts. A more advanced sensor design is being developed as well.

Proposed gasket materials will be tested in a press to determine their yield strength and behavior after yield. The sensors will be tested in a separate pressure vessel before being installed in the

loop. We will also test a backup tantalum metal gasket. Other sealing options are being investigated.

The Hazard Control Plan (HCP) and the operational procedures were reviewed to implement changes derived from the operations. They have been submitted to the responsible line management for approval.

LBE Technology Development. The main activities in this area are the continued oxygen sensor development and calibration, corrosion modeling for transients, and TRAC modeling of DELTA Loop thermal hydraulics.

Oxygen Sensor Development and Calibration. We completed an evaluation of the candidate electrolyte materials and reference electrodes for low temperature sensors, and the experimental results from the LANL YSZ | Bi/Bi_2O_3 sensors operating in the calibration stand and the DELTA loop. It is decided that this type of sensor will continue to represent the baseline technology, with several forms of zirconia electrolytes, reference electrodes, and sensor configurations as backup. Emphasis will be placed on developing and testing compact sensors and the matrix for large vessel deployment, where flow conditions and oxygen distribution are more complex than in forced-circulation pipe flows.

Three more oxygen sensors were tested in the entire range of magnetite dissociation (depletion of oxygen, limited by the SS-316 vessel) and saturation. Their dynamic responses were also measured (cf Fig. 6-17).

At 420°C, the confirmed OS dynamic range is more than 5 orders of magnitude, and the sensitivity is roughly 70 mV per decade of oxygen concentration (the sensor emf depends on the logarithm of concentration). This value is temperature dependent.

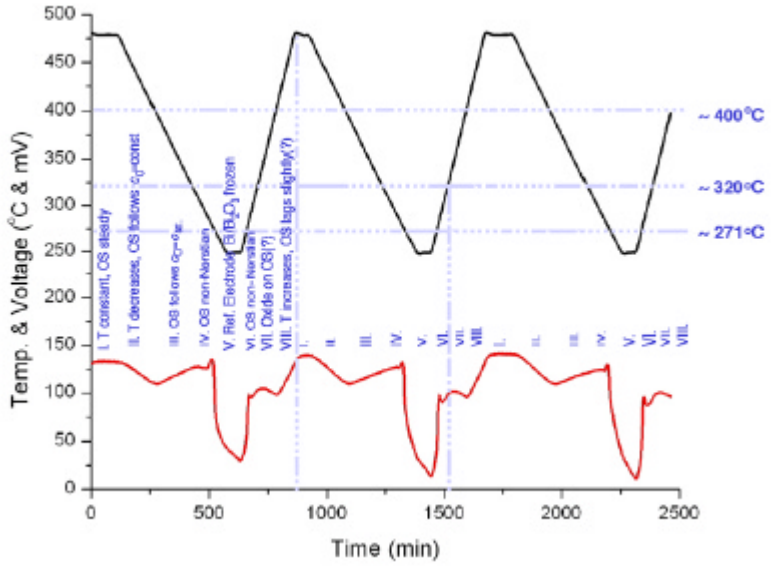

Figure 5-17. The oxygen sensor's (LA-OS-009) dynamic responses to thermal cycling. The starting oxygen concentration is approximately 2ppm.

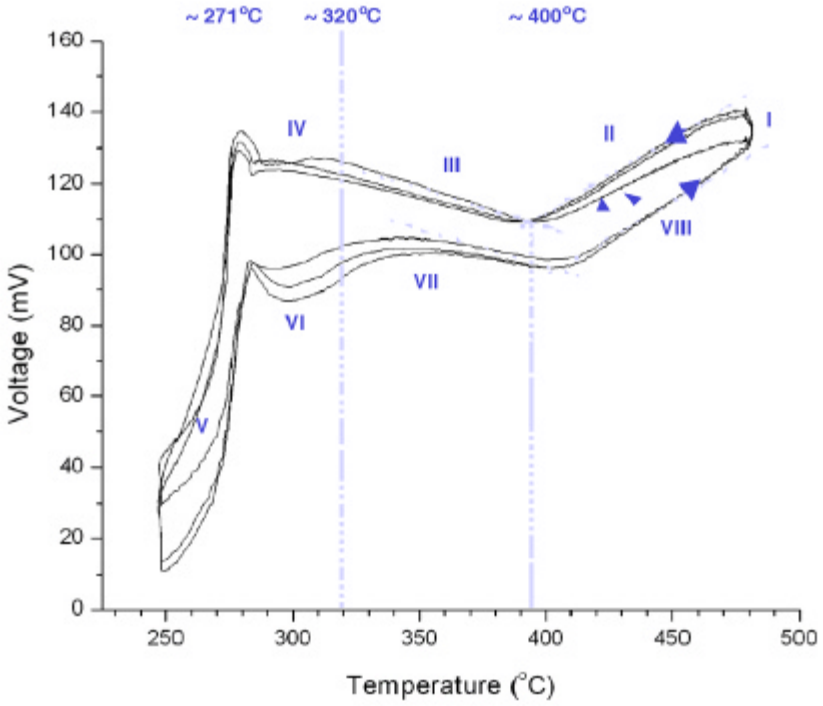

Figure 5-18. The V-T plot of the oxygen sensor data shown in Fig. 17, showing an apparent hysteresis.

We now have the calibration curves for 5 sensors. They behave quite uniformly according the Nernst Law in the range of 350–550°C, with an estimated uncertainty of less than 20% within the theoretical values. The sensors' lifetimes may be drastically reduced by prolonged exposure to hydrogen and thermal cycling.

The results have been submitted to ICONE-11 and to the Accelerator Application Division of the ANS for its annual summer meeting with embedded topical AccApp'03.[27]

A new sensor calibration stand is being designed. This configuration (a crucible of LBE stirred by a mixer in an atmosphere-controlled vessel) will have multiple sensor wells for cross-calibrations, and should improve reaction kinetics and shortened calibration times. The design will be first used for a UNLV Transmutation Research Project.

Corrosion Model. The kinetic corrosion model for oxygen-controlled LBE systems is expanded to include transient behaviors. The model reveals important differences for corrosion and precipitation distributions during transients, in steady states, and in closed-loop flows.

The differences can be illustrated in the following way. In Figure 6-19, the evolution of corrosion and precipitation distribution in a simple test loop shows that in a few hours (very short in comparison to typical corrosion test times), the behaviors differ substantially. At the very early

[27] "Oxygen Sensor Calibration for LBE Coolant Chemistry Control," ICONE11-36561, and "Oxygen Concentration Measurement and Control for Liquid Pb-Bi Eutectic," AccApp'03.

stage, the corrosion proceeds in uncontaminated fluid and behaves like in open-pipe flows. A simple sectioned conventional mass-transfer correlation may predict very similar results.

As the transient quickly evolves toward the steady state, the corrosion product in the fluid builds up, and the upstream transport also begins to affect the local corrosion and precipitation. The resultant corrosion and precipitation distribution cannot be predicted by linking local mass transfer models in *ad hoc* manners. These differences have led to over-prediction of corrosion rates, and the mistaken prediction of maximal corrosion and precipitation. The latter may lead to severe safety problems resulting from leaking or plugging.

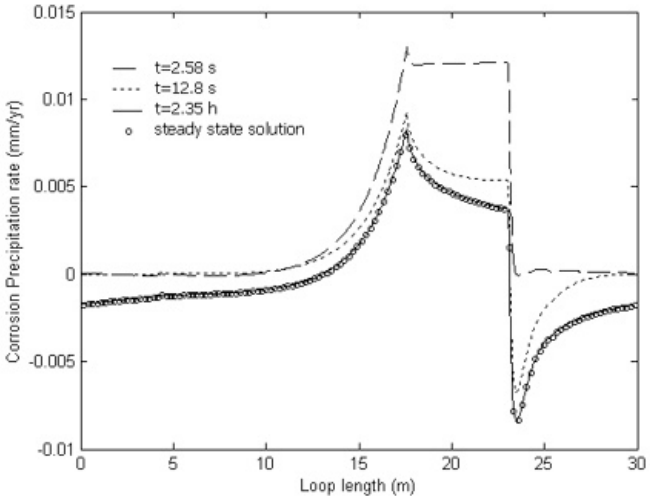

Figure 5-19. Transient Fe corrosion and precipitation distribution in a simple test loop (Tmin=350°C, Tmax=550°C, *cO*=0.01ppm).

In Figure 6-20, the average corrosion rates in the hot test section of a simple test loop with various temperature differences are shown. It again demonstrates the substantial change during the relatively short transient.

TRAC Modeling. The Delta Loop TRAC Model was benchmarked to the 48-hr. test that was conducted in August 2002. The 48-hr. test showed that there were significant external piping heat losses. The measured temperature increase across the heater section was ~23°C compared to temperature drop across the heat exchanger of ~15°C.

The Delta Loop model was updated to model external heat losses. The external heat losses were represented by modeling the pipe walls and assuming a constant heat transfer coefficient to standard room temperature. The heat transfer coefficient was adjusted until the calculated temperatures at selected points in the loop matched the measured temperatures.

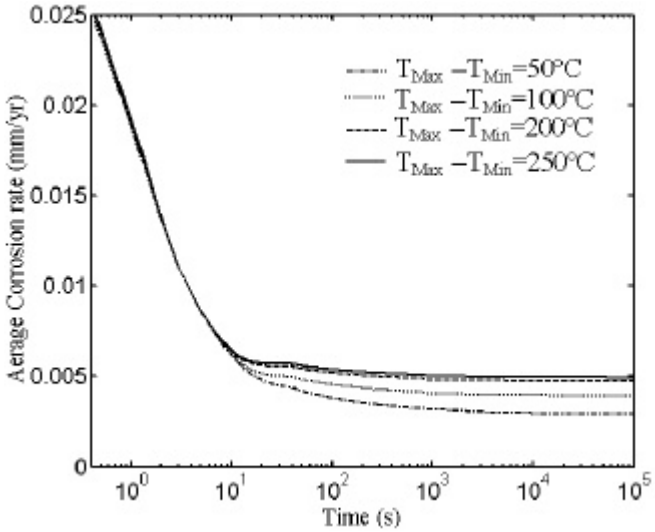

Figure 5-20. Average corrosion rate in the hot test section of a simplified loop.

The Delta Loop model was updated to model the water-to-PbBi heat exchanger. The heat exchanger model was integrated to into the Delta Loop model and the full Delta Loop model was then benchmarked against the 48-hr. test. Figure 6-21 shows the noding diagram of the integrated Delta Loop model; Fig. 6-22 shows a comparison of the measured temperatures to the TRAC calculated temperatures; and Fig. 6-23 shows a comparison of the measured temperature differences across the recuperator, heater section, and heat exchanger to the TRAC calculated results.

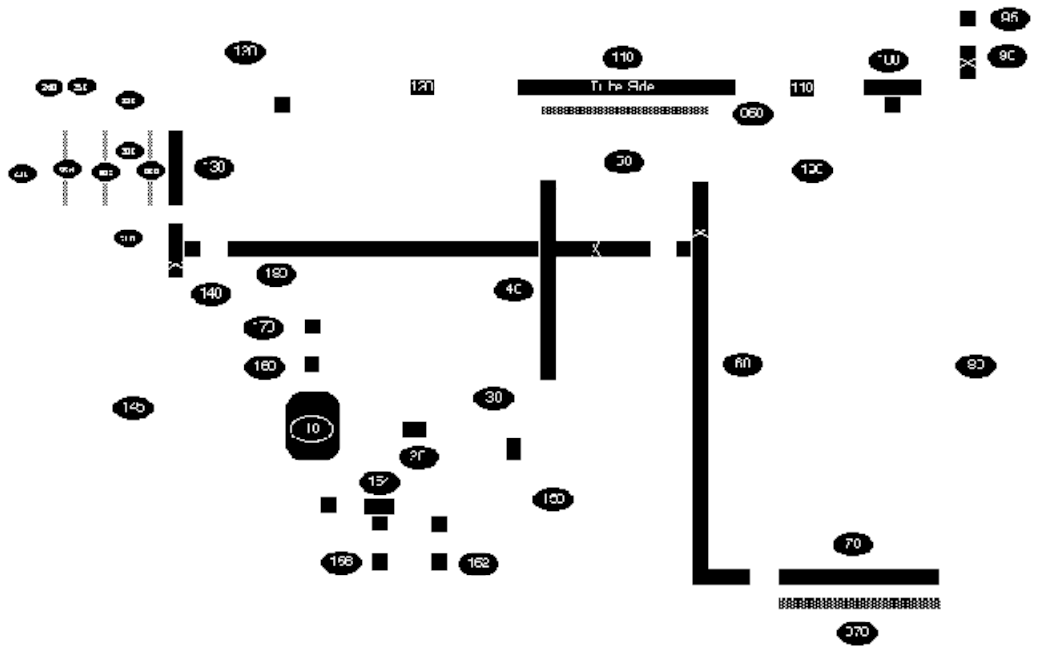

Figure 5-21. A near complete TRAC model of DELTA, with a variable capacity heat exchanger incorporated.

Figure 5-22. Comparison of the measured and TRAC calculated temperatures at 5 locations in the DELTA Loop.

Figure 5-23. Comparison of measured temperature differences across the recuperator, heater section, and heat exchanger to TRAC calculated results.

The heat exchanger modeling was improved so that the PbBi height in the PbBi intermediate channel could be varied to control the heat transfer. Control modeling was added so that the height of the PbBi intermediate channel could be varied to control the heat transfer to the water-side so that the PbBi coolant outlet temperature could be controlled to a specified value. The modifications were done first on a stand-alone heat exchanger model and then added to the Delta Loop model.

The TRAC code will allow PbBi and a noncondensible gas together in the same hydro component. However, the code had to be updated to correct an error in the heat transfer. The PbBi intermediate channel and adjacent heat structure components had to be re-noded more finely in order to get the control modeling to work. The Delta Loop model was modified to add the changes made in the stand-alone heat exchanger. The TRAC code was also updated to provide a more smooth heat transfer calculation in the PbBi intermediate coolant channel.

Corrosion. The focus of our activities was the analysis of data generated during the FY02 WNR irradiation experiments. The oxide dielectric properties of the martensitic-ferritic steel HT-9 were characterized during proton irradiation. Prior to the irradiation experiment, samples were pre-oxidized in moist air resulting in an oxide scale that was on the order of 3 m in thickness. Samples were then irradiated during immersion in 200°C lead-bismuth eutectic at a proton current of approximately 63 nA.

To assess the electrical properties of the oxide in real-time, a sinusoidal voltage perturbation was applied across the oxide surface as a function of frequency. By measuring the magnitude and phase shift in the current response, oxide impedance and capacitance values were obtained. For HT-9, proton irradiation was associated with a decrease in oxide impedance in 2-out-of-3 experiments (Figure 6-24). This change in oxide electrical properties is consistent with increased corrosion rates during proton irradiation. This decrease in corrosion resistance is most likely due local chemical, structural, or electronic changes in oxide properties, though global changes in oxide properties are possible as well. Defects in the oxide that permit direct contact between the LBE and metal surface are ruled out. Although we were prepared to examine the oxide properties of SS-316, time constraints did not permit these experiments.

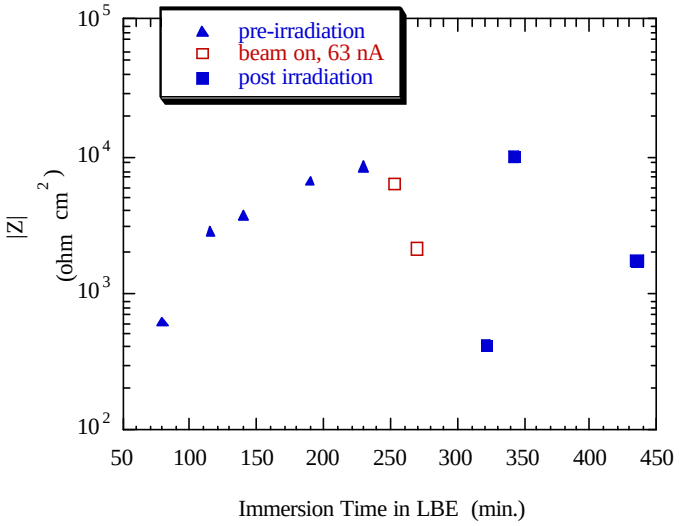

Figure 5-24. Oxide impedance as a function of LBE immersion time for a preoxidized HT-9 sample (48 hrs@800oC). Plot shows pre-irradiation, irradiation and post-irradiation data.

University of Illinois, Urbana-Champaign. Work on corrosion probe development and testing continued. The design of the test LBE apparatus was modified to mitigate corrosion and coolant

chemistry control problems. Purchasing of equipment and supplies is 80% complete. The feasibility of impedance spectroscopy based corrosion probes will be tested.

University of Florida. The study on the influence of radiation on passivating oxides continued. SS-316L and HT-9 samples were procured, and test conditions were selected. Oxidation studies will be carried out in dry air at 300ºC, 400ºC, 500ºC, 600ºC, and 700ºC with exposure times ranging from 12–48 hours. As a first choice for irradiation, a 3.2-MeV proton-ion beam and an irradiation temperature of 360ºC are the selected conditions to irradiate the samples to a dose of 1dpa. Based on these parameters, the ion beam facility at the University of Michigan is a potential irradiating facility, however, the cost of irradiations may be prohibitive.

5.4 Accelerator-Driven Systems (ADS)

Transmutation engineering activities in accelerator driven systems will provide necessary information on the physics of coupling an accelerator to a subcritical system and the operation and start-up of such systems. In addition, the target technology necessary to drive these systems will be developed to support the technology decisions.

The accelerator-driven systems tasks involve the codes and methods used to assess the transmutation process. The objective also includes defining and designing long-term experiments needed to advance the TRL in this area. International support and collaboration is a strong part of the ADS research conducted under transmutation science. A major collaborator is CEA in France. However, this collaboration is defined at the basic research level, and there are no tasks specifically conducted or funded in support of CEA's efforts. Some tasks are specifically funded in support of the MEGAPIE Project at Paul Scherrer Institute (PSI) in Switzerland.

5.4.1 Accelerator-Driven Systems Technical Summary

MUSE (ANL)

Experimental Activity. The MUSE-4 reference measurements (without the GENEPI accelerator) were completed at the end of September, and the core transitioned back to the SC0 configuration. In October, SC0 measurements (which include irradiation of foils for spectral unfolding), fission reaction rate traverses, and noise measurements, were performed. The experiment analysis team is making an effort to better understand the effects of polyethylene on ^{235}U detector response.

When it was attempted to restart the GENEPI accelerator after the 6+ months of non-operation, it was found that there was a problem with one of the power supplies. This was fixed, but cost about a week of lost time to the schedule. Another problem was found in GENEPI in November, which is degrading the performance (a very small air leak). In spite of the degradation, the tritium target was tested, and found to give much superior performance as expected. Another problem with the GENEPI accelerator occurred in early December that prevented GENEPI from operating. As a consequence, the experimental program made no progress during this period.

The biennial MUSE partners meeting was held in November at Cadarache. Because the MUSE-4 program must definitively terminate at the end of 2003, there was much discussion regarding what experiments can and should be performed during this last year. It was agreed that a Technical Program Committee would be formed to advise CEA, and includes members from ANL, BNFL, SCK, Delft, CEA, and ISN. The first meeting will be held in January at Cadarache.

Analysis Activity. Adjoint flux distribution measurements were analyzed for the MUSE4 reference configuration. Satisfactory agreement between calculation and experiment (within uncertainty margins) was found when a large number of energy groups (=299) is used. In Fig. 1-25 we show a comparison between calculated and experimental values of the adjoint flux distribution.

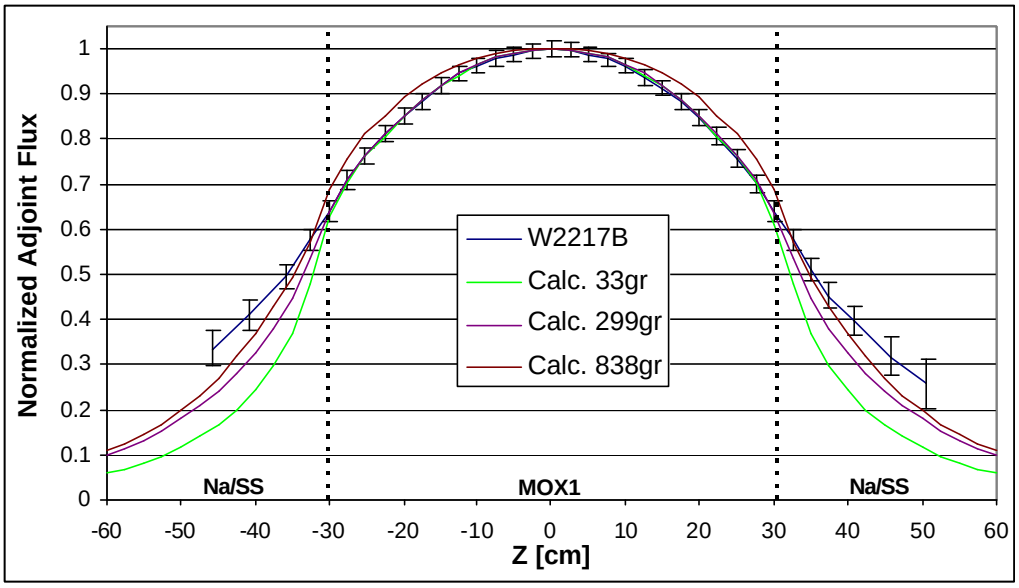

Figure 5-25. Adjoint flux radial distribution calculation/experiment comparison.

The calculations on MUSE4 Benchmark have been completed. These include the deterministic calculations of the dynamic results. The agreement with the other participants to the Benchmark is now satisfactory. The deterministic dynamic results of the point 5 of the MUSE4 Benchmark - Step 3 (MUSE4 subcritical configuration) have been improved by fixing several bugs in the KIN3D code, done in cooperation with FZK-Karlsruhe (Germany). The new results lead to the conclusion that the agreement between KIN3D and Monte-Carlo is extremely good for those detectors located near to the external source. Some improvements are still needed for the behavior of those detectors located in the reflector and in the shielding. Figure 6-26 shows the new results obtained with KIN3D for each detector, and Figs. 6-27 and 6-28 show the case of the detector in the reflector. We can observe that agreement with other participants to the Benchmark (mostly a Monte-Carlo code) is now satisfactory.

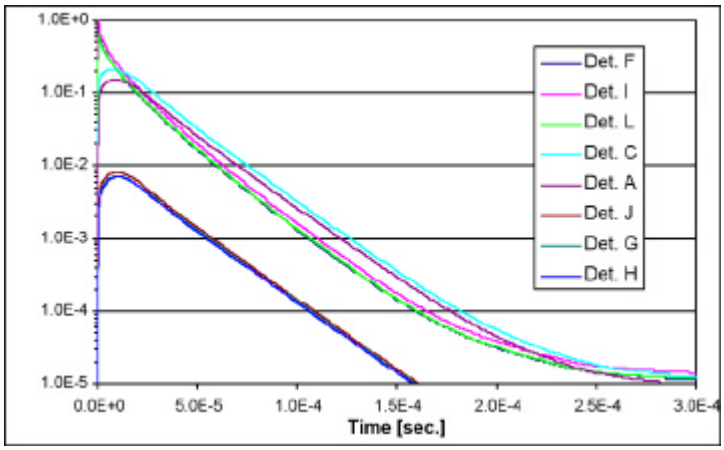

Figure 5-26. KIN3D Direct Method – All Detector Behaviors.

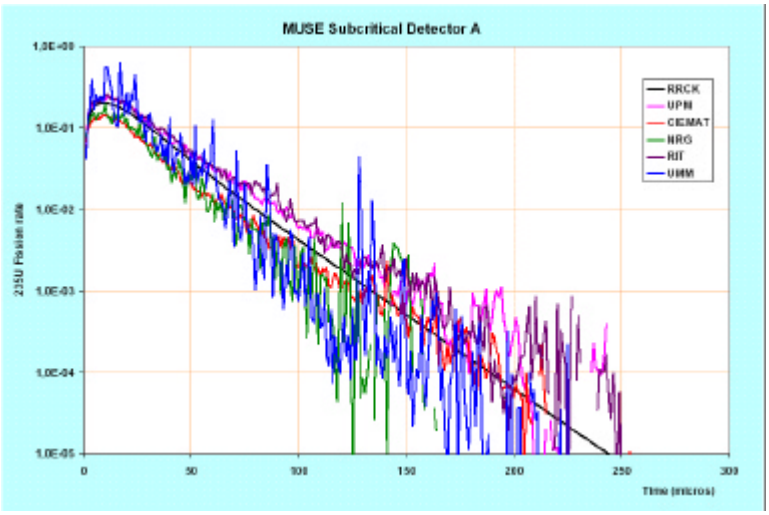

Figure 5-27. Detector A – Monte-Carlo Results.

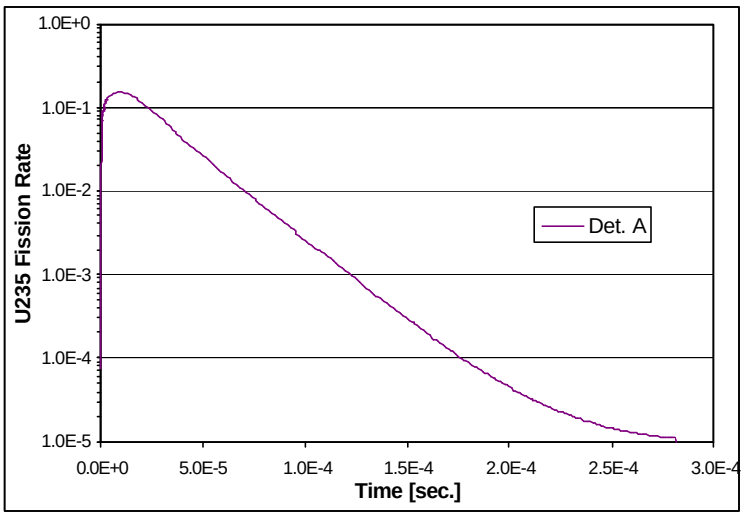

Figure 5-28. Detector A – KIN3D.

It has been found that the discrepancy observed between ECCO and MC^2-2 was minimal when calculations were performed using the total cross section weighted with the current, instead of the flux. The discrepancy observed when using a flux-weighted total cross section has been attributed to an incorrect formulation of MC^2-2. In this latter case the group-to-group P1-scattering cross section needs to be corrected. A theoretical demonstration has been provided.

TRADE (ANL)

Coordination. The TRADE experimental program plan for Phase IA was presented to the TRADE working group at the Third Enlarged General Progress meeting in Rome in October.

In November, a coordination meeting on the TRADE neutronic activities was held in Cadarache, France, with participants from ANL (via phone), CEA, ENEA, and FZK. Several actions have

been agreed for the short term on five different lines of activities: (1) Benchmark, (2) Calculations by deterministic codes, (3) Data, (4) Burnup, and (5) Experimental Phase IA.

A TRADE coordination meeting was held in Paris in December, where several items were discussed and agreement reached, including:

- Neutronic activities
- Following a workshop in Los Alamos, a new design for the target is being explored (pure tantalum)
- Forced vs. natural convection of the target - a first full 3D natural convection cooling calculation has been produced by CEA
- An increase of the proton energy (E_p~ 140 MeV instead of E_p~ 110 MeV) has been considered and a first evaluation (cost, feasibility, associated beam transport line) is underway

Experimental Activity. The experimental program plan for Phase IA was revised to reflect the realistic procurement times for the needed fission chambers and associated electronics. This was presented to the TRADE working group and contact persons at the Third Enlarged General Progress meeting in Rome in October. The plan was accepted, and a subsequent visit to Casaccia allowed a better definition of the Phase IA activities.

Phase IA can be split into two general sub-phases: a very preliminary set of reactivity measurements and equipment testing to take place toward the end of 2002, and a more expanded set of measures leading to measurements in a TRADE mock-up core in the late spring of 2003.

The TRADE Phase IA experimental program commenced on November 18. The following types of measurements were performed until the end of the month:

- Chamber testing
- Fuel element reactivity worth
- Flux measurements
- Temperature coefficient of reactivity
- Control rod calibrations

The shutdown (all rods in) and excess (all rods out) reactivities as estimated are shown in Table 4.

Table . Shutdown and Excess Reactivities

Config	Excess	S.D. $	SD pcm
4 B-ring	0.04	6.57	4730
1 B-ring	3.58	7.00	5040
Full core	4.42	6.16	4440
G-ring	4.16	6.42	4620

Flux measurements were made using the Pu-239 miniature fission chamber and are presented in Table 5. The chamber has an effective mass of 23.6 μg.

Table. Flux Measurements with ^{239}Pu Miniature Fission Chamber

Config	Flux
1	0.8 E05 (center)
2	1.0 E05 (center)
4	4.0 E04 (periphery)

Analysis Activity. A study on the time dependence of the neutron population in different parts of the TRADE experiment after the external neutron source is turned off was performed. It was found that several microseconds after the source had been turned off, the spallation neutron population constituted at best 5% of its initial value. At the same time in the case of a 1-GeV proton beam, the neutrons disappear faster than in the case of a 110-MeV beam. Tables 6 and 7 illustrate some selected results for water and LBE-filled B ring in terms of the time dependence of the neutrons flux, defined as a fraction as compared to the flux at t=3e-6 s (the time of the beam turn off). The Figures 6-29 and 6-30 illustrate the tables.

Table. Evolution of the Neutron Flux as Function of Time in the TRIGA Fuel. Ring B is Filled with Water.

Time (s)	110 MeV (spallation)	1 GeV (spallation)	110 MeV (total)	1 GeV (total)
0	1.00E+00	1.00E+00	1.00E+00	1.00E+00
2.00E-06	9.99E-02	7.62E-02	1.34E-01	1.05E-01
4.00E-06	5.92E-02	4.48E-02	1.02E-01	7.74E-02
6.00E-06	4.69E-02	3.52E-02	8.75E-02	6.77E-02
8.00E-06	4.10E-02	3.04E-02	7.71E-02	6.55E-02
1.00E-05	3.77E-02	2.76E-02	8.77E-02	6.31E-02
2.00E-05	2.82E-02	2.09E-02	7.80E-02	6.01E-02
4.00E-05	1.97E-02	1.41E-02	7.46E-02	5.72E-02
6.00E-05	1.41E-02	1.02E-02	7.40E-02	5.57E-02
8.00E-05	1.10E-02	7.55E-03	7.22E-02	5.53E-02
1.00E-04	8.68E-03	5.66E-03	7.24E-02	5.18E-02
1.10E-04	7.62E-03	4.92E-03	7.13E-02	5.18E-02
1.18E-04	6.62E-03	4.51E-03	6.91E-02	5.11E-02

Table. Evolution of the Neutron Flux as Function of Time in the TRIGA Fuel. Ring B is Filled with LBE

Time (s)	110 MeV (spallation)	1 GeV (spallation)	110 MeV (total)	1 GeV (total)
0	1.00E+00	1.00E+00	1.00E+00	1.00E+00
2.00E-06	1.04E-01	7.87E-02	1.48E-01	1.09E-01
4.00E-06	6.13E-02	4.60E-02	1.06E-01	8.11E-02
8.00E-06	4.22E-02	3.10E-02	8.75E-02	7.21E-02
1.00E-05	3.84E-02	2.81E-02	9.72E-02	6.60E-02
2.00E-05	2.84E-02	2.11E-02	7.34E-02	6.25E-02
4.00E-05	1.94E-02	1.42E-02	7.53E-02	5.53E-02
6.00E-05	1.35E-02	1.01E-02	7.69E-02	5.86E-02
8.00E-05	1.08E-02	7.41E-03	7.48E-02	5.58E-02
1.00E-04	8.37E-03	5.59E-03	7.73E-02	5.49E-02
1.10E-04	7.32E-03	4.87E-03	7.18E-02	5.46E-02
1.18E-04	6.42E-03	4.45E-03	7.66E-02	5.44E-02

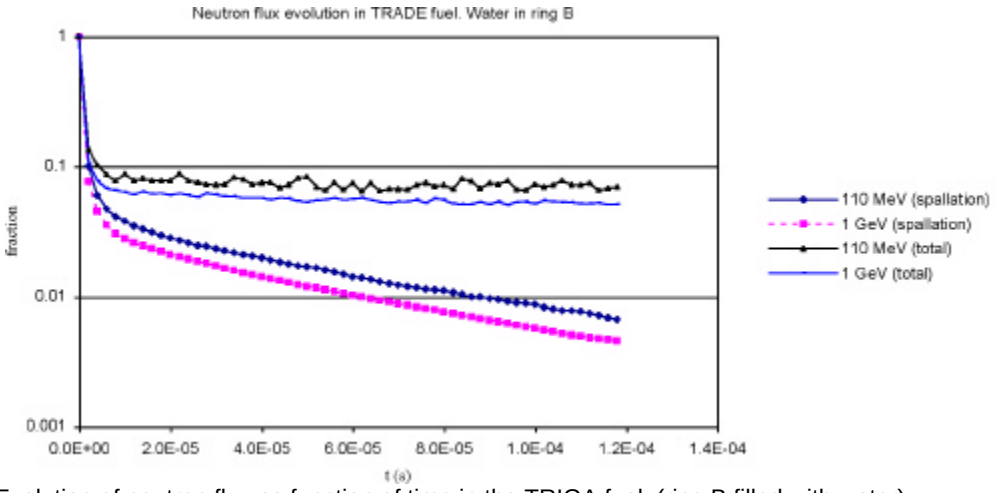

Figure 5-29. Evolution of neutron flux as function of time in the TRIGA fuel. (ring B filled with water).

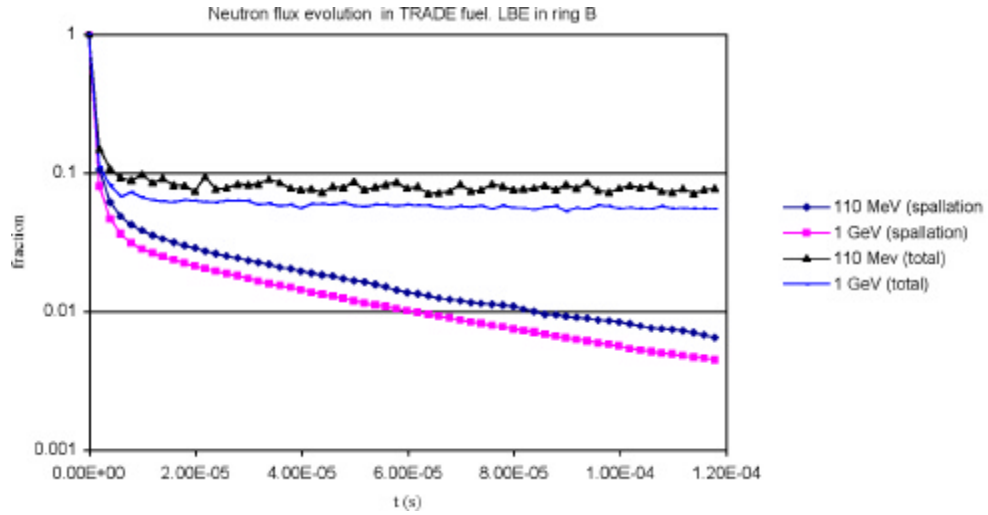

Figure 5-30. Evolution of the neutron flux as function of time in the TRIGA fuel. Ring B is filled with LBE.

The development of a deterministic model for MSM and dynamic calculations of the TRADE experiment has started. Hexagonal-Z geometry and 2 and 9 multi-group cross sections in conjunction with the DIF3D nodal diffusion code have been used.

Fuel-Cycle Method Code Development (ANL)

Several updates have been done on the lattice codes DRAGON and WIMS-ANL, the Monte Carlo code MCNP (parallel version), and their associated libraries. An effort is underway to provide the capability of displaying in the ISOTXS data set (generated by the DRAGON code) the partial cross sections, viz., the vector (n,p), (n,alpha), (n,d), (n,t), and (n,capture). The P0 and P1 matrices for elastic, inelastic, and (n,2n) data can also be included.

Modifications to the VARIANT module of the DIF3D code were made to improve the angular and spatial approximations available. This allowed the extension of the angular approximation from maximum P_5 or SP_5 approximation to a P_{99} or SP_{99} approximation.

In order to test a viable approach for the treatment of low density regions in the variational nodal-transport methodology, we tried to implement the first-order transport equation-response matrix formulation in the x-y geometry option of the VARIANT code. After some difficulties were encountered, it was decided to modify the MathCAD programming that was written to prototype the method on simple model problems before attempting to integrate it into a FORTRAN coding. This will allow testing the first-order treatment on a very simple problem and help decide whether it would be worth trying to include it in VARIANT for vacuum nodes.

MEGAPIE

Project Status and Activity. The target system design is essentially complete. However, resolution of the last remaining unresolved details and issues is progressing slowly. Since manufacturing is already behind schedule, this has the potential to seriously impact the 2005 irradiation date. To speed progress, PSI has met with Subatech and has agreed to accept the work and responsibility for some tasks. PSI has accepted responsibility for the lower target enclosure (the water-cooled jacket).

A contract was awarded for target manufacture to ATEA—the only company to bid on the job. The contract was awarded prior to resolving all design details; however, project management felt it was important to begin the formal work to plan the manufacturing and assembly. A Readiness For Manufacturing milestone is set for March 2003. Scheduled delivery of the target system is December 2003.

During the PCG meeting in October, CEA presented stress analysis of the heat exchanger, indicating unacceptably high stresses in the region at the top. The heat exchanger has been redesigned; and even though the resulting geometry is more complex, the stresses are now acceptable according to CFD analysis.

Continuation of pump cavitation testing, initiated last summer, was performed, confirming no cavitation under more extreme testing. This testing confirms that the cover gas pressure can be reduced to 0.2 bar.

In a protracted test of the pump/flow meter system, the flow meter failed after 600 hours. It is now being evaluated for improved performance and mechanical integrity.

FZK flow visualization experiments, called HYTAS, continued. These tests simulate the flow in the target window region. Water flows through a transparent mock-up, and flow fields are observed with light sheets. Within the parameter range studied, it is possible to observe the location of the stagnation point, recirculation, and the degree of rotational "swirl" in the riser tube.

KILOPIE, the low-power window-cooling experiment, also to be conducted by FZK, has been delayed again. Expected test date is now in February. The delay is from leaking flange seals and the need for additional safety features.

The ability to operate at reduced cover gas pressure introduced some options for handing gases and vapors produced by radiolysis. The most extreme and simplifying option would be to enclose the cover gas system. However, this option was rejected because 1) the absorber system must be proven experimentally before it can be relied upon to do this job, and 2) in the event of an accident, a rise in absorber temperature may result in release of gases and consequently unacceptable gas pressures. A second option has been adopted that eliminates the in-target absorbers in favor of venting all the gases, including the H_2, to a decay tank, followed by venting

to stack after decay and dilution with sufficient inert gas to eliminate flammability hazards, if necessary. Eliminating the in-target absorber system has the added benefit of allowing more space for in-target shielding.

The LBE Fill and Drain system will be a non-automated system, with freezing of the LBE in the target at the end-of-life. Filling and draining will be done by manual manipulation of the valve system during the integral tests. In SINQ, the target will be filled only once, prior to startup, then the fill system will be disconnected. A reversible seal will allow for later reconnection if it is necessary to make repairs and the target is not yet too active. At end-of-life, the LBE will be frozen in place and removed in the hot cell. Analysis and experimentation indicate that this freezing can be accomplished while preserving the window for PIE, although the precise freezing procedure remains to be prescribed. The TAC request was to keep the LBE drain capability because this function is of general interest to the partners; however, it is argued that the MEGAPIE situation is so unique that the draining experience is only partially relevant to the general community. Written documentation of the changes and their impact will be prepared in the near future.

The Heat Removal System (HRS) is complete and the contract has been awarded for fabrication. The HRS is scheduled for delivery at the end of 2003.

A meeting was held with the Swiss nuclear safety authorities. They presented to PSI a list of 29 questions on the safety report. Most of these questions where adequately addressed during the meeting. The remaining points will be dealt with in a written statement, to be issued before Jan. 1. The approval process will continue, with approval milestones in March and May, 2003.

DOE Contribution

Oil-LBE Interaction Experiments. We are working with PSI personnel to investigate any possibility of interactions between cooling oil and LBE. A 2-hour test was conducted, resulting in no measured reaction between the fluids. The time chosen for these tests was based on an estimated cool-down time in the event of an accidental leak of oil into the LBE (assuming immediate beam interrupt). To investigate the possibility of a small slow leak that could remain undetected for a longer time, these tests will be extended to several days. Plans for the longer tests have been made requiring some system modifications. Tests will proceed when the modifications are complete. We do not anticipate any interaction between the oil and water.

TRAC Model. A TRAC model of the MEGAPIE 3-loop system is being set up evaluate the system transient performance during operation in SINQ as well as during reduced power tests on the integral test stand. Currently, a full model of the LBE side of MEGAPIE is operational, with main and bypass pumps and circuits, beam heating, pump heating and transient analysis capability. All thermal masses and conductances have been verified. This TRAC model will closely follow the RELAP5 model developed by Ansaldo for the heat removal system design basis.

Integral Test Stand. We are working with PSI personnel on preparing the MEGAPIE Integral Test Stand (MITS). Specific activity is sizing and selecting a heater system for steady-state and transient system performance tests. Heaters have been selected and procured for preliminary testing in the PSI LBE loop. The plan is to have 18–19 heaters in a hexagonal array.

Preliminary testing will investigate surface corrosion and the envelope for pushing the heat flux beyond the manufacturers rated performance limit. The corrosion rate of the heaters has been

analyzed using models developed at LANL, and the maximum corrosion rate is expected to be less than 260 m/year at a heater surface temperature of 450ºC. With a total life of heater operation expected to be a few hundred hours, this is acceptable. A report on this analysis has been submitted.

Three heaters were received for testing. These test heaters are equipped with internal thermocouples to monitor heater-element temperature as a function of power. One of these heaters was mounted in the PSI loop to verify performance. Heat flux was limited by the power supply, but 125% of rated power was achieved. A small hole in the heater sheath developed while the internal temperature of the heater was only 450ºC at peak power. Based on this, one can expect that higher power densities can be achieved but the quality of manufacturing is suspect. X-rays of the failed heater are in progress. After fully assessing the heater failure, the manufacturer will be consulted and a superior product procured.

Absorber Tests. During this quarter, refinements in the designs of both the target system and the HRS resulted in the elimination of both the HRS and the in-target absorber systems. Nonetheless, in the interest of fully documenting the technology and the MEGAPIE decision basis, and because of the potential usefulness of absorber systems in other applications, some level of testing will be conducted.

Vent Line Sizing. A model of a maximal leak event on the MEGAPIE target vent line prepared earlier was revived and improved, with better bounding assumptions, and a report was written and submitted. According to this analysis, the 4-cm diameter vent line is full satisfactory. The remaining issue is the possible break of the window due to quenching with water. Thermal stress analysis is being conducted.

Cost and Schedule. A detailed schedule has been prepared, indicating irradiation starting in early 2005. Key milestones are the completion of the target design (Feb 2003), completion of the Readiness for Manufacturing (March 2003), and delivery of the target and heat removal system (Dec 2003), leaves sufficient time for integral testing and installation in SINQ in 2004.

The cost to completion is 6.9 M Euro. There is very little contingency, and what there is will most likely be taken up by additional target manufacturing costs.

6 IDAHO ACCELERATOR CENTER

6.1 Idaho Accelerator Center Scope

The Idaho State University is a component of the national Advanced Fuel Cycle Initiative. Through this research project, which is centered in the Idaho Accelerator Center (IAC), research is conducted to support activities in the research programs of the AFCI: Transmutation Engineering, Separations, and Fuels. Most of our work is concentrated on Transmutation Engineering. In the two separate multifaceted research projects support is provided for undergraduate and graduate students, administration of the program, and provides infrastructure for conducting the research. The research includes the use of electron accelerators to produce photons and neutrons for use in experiments.

Experiments may include radiation damage to materials and/or cooling systems, investigations of neutron production and multiplication, reactor dynamics, and other topics that may be added as research needs are identified in the future. In addition a new method for positron-annihilation spectroscopy (PAS) has been developed at IAC that allows stresses and defects to be measured in bulk materials. The application of this new PAS technique to AFCI nuclear materials problems such as the examination of the zone of a weld between dissimilar materials is under way. Both of these research and development activities are being conducted in collaboration with other AFCI member organizations.

6.1.1 Idaho Accelerator Center Technical Summary

The following summarizes principle activities for AFCI at IAC in the 4th quarter. The 1st two projects have led to papers submitted to peer reviewed journals and all but the last two have led to talks presented at national meetings. The neutron producing target development were the subject of an MS thesis successfully defended by Suresh Sardineni, a UNLV engineering student.

Positron Annihilation for Materials Stress Analysis: A new technique has been demonstrated at IAC this past quarter, for performing PALS, Positron Annihilation Lifetime Spectroscopy, another a useful probe of defects in materials. The new method allows PALS to be performed on bulk samples for the first time. The new PALS scheme, shown in Figure 7-1, relies on the prompt gamma decay that results from proton capture reactions in many light nuclei (Al in our case). Two gamma rays are produced, one starts the TAC the other is converted to positron electron pair in the sample. When the positron thermalizes then annihilates in the sample the annihilation gamma provides the TAC stop. This allows the lifetime in the bulk material to be measured that is not possible by any other technique.

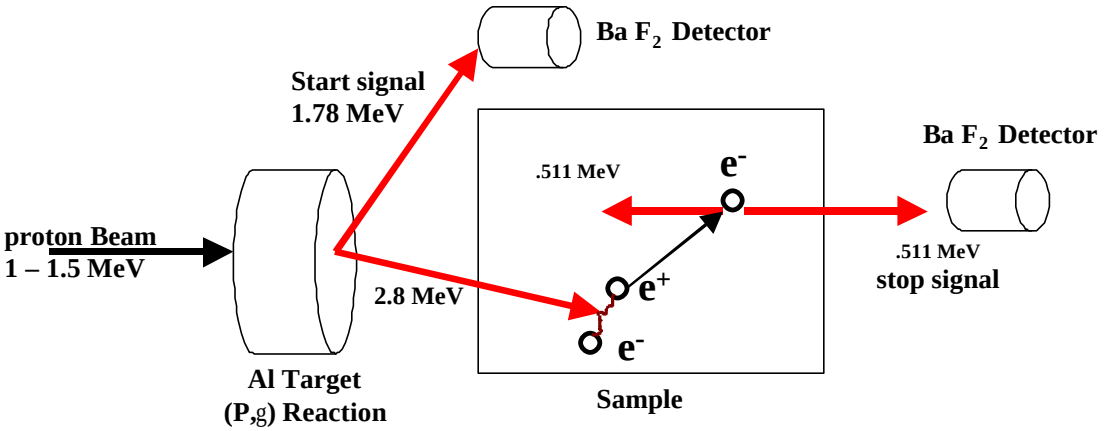

Figure 6-1. Positron Annihilation Lifetime Spectroscopy Scheme.

A positron life time measurement on lead is shown in Figure 7-2, the result is in excellent agreement with literature values and exhibits a much cleaner decay than the conventional methods, which are bedeviled with complex decay curves due to positron source and sample surface effects. The lifetime measured, 194 ps, is in excellent agreement with the literature value and may set a new standard for this number.

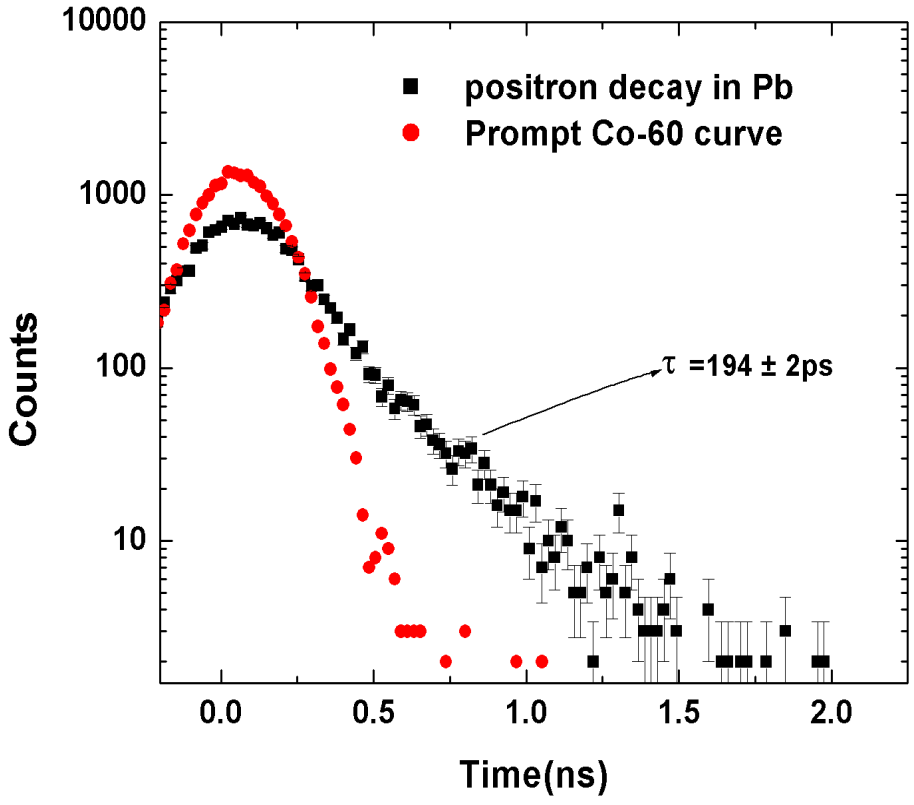

Figure 6-2. Positron life time measurement on lead.

Positron Measurements in Laser Pulse Shocked Silicon. This methodology uses an electron accelerator to perform positron Doppler Annihilation Spectroscopy (PAS) in bulk materials, as previously reported, but now during and shortly after a thermal stress is induced in a sample with an intense 10ns laser pulse. The experimental setup and the first results are shown below (Fig 7-3 and 7-4). A 100MW YAG laser and the FPL accelerator were used for this work. The data displays the longitudinal momentum of the electrons in bulk silicon during laser pulses and after laser irradiation. Refinements of this technique are scheduled for testing in Jan.2003.

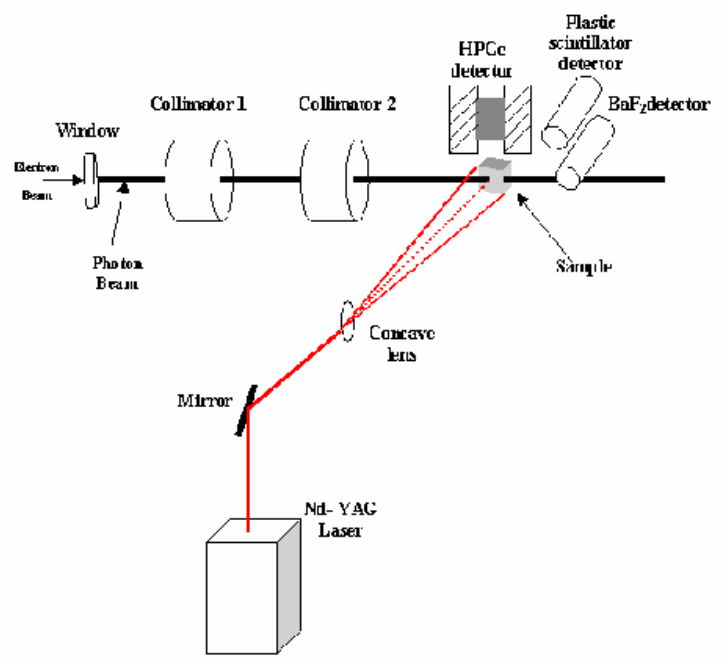

Figure 6-3. Setup for correlated PAS/ thermal stress measurements

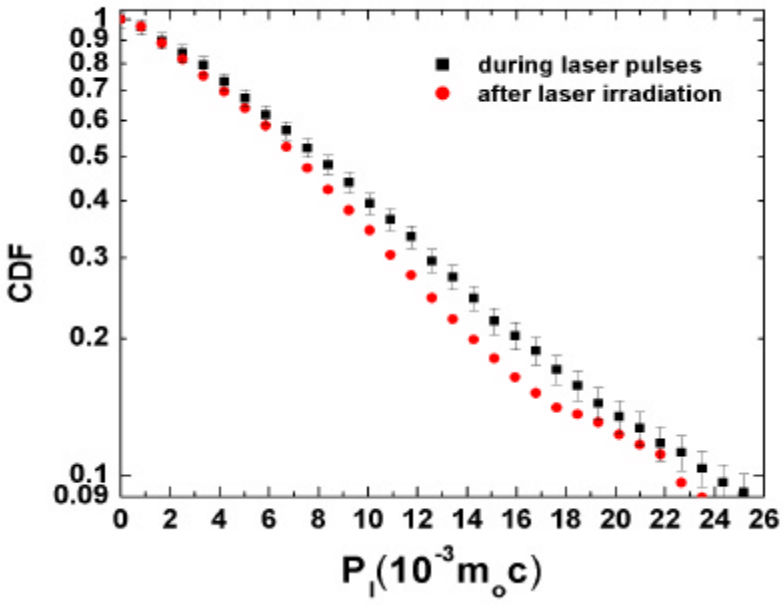

Figure 6-4. Transverse electron momentum in silicon as measured by PAS during and after an intense laser pulse.

LeANS Neutron Source. A transportable linear electron accelerator driven neutron source (LeANS) (Figure 1-5) for possible coupling with a suitable subcritical facility is being set up and tested. The accelerator, which provides a pulsed neutron fluence of ~10e11n/pulse and ~10e13n/sec time average fluence, can also be used to perform dynamic reactivity measurements in multiplying and non-multiplying assemblies. Building modifications at the IAC main building provide a separate shielded space to house this facility, and accelerator set up were 60% completed as of 31 December. Final accelerator tests will begin in March 2003.

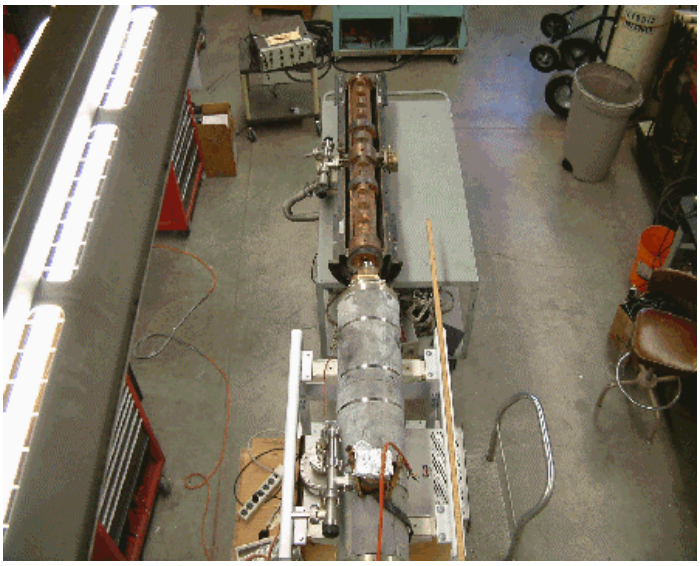

Figure 6-5. Mock up of LeANS Accelerator.

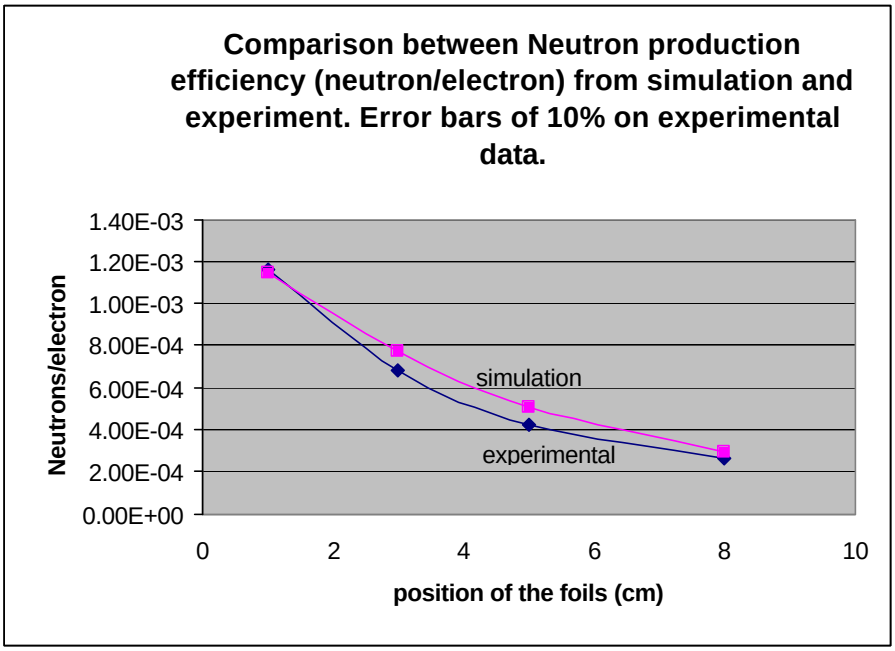

Figure 6-6. Data on the neutron target performance has been taken using the "20" accelerator at IAC.

Upgrading DOE Accelerators. This part of the project assures the continued viability of the ISU Fast Pulsed Linac (FPL) (Fig. 7-7). Upgrading of the FPL magnet power supplies has been completed and tests of the short pulse capability has been completed. The long pulse injector electronics have been replaced and tests will be conducted during a series of experiments scheduled for Jan. and Feb. 2003.

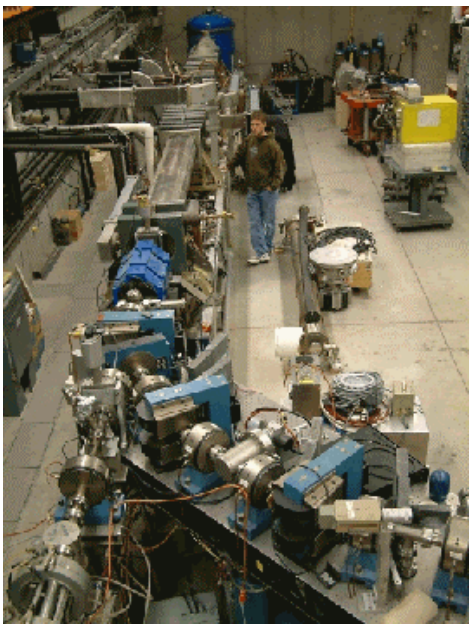

Figure 6-7. Fast Pulsed Linac at IAC.

Dose Conversion Coefficients Collaboration. This part of the project is a continuing collaboration with the UNLV AAA UPP Dose Conversion Coefficients Program. This activity generates internal and external dose conversion coefficients for radio nuclides produced in spallation neutron sources. This work allows the assessment of health physics issues attending exotic nuclides that will be produced in the high-energy-proton/neutron targets. The first round of DCC intercomparisons (Table 1) have been completed and data is being analyzed and the software for the DCC analysis has been upgraded.

15. Table. Dose Coefficients Calculated for Sb-113

Nuclide	**Age**	**AMAD**	**Class**	**Bone_Sur**	**E_50**
Sb-113	7300	5	F	6.85E-13	9.55E-12
Sb-113	7300	5	M	4.49E-13	1.23E-11
Sb-113	7300	5	S	4.20E-13	1.26E-11

The following is a list of presentations and publications:

- J. Kwofie, D.P. Wells, F. Selim, J.F. Harmon, T. White, T. Roney, J.L. Jones, and G. Erickson, "Bremsstrahlung-Based Imaging and Assays of Radioactive, Mixed and Hazardous Waste," 17th International Conference on the Application of Accelerators in Research and Industry CAARI 2002, to be published in *Application of Accelerators in Research and Industry*," AIP Press, Denton, Texas (anticipated publication date Fall 2003).
- K. Chouffani, D.P. Wells, J.F Harmon, J.L. Jones, G. Lancaster, "Exotic X-ray Sources from Intermediate Energy Electron Beams," presented at 17th International Conference on the Application of Accelerators in Research and Industry CAARI 2002 November 12-16, *2002* University of North Texas Department of Physics Denton, Texas, USA. to be published in *Application of Accelerators in Research and Industry*, AIP Press, Denton, Texas (anticipated publication date Fall 2003).
- F. A. Selim, D.P. Wells, F. J. Harmon, J. Kwofie, R. Spaulding, G.Erickson, and T. Roney, "Bremsstrahlung Based Positron Spectroscopy For Material Defect Analysis," *Proceedings of 17th International Conference on Applications of Accelerators in Research and Industry* (CAARI 2002), Denton, TX, 2002, (anticipated publication date: Fall 2003).
- M.A. Reda, J.F. Harmon, and S.B. Sadineni; "A Photo-neutron Source for a Sub-Critical Nuclear Reactor Program" 17th International Conference on the Application of Accelerators in Research and Industry CAARI 2002.
- J. F. Harmon, Idaho Accelerator Center; "Radiation Research Opportunities at the Idaho Accelerator Center" 17th International Conference on the Application of Accelerators in Research and Industry CAARI 2002

J. L. Alvarez, R. Geddes, J. E. Rice, T. F. Gesell, and D. Wells, "Elemental Phosphorous Slag Exposure Study in Southeastern Idaho, USA," 5th International Conference on High Levels of

Natural Radiation and Radon Areas: Radiation Dose and Health Effects, Munich, Germany, 2000, 5th International Conference on High Levels of Natural Radiation and Radon, 2002.

7 UNIVERSITY OF NEVADA LAS VEGAS

7.1 University Programs Scope

UNLV Transmutation Research Program. The University of Nevada, Las Vegas supports the AFCI through research and development of technologies for economic and environmentally sound refinement of spent nuclear fuel. The UNLV Program has four components: student-based research, infrastructure, international collaborations, and management support.

7.1.1 University Programs Highlights

UNLV Transmutation Research Program

- Last quarter, UNLV purchased a state-of-the-art Transmission Electron Microscope (TEM) to enhance their materials science capability. The Architectural and Engineering Design drawings for a new User Facility to house the TEM were approved and the remodeling will commence.
- The UNLV Mechanical Engineering Department submitted a proposal for new Master of Science Degree programs in Materials and Nuclear Engineering to the University and Community College System of Nevada. This proposal comes at the request of the Dean of the UNLV College of Engineering and the expectation of the UNLV President.
- UNLV, along with the University Research Alliance and Idaho State University, initiated an effort to develop the conceptual design of a University Consortium for Transmutation Research (UCTR). The UCTR has the intent of complementing the AFCI and Generation IV programs and of being a key element in participation in international collaborations in accelerator-driven transmutation system technologies.

UNLV Transmutation Research Program graduate students successfully defended two master's theses entitled "Experimental Investigation of Steel Corrosion in LBE: Characterization, Species Identification, and Chemical Reactions" (Physics Department) and "Benchmarking Photoneutrons from MCNPX Simulations with Experimental Results" (Mechanical Engineering Department).

8 UNIVERSITY RESEARCH ALLIANCE – FELLOWSHIP PROGRAM

8.1 University Research Alliance Scope

Managing the on-going fellowship program. University Research Alliance continues the ongoing detailed management of the fellowship program, including ensuring the fellows receive their stipends in a prompt manner, ensuring that special needs are addressed and accommodated appropriately, and ensuring students stay on track for completing their fellowships in a timely manner. In addition to these tasks, University Research Alliance worked with each of the 2002 fellows and their universities to ensure the financial aspects of enrollment, tuition and stipends went well and ensure prompt reimbursement to the students for appropriate and allowable expenses.

8.1.1 University Research Alliance Highlights

- FY01 AFCI Fellow Ben Milliron has graduated from Ohio State University with an MS in Nuclear Engineering. His thesis is on the Use of the Fluoride Volatility Process to Extract Technetium from Transmuted Spent Nuclear Fuel.
- FY01 Fellow Jim Platte, University of Michigan has graduated. He will complete his thesis later this spring. The topic of his thesis is Neutron Spectra Unfolding with an Accelerator Driven System.
- FY01 Fellow Preston Pratt graduated from Texas A&M University with a master's degree in nuclear engineering. His thesis is on Computational Simulation of the Thermal Experiment by the Accelerator Driven System Target Model Using a Computational Fluid Dynamic Program. Preston has accepted a job with Pennsylvania Power and Light, Susquehanna Nuclear Power Plant as a Senior Reactor Operator, Unit Supervisor.
- FY01 Fellow Thomas Roddey has gone to work for Exelon Nuclear in Warrenville, Illinois as a Reactor Licensing Engineer. Thomas will graduate in May 2003, with a master's degree in Energy and Resource Management pending completion of his project report and the presentation of the report to faculty in his department at UC Berkeley. Thomas' project report is titled: Assessment to Research the Correlation Between Funding for Proliferation Abatement and Waste Management Projects and the Risks Associated with Political Instability in Countries Thought to be Without Nuclear Weapons Capabilities.

ANRC has received and approved thesis topics for all of the '02 fellows:

- Shafaq Amdani (U of Illinois-Chicago): Electronic Structures of Clusters and Nanowires of Be
- Tom Carter (U of Florida): Feasibility of Mixed Carbide Fuels for Use in Transmutation Systems
- Lisa Cordova (UNM): An Investigation of the Angular and Spatial Spreading of a Relativistic Proton Beam in a High Z Target, Like Tungsten
- Michael Gregson (U of Texas): Review of Target Materials for Accelerator Transmutation of Waste (ATW) Systems

- Jennifer Ladd (U of Tennessee): Separation of Residual Fluorinated Slag Containing Transuranium and Fission Products
- Billy Rothstein (U of Illinois-Urbana-Champaign): The Effect of Irradiation on Neutron Super Mirrors
- Matthew Sowa (U of Michigan): Investigate Pyrochlore and Zirconia as Inert Matrix Target Materials for Transmuting Transuranics
- Frank Szakaly (A&M): Study of Nitride Fuels for Use in Fast Reactors for the Purpose of Waste Minimization and Waste Transmutation
- Lee Van Duyn (GA Tech): Evaluation of a Non-Fertile Metal-Matrix Dispersion Fuel for use in Plutonium Burning Light Water Reactors
- William Wieselquist (NC State): Investigation of the Impact of Specific Cross-Sections' Uncertainties on AAA Nuclear Fuel Assembly Design

The ’02 fellows were required to provide research proposals during this quarter. All research proposals have been approved.

University Research Alliance has continued developing a program announcement for a potential fellowship program for Ph.D. students. The program is dependent upon the availability of funding. University Research Alliance is also revising the program announcement for master’s degree students.